

**LABORATORY TESTS TO STUDY STABILITY  
MECHANISM OF RAINFALL INFILTRATED  
UNSATURATED FINE-GRAINED SOIL SLOPES  
DEVELOPING INTO SHALLOW LANDSLIDES  
AND THEIR HYDRAULIC PROPERTIES**

**A Thesis Submitted to  
the Graduate School of Engineering and Sciences of  
İzmir Institute of Technology  
in Partial Fulfillment of the Requirements for the Degree of**

**MASTER OF SCIENCE**

**in Civil Engineering**

**by  
Yavuz ŞAHİN**

**July 2013  
İZMİR**

## ACKNOWLEDGEMENTS

I would like to express my extensive gratitude to my supervisor, Assoc. Prof. Dr. İsfendiyar Egeli, for his continued vision, support and priceless guidance during my study. It would not have been possible to complete this study without his endless efforts and experienced guidance. Also Gazi University-Technical Education Faculty, Construction Dept's academic staff, in particular to Assoc. Prof. Dr. Mehmet Özer for his helping for conducting the Laser Diffraction Tests, to Ege-Zemin Laboratory and Ege-Zemin Construction. Ltd. for providing the undisturbed soil samples and for conducting some basic index tests, to Assoc. Prof. Dr. Selim Altun and Assist. Prof. Dr. Devrim Erdoğan for allowing some laboratory tests to be conducted at their soil mechanics laboratory to Prof. Dr. Deniz Dölgen, DEU- Env. Eng. Dept-Chairwoman and Vice-Dean of the Eng. Faculty for providing some help with the review on contamination literature on colloids, and to Izmir Institute of Technology's İYTEBAP022 project, for providing financial support to purchase the automatic HYPROP equipment made by [www.decagon.com](http://www.decagon.com), Thanks are also extended to METU and IYTE's jointly obtained TUBITAK T1001 Project (#109M635) for providing financial support and to METU staff; Assist. Prof. Dr. Nejan Huvaj Sarihan, Assist. Prof. Dr. Kartal Toker and research assistant Mr. Mohammad Ahmadi Adli. I also dedicated the thesis to my mother Deniz Şahin.

## **ABSTRACT**

### **LABORATORY TESTS TO STUDY STABILITY MECHANISM OF RAINFALL INFILTRATED UNSATURATED FINE-GRAINED SOILS SLOPES DEVELOPING INTO SHALLOW LANDSLIDES AND THEIR HYDRAULIC PROPERTIES**

This study consists of two parts. In the first part, saturated soils wetting band infiltration theories and the most widely used in the world by Lumb, 1975 and Pradel and Raad, 1993 compares theoretical predictions were compared with observed results which gave poor correlations. Results showed that both theories grossly underestimated wetting-band thicknesses. Because above mentioned two theories result in constant values, instead of giving values changing as functions of time. These theories need corrections, which indicate need for further studies.

In the second part, hydraulic properties were determined (water-retention, hydraulic-conductivity) of locally obtained 3 undisturbed soils near saturation with a new Hyprop testing technique using the evaporation method. As the Unified Soil Classification System (USCS) does not distinguish inorganic clay colloids by size (size  $<0,001$  mm or 1000 nanometers), Lazer Diffraction Method was used. Results have shown that under zero overall stress; Matric suction does not stay constant, but increases with time up to a maximum point and then decreases, whereas time to reach maximum matric suction increases with decreasing plasticity index (PI) and colloid content (c). While maximum matric suction increases with PI and c, hydraulic conductivity and volumetric water content decreases with increasing matric suction. Also, hydraulic conductivity at maximum matric suction decreases with increasing PI and c.

## ÖZET

### İNCE DANELİ DOYMAMIŞ ZEMİN ŞEVLERİNE YAĞMUR SUYU İNFİLTASYONU İLE SİĞ HEYELANLARA YOL AÇABİLEN DURAYLILIK MEKANİZMASININ VE HİDROLİK ÖZELLİKLERİNİN LABORATUVAR DENEYLERİ İLE İNCELENMESİ

Bu çalışma iki kısımdan müteşekkildir. Birinci kısımda; doymuş zeminlerdeki ıslatma bandı infiltrasyon teorilerinden olan ve dünyada en çok kullanılan Lumb, (1975) ve Pradel-Raad, (1993) teorik hesaplama(tahmin) neticelerinin ve gözlemsel sonuçlarının karşılaştırılması ve birbirleriyle olan ilişkilerinin incelenmesi konusu çalışılmıştır. Sonuçlar göstermektedir ki her iki teoride de gözlemsel ve teorik hesaplamalarda iyi sonuçlar vermemekte, ıslatma bandı kalınlığı hesapları gözlemlerin altında kalmaktadırlar. Çünkü yukarıda bahsedilen mevcut iki teori zamanla değişken değerler yerine sabit değerler vermektedir. Bu teorilerin düzeltilmesi gerekmektedir. Bu konu daha geniş ve gelecek çalışmalar halinde yine incelenmelidir.

İkinci kısımda ise; 3 farklı örselenmemiş zemin numunesinin hidrolik özelliklerinin (su tutma, hidrolik iletkenlik) belirlenmesinde, evaporasyon methodunu kullanan Hyprop adlı yeni bir deney teçhizatının kullanılmasıdır. Birleştirilmiş zemin sınıflandırma sistemi'nin (USCS) ayırt edemediği kil kolloid ebadları (boyut<0,001 mm ya da 1000 nanometre) için Lazer Kırınım Methodu kullanılmıştır. Sonuçlar göstermektedir ki; numune herhangi bir dış basınca maruz kalmasa da, matrik emme sabit kalmaz ve bir maksimum değere ulaşana dek zamana bağlı olarak artış gösterir. Maksimum noktadan sonra azalmaya başlar. Oysa ki; plastisite indeksi (PI) ve kolloid muhtevası (c) azaldıkça, zeminin maksimum matrik emme değerine ulaşması daha hızlı olur. Plastisite indeks (PI) ve kolloid muhtevası (c) ile maksimum matrik emme artarken, artan matrik emme ile hidrolik iletkenlik ve volumetrik su içeriği azalır. Ayrıca, plastisite indeks (PI) ve kolloid muhtevası arttıkça, maksimum matrik emmedeki hidrolik iletkenlik azalır.

# TABLE OF CONTENTS

LIST OF FIGURES.....	x
LIST OF TABLES.....	xiv
CHAPTER 1. INTRODUCTION .....	1
1.1. General .....	1
1.2. Scope of Study .....	2
1.3. Organization of the Thesis .....	3
CHAPTER 2. LITERATURE REVIEW ON RAINFALL INFILTRATION	
PARAMETETERS AFFECTING SLOPE STABILITY .....	5
2.1. Introduction .....	5
2.2. Infiltration.....	5
2.2.1. Factors Affecting Infiltration.....	6
2.3. Influence of Seepage on Slope Instability .....	6
2.4. Rainfall Infiltration and Shallow Landslides.....	7
2.5. Uncertainties with Slope Stability under Rainfall Conditions .....	8
2.6. Definition of Saturated and Unsaturated Soils .....	9
2.6.1. Shear Strength Characteristics of Saturated and	
Unsaturated Soils .....	10
2.7. Stages of Saturation.....	16
2.8. Wetting Front and Moisture Redistribution .....	17
2.9. Wetting Band Theory by Lumb's Equation .....	19
2.9.1. Wetting Band Theory by Pradel-Raad Equation.....	20
CHAPTER 3. DETERMINATION OF ENGINEERING PROPERTIES OF	
SOILS WITH LABORATORY TESTS .....	23
3.1. Introduction .....	23
3.2. Soil Classification Tests .....	23
3.2.1. Particle Size Distribution.....	23
3.2.2. Atterberg Limits Tests.....	27

3.3. Standard Proctor Compaction Test for Soils .....	32
3.3.1. (Static) Direct Shear Tests for Various Soils Used .....	34
3.3.2. (Static) Triaxial CU Test for the CL-ML Soil Used .....	40
3.4. Permeability Tests for Saturated Soils .....	43
3.4.1. Falling Head Permeability Test .....	44
3.4.2. Constant Head Permeability Test .....	45
CHAPTER 4. LITERATURE REVIEW OF STUDIES ON UNSATURATED SOIL'S HYDRAULIC PROPERTIES .....	46
4.1. Introduction .....	46
4.2. Suction.....	48
4.2.1. Total Suction .....	49
4.2.2. Total Suction Measurements .....	51
4.2.3. Matric Suction Measurements .....	52
4.3. Evaporation Method .....	55
4.3.1. Tensiometer Use on Wet End in a Soil Drying from Saturation .....	57
4.4. Principle of the Extension of the Measurements.....	58
4.5. Material and Methods.....	58
4.5.1. Evaporation Method According to Schindler.....	59
4.5.2. Discrete Data for Retention and Conductivity Relation.....	63
4.6. Retention and Conductivity Functions .....	64
4.6.1. Van Genuchten/Mualem Model .....	65
4.6.2. The Bimodal Van Genuchten/Mualem Model .....	65
4.6.3. The Brooks and Corey Model .....	66
CHAPTER 5. LABORATORY TESTS ON WATER INFILTRATION INTO UNSATURATED FINE GRAINED SOIL SLOPES .....	67
5.1. Introduction .....	67
5.2. Soil Container.....	68
5.2.1. Artificial Rainfall System.....	70
5.2.2. Infiltration Bands and the Discharge System .....	72
5.3. 2-D Infiltration Study Experiments .....	74

5.3.1. Previously Conducted 2-D Experiments .....	74
5.4. 1-D Infiltration Study Experiments .....	79
5.4.1. Materials and Test Procedure Used .....	79
5.4.2. 1-D Experimental Results .....	82
5.5. Conclusion on the Combined Results of 1-D and 2-D Experiments .....	84
CHAPTER 6. TESTING UNSATURATED FINE GRAINED SOIL FOR ITS HYDRAULIC PROPERTIES .....	86
6.1. Introduction: Review of Suction and Hydraulic Conductivity Measurements in Unsaturated Soils .....	86
6.2. Hyprop Testing Technique for Unsaturated Soil's Water Retention and Hydraulic Conductivity Properties .....	87
6.2.1. Sample Preparation .....	87
6.3. Hyprop Testing Theory Using the Evaporation Method .....	89
6.3.1. Discrete Data for Retention and Conductivity Relation .....	90
6.3.2. Water Retention and Hydraulic Conductivity Functions .....	91
6.3.3. Optimization of the Parameters .....	92
6.4. Testing Materials and Laboratory Tests on the Samples .....	92
6.5. Hyprop Test Results .....	94
6.5.1. Matric Suction vs. Time .....	94
6.5.2. Hydraulic Conductivity vs. Matric Suction .....	97
6.5.3. Volumetric Water Content vs. Matric Suction .....	99
6.5.4. Correlations with the Hyprop Test Results .....	102
6.6. Calibration of the Hyprop Tensiometers .....	109
6.7. Discussion of the Results .....	110
CHAPTER 7. CONCLUSIONS .....	112
7.1. Conclusion with Tests on Unsaturated Soil's Infiltration Theories .....	112
7.2. Conclusions with Tests on Unsaturated Soil's Hydraulic Properties .....	113

7.3. Significance of this Research for Use in Geotechnical Engineering Practice.....	114
7.4. Suggestions for Future Research.....	114
REFERENCES .....	116

# LIST OF FIGURES

<b><u>Figure</u></b>	<b><u>Page</u></b>
Figure 2.1. Anatomy of a Shallow Landslides.....	8
Figure 2.2. Places of Unsaturated and Saturated Soil Zones .....	10
Figure 2.3. Mohr-Coulomb Failure Envelope Criterion Model.....	14
Figure 2.4. Mohr-Coulomb Failure Surface for an Unsaturated Soil .....	16
Figure 2.5. Development of Wetting Front.....	18
Figure 2.6 Schematics of moisture and pressure redistribution with respect to the amount of initial application: (a) hysteresis effects, (b) $L < S$ , (c) $L > S$ , (d) water blob at the front. ....	19
Figure 3.1. Particle Size Distribution Graph of CL-ML soil used in this study .....	24
Figure 3.2. Hydrometer Tests Performed in this study.....	25
Figure 3.3. Illustration of Laser Diffraction Test Method .....	27
Figure 3.4. Typical Test Graph of the LDM Equipment used.....	27
Figure 3.5. Casagrande Apparatus used for the Multi-Point Liquid Limit Test.....	29
Figure 3.6. Liquid Limit Test Plot of the CL-ML Soil .....	29
Figure 3.7. The Plastic Limit (PL) Test Equipment .....	30
Figure.3.8. The Unified Soil Classification System (USCS)'s Plasticity Chart.....	30
Figure 3.9. Specific Gravity Test Equipment .....	31
Figure 3.10. Standard Proctor Compaction Test.....	33
Figure 3.11. Result of Standard Proctor Test of the CL-ML soil conducted in this study	33
Figure 3.12. Direct Shear Test (DST) concept .....	35
Figure 3.13. Direct Shear Test Results of the 100% SP Soil Sample at the Relative Compaction of 45 %.....	36
Figure 3.14. Direct Shear Test Results of the 100% SP Soil Sample at the Relative Compaction of 90 %.....	36
Figure 3.15. Direct Shear Test Results of the (%25 CL - ML+%75 SP) Soil Sample at the Relative Compaction of 45 %.....	37
Figure 3.16. Direct Shear Test Results of the (%25 CL - ML+%75 SP) Soil Sample at the Relative Compaction of 90 %.....	37
Figure 3.17. Direct Shear Test Results of the (%50 CL - ML+%50 SP) Soil Sample at the Relative Compaction of 45 %.....	38

Figure 3.18. Direct Shear Test Results of the 100 % CL-ML Soil Sample at the Relative Compaction of 90 %.....	38
Figure 3.19. Direct Shear Test Results of the (%50 CL - ML+%50 SP) Soil Sample at the Relative Compaction of 90 %.....	39
Figure 3.20. Automatic Static-Direct Shear Test Set-up Used.....	39
Figure 3.21. Automatic (Static) Triaxial CU-Test set-up used by (Courtesy of Ege University-CED-Geotechnical laboratory).....	41
Figure 3.22. (Static) Triaxial CU-Test results of the CL-ML Soil Used (Courtesy of Ege University-CED-Geotechnical laboratory).....	42
Figure 3.23. Falling Head and Constant Head Permeability Test-Equipment.....	44
Figure 4.1 A Typical Soil-Water Characteristic (SWC) Curve .....	47
Figure 4.2. Typical Water-Retention Curve of Some Soils.....	48
Figure 4.3. Osmotic Suction Illustration.....	51
Figure 4.4. Tension Dynamics during Evaporation (left) and Interpolation to Air-Entry Pressure (right) for Clay Soil .....	58
Figure 4.5. Refilling Window View of Hyprop Test.....	61
Figure 4.6. Assembly of the Tensiometer.....	61
Figure 4.7. Soil Sample with Two Shaft Holes .....	62
Figure 4.8. The Schematic Illustration of Hyprop Measurement Device.....	62
Figure 5.1. Sloped Soil Container View during the Previous Slope Stability Study.....	68
Figure 5.2. Top View of the Soil Container's Bottom.....	69
Figure 5.3. General View of the Test Set-Up with Horizontal Empty Soil Container .....	70
Figure 5.4. Lateral View of the Water Storage Tank.....	71
Figure 5.5. Water Pump, Rainfall Hoses and Main Water Valves .....	71
Figure 5.6. Filled Soil Container and Placed-in Tensiometers to Measure Soil-Suction ..	73
Figure 5.7. Another View of The Filled Soil Container and Placed-in Tensiometers.....	73
Figure 5.8. Discharge Water Collection Bin Under the Soil Container .....	74
Figure 5.9. Infiltration (wetting band) Depth Measurement after the Experiment.....	75
Figure 5.10. Thin-Walled Soil Sampler Used to Obtain Undisturbed Soil Samples after Rainfall .....	78
Figure 5.11. 1-D Test Equipment .....	80
Figure 5.12. Artificial Rainfall Supplier.....	80
Figure 5.13. To Assembly a Tensiometer in 1-D Test Set-Up .....	81

Figure 5.14. Parts of the Used Tensiometers (model:T5-2100F) .....	81
Figure 5.15. 1-D Experiments - Soil Compaction via 2 kg Weight/10cm Soil Layer .....	82
Figure 6.1. Dish with Water and Sample during the Initial Saturation Process. ....	88
Figure 6.2. Assembling the Hyprop's Sensor Unit with the Sampler Ring .....	88
Figure 6.3. Test Set-up of the HYPROP Equipment .....	89
Figure 6.4. Experimental Sets-up of the Hyprop Tests.....	92
Figure 6.5. A Hyprop Test is in Progress .....	92
Figure 6.6. Particle Size Distributions of 3 Undisturbed Soil Samples .....	93
Figure 6.7. Variation of Matric Suction with Time for the ML Soil Sample .....	95
Figure 6.8. Variation of Matric Suction with Time for the CH Soil Sample.....	95
Figure 6.9. Variation of Matric Suction with Time for the OL Soil Sample .....	96
Figure 6.10. Variation of Matric Suction with Time of 3 Soil Samples used .....	96
Figure 6.11. Variation of Hydraulic Conductivity with Matric Suction for the ML Soil Sample .....	97
Figure 6.12. Variation of Hydraulic Conductivity with Matric Suction for the CH Soil Sample .....	98
Figure 6.13. Variation of Hydraulic Conductivity with Matric Suction for the OL Soil Sample.....	98
Figure 6.14. Variation of Hydraulic Conductivity with Matric Suction of 3 Soil Samples Used .....	99
Figure 6.15. Variation of Volumetric Water Content with Matric Suction for the ML Soil Sample.....	100
Figure 6.16. Variation of Volumetric Water Content with Matric Suction for the CH Soil Sample.....	101
Figure 6.17. Variation of Volumetric Water Content with Matric Suction for the OL Soil Sample.....	101
Figure 6.18. 3 Undisturbed Soils Water-Retention (WRC) Tests Results by Using HYPROP .....	102
Figure 6.19. Variation of Plasticity Index against Time to Reach the Maximum Matric Suction .....	103
Figure 6.20. Variation of Colloid Content against Time to Reach the Maximum Matric Suction .....	104
Figure 6.21. Variation of Plasticity Index against the Maximum Matric Suction.....	105

Figure 6.22. Variation of Colloid Content against the Maximum Matric Suction .....	106
Figure 6.23. Variation of Hydraulic Conductivities at the Max.Matric Suction against the Maximum Matric Suction.....	107
Figure 6.24. Variation of Hydraulic Conductivity at the Maximum Matric Suction against the PI .....	108
Figure 6.25. Variation of Hydraulic Conductivity at the Maximum Matric Suction point against the Colloid Content .....	109
Figure 6.26. Calibration Plot of the Hyprop Tensiometers.....	109

# LIST OF TABLES

<b><u>Table</u></b>	<b><u>Page</u></b>
Table 3.1. Summary of DST Results .....	40
Table 3.2. Range of Permeability for Various Soils .....	43
Table 3.3. Results of Falling and Constant Head Permeability Tests conducted during this Study .....	45
Table 5.1. Basic Data of the Previously Performed 12 Tests .....	75
Table 5.2. Detailed Data of the Previously Performed 12 Tests .....	76
Table 5.3. Previously Conducted 12 Test Results (*) with Initial-Final Conditions and Comparison of .....	77
Table 5.4. Summary of the 2-D additional tests conducted with initial, final conditions and comparison of observed wetting band depths ( $h_{\text{observed}}$ ) against ( $h_{\text{p-R}}$ ) and $h_{\text{lumb}}$ values. ....	79
Table 5.5. Summary of the 1-D Tests and comparison of average observed wetting band depths ( $h_{\text{observed}}$ ) vs. results obtained from the Prade-Raad, 1993 ( $h_{\text{p-R}}$ ) and Lumb's, 1975 ( $h_{\text{lumb}}$ ) Equations. ....	83
Table 6.1. Comparing the laboratory test results of the 3 undisturbed soil samples .....	93

# CHAPTER 1

## INTRODUCTION

### 1.1. General

A slope is a ground surface that stands at an angle to the horizontal plane. Slopes may be natural or man-made. Each slope possesses unique soil characteristics and geometric features, which may resist gravity or collapse. Slope failure causes soil mass to slide downward and outward, occurring either slowly or suddenly. Slides usually begin from hairline tension cracks, which propagate through the soil layers (Das 1994).

Slope stability problems are among the most commonly encountered problems in geotechnical engineering. Due to practical importance of the subject of slope stability, assessing stability of a natural or man-made slope has received wide attention across the geotechnical community for long decades. The first question should be why a natural slope moves suddenly after long period of its existence. Rainfall effect is one of the most effective factors in this question. Slope failure has a close relationship with rainfall. Numerous natural events have shown that climatic and geomorphic conditions trigger slope failures. In post-failure investigations, parameters that affect slope stability can be found. These are physical properties of the failed slope, effect of the slope angle, moisture content, pore water pressure variation, mechanism of the debris avalanche movement and properties of the resulting deposits (Fisher 1971, Hutchinson and Bhandari 1971, Scott 1972, Williams and Guy 1973, Swanston 1974, Campbell 1975, Hollingsworth and Kovacs 1981, Istok and Harward 1983).

Landslides usually occur during or after wet periods. If said in a different way; slope failures are induced by rainfall infiltration. Field studies on the effect of rainfall infiltration on slope instability have been carried out by many researchers (Brand, et al. 1984, Johnson and Sitar 1990, Affendi and Faisal 1994, Lim, et al. 1996, Gasmu, et al. 1999, Zhang, et al. 2000, Rahardjo, et al. 2003).

In addition to the field studies, many researchers conducted numerical studies to show the effect of rainfall infiltration on the stability of a slope (Fredlund and Rahardjo,

1993; Alonso, et al. 1995; Ng, et al. 1999; Fourie, et al. 1999; Leong, et al. 1999; Gasmu, et al. 2000).

During any rainfall period, negative pore water pressures in an unsaturated soil slope can be gradually reduced by rainfall infiltration. As a result, positive effect of negative pore water pressure to soil strength decreases with time. This process may cause instability to soil slope. Numerous researchers (Lumb, 1962; Ng and Shi, 1998; Sun, et al., 1998; Gasmu, et al., 2000; Tsaparas, et al., 2002; Collins and Znidarcic, 2004) have studied infiltration affecting soil slope stability during a rainfall event.

Tarantino and Bosco (2000) have proposed that rainfall intensity and duration plays an important role on extend and manner of slope failure. A particular slope may be subjected to negative and positive pore water pressures, whose values are subject to change during any rainfall infiltration. Most shallow landslides occur, due to rainfalls infiltration.

According to Haan et al. (1994), a wet soil profile usually has low infiltration rate compared to a dry soil profile. Seepage is one of the most crucial factors to trigger slope instability in the soil mass (Cruden, 1991).

## **1.2. Scope of Study**

Primarily objective of this study is to observe, compare and determine validity of theoretically derived equations against observations made in laboratory also to develop better modeling and mechanisms for shallow landslides and slope failures in fine-grained low plastic soils. Another special objective of this study is to determine various unsaturated soils' hydraulic properties by using a new laboratory testing method with the HYPROP equipment. It provides an easy, cost-effective and continuous measurements of various unsaturated fine soil's (which is near saturation and whose water content is wetter than the optimum) hydraulic properties for the low suction range of 0-100 kPa, using the evaporation procedure. Hence, this thesis covers the following stages;

- Searching and reviewing existing literature on shallow landslides and slope instability analyses and factors causing them.
- Comparing different cause-factors (soil types, rainfall intensity, amount of colloids content etc.) and using equations, methods to

understand/explain mechanism of rainfall infiltrated landslides and slope failures.

- Study of rainfall infiltration and its effect on the instability process,
- Comparing and applying rainfall infiltration and slope stability theories by Pradel-Raad (1993) and Lumb (1975) in İYTE developed two-dimensional (2-D) and one-dimensional (1-D) test models.
- Determining various unsaturated soils' hydraulic properties (i.e. variations of water-retention and hydraulic conductivity functions) against different parameters of various unsaturated soils near saturation by using a newly developed laboratory testing set-up with the HYPROP equipment using evaporation procedure, which is a recent equipment and standard method (ASTM D3404-91 (2013)) to find water retention and hydraulic properties of soils.
- Comparing and commenting on the test results, making observations, discussions and reaching conclusions.

### **1.3. Organization of the Thesis**

This thesis consists of seven chapters. The contents of each chapter are summarized as below;

Chapter 1 gives a brief introduction and contains general themes for the organization of the thesis with brief objectives and an overview of the laboratory tests conducted.

Chapter 2 focuses on the literature review on rainfall infiltration theories affecting slope stability. Background information of two wetting-band theories given by Lumb (1975) and Pradel-Raad (1993) equations are studied.

Chapter 3 Basic engineering properties of SP and CL-ML soils are used in this study per ASTM standards.

Chapter 4 summarizes a brief literature review for determining hydraulic properties of soils. In addition influences of suction capacity to slope stability is studied. It also gives details on how to calculate soil suction in various ways, together with their advantages and disadvantages. Detailed explanations of water-retention and hydraulic

conductivity functions, as expressed by the three theories (Van-Genuchten/Mualem, The bimodal Van Genuchten/Mualem and Brooks-Corey models) are provided, in order to select one for the HYPROP tests to be conducted later.

Chapter 5 gives laboratory tests on saturated slope stability and our conclusions about the validity of Lumb (1975) and Pradel-Radd (1993) theories against the observation made during the previously conducted 12 numbers of 2-D tests and 3 numbers of newly conducted 2-D tests. Laboratory tests also include total of 32 numbers of 1-D tests. Results are summarized in tables, discussions and conclusions are provided.

Chapter 6 contains laboratory tests on various unsaturated soils hydraulic property (water-retention and hydraulic conductivity) tests with the Hyprop equipment using the evaporation procedure. As three USCS types of soils (ML, OL, CH) are used in the Hyprop tests, effects of various soil parameters in the variations of unsaturated soils' hydraulic properties are studied in graphical forms and discussions are provided.

Chapter 7 presents conclusions for the tests done in both chapters 5 and 6.

## CHAPTER 2

# LITERATURE REVIEW ON RAINFALL INFILTRATION PARAMETERS AFFECTING SLOPE STABILITY

### 2.1. Introduction

Several studies have been performed in recent years with numerical analyses to investigate the effect of rainfall infiltration on slope stability. (Haefeli, 1948, Brakensiek, 1977, Fredlund and Rahardjo 1993, Pradel, D. and Raad, G.1993, Fredlund, Xing and Huang 1994, Alonso, et al.1996, Cheng, P.F.K. 1997, Ng and Shi 1998, Ng, et al.1999, Fourier, et al. 1999, Gasmol, et al. 2000). These studies have investigated the effect of soil properties, such as; slope angles, pore water pressure, mechanism of debris flow and rainfall intensity on slope stability. Infiltration increases pore water pressure and causes stress change, which may result in soil swelling. Thus swelling can occur as a result of rainfall infiltration. (Pierson 1980, Premchitt, et al. 1994, Wilson and Dietrich 1987, Iverson and Major 1986, Iverson 2000, Lan, et al. 2003, Chen 1996 & 1997, Du 1991, Xie and Xu 1999, Li, et al. 2001, Huang and Lin 2002).

### 2.2. Infiltration

Infiltration refers to the movement of water into the soil layer. Rate of this movement is called infiltration rate. If rainfall intensity is less than infiltration rate (IR), water will be able to pass into the subsoil. Otherwise, if the rainfall intensity is greater than infiltration rate (IR), water will be accumulated on the surface and surface runoff may result. If the soil surface is undulated or has a slope, water may fill depressions immediately, if rainfall intensity exceed the infiltration capacity. High infiltration reduces runoff and increases recharge. Low infiltration increases runoff, causes erosion and decreases recharge. Rainfall water quantity is equal to sum of surface runoff, recharge (or infiltrated) water and evaporated water.

### **2.2.1. Factors Affecting Infiltration**

A number of factors affect soil infiltration. Some of these factors are; texture of soil, composition and initial water (moisture) content and degree of saturation of soil, surface properties (frozen or covered or not), plasticity, cohesion, compaction and pore size, stratigraphy (presence of impermeable layer within soil) also affect infiltration rate. For example wet soil profile has low infiltration rate than drier one (Haan, et al. 1994). Additionally, coarse grained soils with bigger pore sizes can have more infiltration rate than fine grained soils. Soils that have many large surface connected pores have higher intake rates than soils that have few such pores. In contrast; a compacted soils or an impervious layer close to the surface restricts the entry of water into the soil and tends to cause ponding on the surface.

An increased amount of plant material-dead or alive (organic matter), generally assists the process of infiltration. Organic matter increases entry of water by protecting soil aggregates from breaking down during rainfall. Particles broken from aggregates may clog pores and seal the surface and decrease infiltration during a rainfall.

Another important parameter is climate factor, which can be divided into 5 distinct parts. These are; precipitation type, rainfall intensity, rainfall duration, rainfall distribution, temperature, and soil surface is frozen or not (Skaggs, 1980). High intensity rainfall may also form an impermeable soil surface (seal) layer, which has low infiltration. Though low intensity rainfall does not cause such a result, but if short duration rainfall is connected with high rainfall intensity, this may yield to surface sealing and low infiltration. The longer the duration rainfall with low infiltration rate is more soil swelling may occur (Schwab et al. 1993).

### **2.3. Influence of Seepage on Slope Instability**

Seepage is one of the crucial factors to trigger slope instability in the soil mass. Slope instability may cause landslides. A mass of rock, debris or earth moving as a mass down a slope is defined as a landslide (Cruden 1991). Landslides are one of the major natural disasters, which cause significant property damages and deaths each year. We can group the factors to trigger landslides as follows;

1. Change of soil's stress conditions,
2. A decrease of soil's material strength

Change of soil's stress conditions defines that; removal of lateral and underlying support (erosion, previous slides, road cuts, quarry cuts), increase of load (weight of rain/snow, fills, vegetation), increase of lateral pressure (hydraulic pressures, roots, crystallization, swelling of clay), transitory stress (earthquakes, vibrations of trucks, machinery, blasting), regional movements (tilting), geological movements etc.

Decrease of material strength defines that; factors related to weathering, change in state of consistency, changes in inter-granular forces (in pore water pressure, in solution-chemically), changes in structure (strength decrease in failure plane, fracturing, due to unloading) etc.

Before a slope fails, the driving forces are equal to the resisting forces. Seepage is one of the main driving forces for a slope. To decrease a seepage hazard, drainage path of seepage should be provided. Following methods are for reduction of seepage;

- Horizontal drains (if failure is a deep-seated one)
- Cut-off trenches (if failure is shallow one)

Horizontal drains are placed into the soil mass horizontally from the slope surface and seepage force reduced vertically down. Cut-off trenches are typically placed to be parallel to the top (crest) of a slope to remove seepage from the slope, if the water table can be intercepted before groundwater reaches the slope. If the water table cannot be intercepted before the slope crest, longitudinal trenches parallel to each other on the slope and in the direction of maximum slope inclination can be used (Stanic 1984).

## **2.4. Rainfall Infiltration and Shallow Landslides**

Rainfall raises groundwater level. Also rainfall decreases matric suctions (negative pore water pressure), which may cause slope failure. Shallow landslides are one of the most common types of landslides, occurring frequently in nature (Kirkby 1987, Benda and Cundy 1990, Selby 1993).

Landslides triggered on forested slopes may discharge such energy to cause debris flow. This flow erodes the unstable material in its path and continues to move

downslope until the movement causing force falls below the one needed to maintain the flow (Burton and Bathurst, 1998).

In order to study the subject of rainfall-induced landslides within slope erosion processes over the long term, it is important to know the spatial distribution of possible landslide initiation sites and characterization of erosion-deposition patterns caused by slope failure. Removal of failed landslide material can potentially increase the local slope's weight and may trigger another slope failure. Once a debris flow emerges, the problem of determining its path becomes complicated by the ability of the flow to erode, to spread, to plug and to alter its direction. The rate of volume transport of a debris flow and its change with time, viscosity and hill-slope morphology are some important factors for debris flow erosion and deposition. (Figure 2.1)

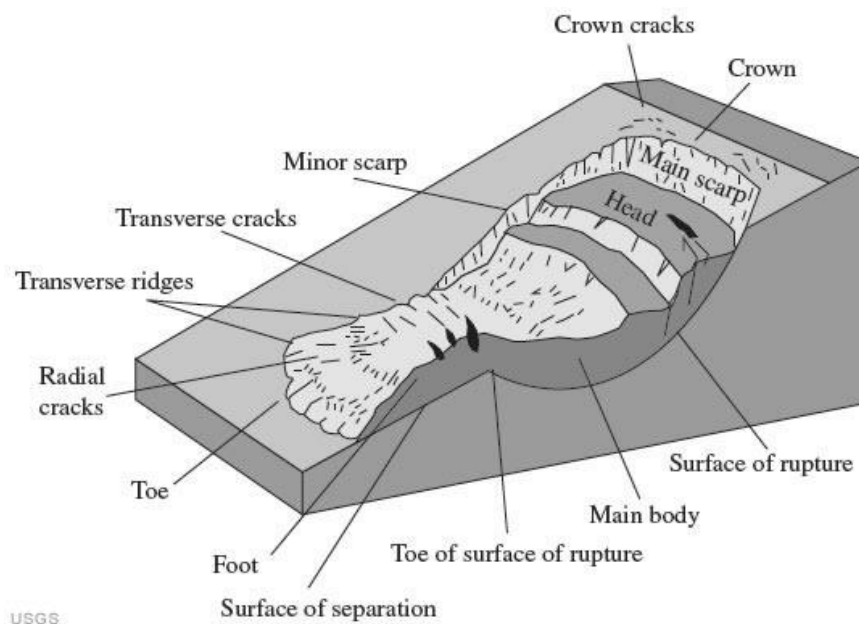


Figure 2.1. Anatomy of Shallow Landslides  
(Source: USGS)

## 2.5. Uncertainties with Slope Stability under Rainfall Conditions

Several uncertainties exist with the stability of slopes affected by rainfall infiltration. Firstly, soil properties that can cause instability of a slope exhibit considerable variation from point to point. Soil properties, such as; soil permeability

varies with time, because of change of pore water pressure and stress. Secondly, estimation of soil properties by laboratory tests or by empirical models may cause some errors. Thirdly, prediction model for slope stability analysis may cause some errors. These errors can affect the results of slope stability prediction. The intensity, duration and pattern of rainstorm are not exactly known. The initial pore water pressures cannot be measured reliably at each and every point in the slope. Soils are geological materials shaped by weathering conditions, transported by physical means to their present locations. They have been subjected to various stresses, physical and chemical changes. Consequently, soil properties may show differences from place to place.

## **2.6. Definition of Saturated and Unsaturated Soils**

A soil sample consists of 3 materials in 3 phases. These phases are; solid matter, air and water. If a soil sample is subjected to rainwater for a certain time, voids (pores) can be filled with water. If all pores are filled with water (no air is present in voids), such soils reach their maximum water contents and are named saturated soils. The same process also occurs, even if the soil is under the groundwater table (GWT). In this condition, the degree of saturation ( $S_r$ ) is equal to one and the soil is classified as ‘saturated soil’. Slope stability problems in saturated can be analyzed using the effective stress equation (Equation 2.2), requiring pore water pressure value ( $u_w$ ) to use.

The terms ‘partly saturated’ or ‘partially saturated’ should not be used, but the term unsaturated should be used. This refers to a condition, where the voids in the soil are filled by both air and water, even if the soil is not directly subjected to the groundwater table action. This event may occur, even if soils are located above the groundwater level. Figure 2.2 shows places of unsaturated ( $S \neq 1$ ) and saturated ( $S = 1$ ) soil zones.

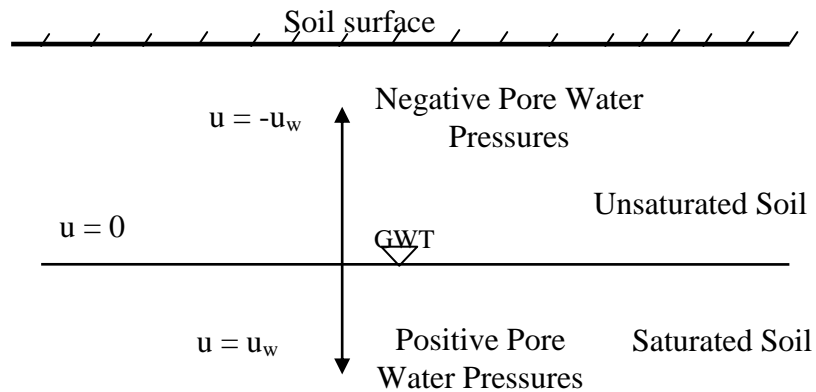


Figure 2.2. Places of Unsaturated and Saturated Soil Zones

## 2.6.1. Shear Strength Characteristics of Saturated and Unsaturated Soils

In saturated soils, all the measurable effects of a change of stress, such as compression, distortion, shearing resistance and volume change are exclusively due to changes in effective stress. Every investigation of the stability of a saturated body of earth requires the knowledge of both the total and water pressures. In this thesis geotechnical instability circumstances are investigated, especially to include shallow landslides occurring in the fine grained soils.

In unsaturated soils, the stress-state of soil consists of two stress-state variables which are effective normal stress  $(\sigma - u_a)$  and matric suction,  $(u_a - u_w)$ .  $\sigma$  is normal stress of soils,  $u_a$  is air pore pressure and  $u_w$  pore water pressure.

### 2.6.1.1. Shear Strength Equation for Saturated Soils

In saturated soils, effective stress principle influences soil's shear strength;

$$\sigma' = \sigma - u_w \quad (2.1)$$

Where;  $\sigma'$  is effective stress,  $\sigma$  is normal stress; Then, shear strength ( $\tau$ ) of a saturated cohesive soil can be defined by the Mohr-Coulomb failure criterion using the effective stress principle as in (D.G. Fredlund, N.R. Morgenstern, R.A. Widger, 1978);

$$\tau = c' + (\sigma - u_w) \times \tan \phi' \quad (2.2)$$

Where;  $\tau$  is the shear strength,  $\sigma$  is the normal stress,  $c'$  is the effective cohesion intercept of the failure envelope with the  $\tau$  axis, and  $\phi'$  is called the angle of internal friction. In literature; there are some failure criterion methods (i.e. Mohr-Coulomb, 1776, Tresca, H. 1864; Von Mises, R. 1913; Griffith, 1924; Drucker, D.C. 1949; Drucker, D. C. and Prager, W. 1952 Hoek, E. and Brown, E.T, 1980; Deshpande, V.S. and Fleck, N.A. 2001; Cazacu, O. and Barlat, F. 2001 etc.). These are also failure criterion applicable to plastic failure showing materials like fat saturated clay, soft metals etc. The Drucker-Prager (1952) yield criterion is one of plastic failure model showing/behaving materials failure criterion (e.g. saturated fat clays) and is a kind of pressure dependent for determining whether a material has failed or undergone plastic yielding. The criterion was introduced to deal with the plastic deformation of soils like highly plastic saturated clays yielding by bulging only under large strains, but without showing any shear plane type failure. So it has limited applications, though its many variations have been applied to some rocks, polymers and other pressure dependent materials. The Drucker-Prager yield criterion has the form;

$$\sqrt{J_2} = A + BI_1 \quad (2.3)$$

Where;  $I_1$  is the first invariant,  $J_2$  is the second invariant of the deviatoric part of the Cauchy stress. The constants A, B are determined from experiments.

Also; the Drucker-Prager criterion should not be confused with the earlier Drucker criterion which is independent of the pressure ( $I_1$ ). The Drucker yield criterion has the form;

$$f := j_2^3 - \alpha \times J_3^2 - k^2 \leq 0 \quad (2.4)$$

Where;  $J_2$  is the second invariant of the deviatoric stress,  $J_3$  is the third invariant of the deviatoric stress,  $\alpha$  is a constant that lies between  $-27/8$  and  $9/4$  (for the yield surface to be convex),  $k$  is a constant that varies with the value of  $\alpha$ .

Deshpande-Fleck (2001) yield criterion for foams has the form given in above equation. The parameters  $\alpha$ ,  $b$ ,  $c$  for the Deshpande-Fleck criterion is;

$$\alpha = (1 + \beta^2)\sigma_y^2, \quad b=0, \quad c=-\beta^2/3 \quad (2.5)$$

Where;  $\beta$  is a parameter that determines the shape of the yield surface and  $\sigma_y$  is the yield stress in tension or compression.

For thin sheet metals, the state of stress can be approximated as plane stress. In that case the Cazacu-Barlat (2001) yield criterion reduces to its two dimensional version with parameters. The William-Warnke (1975) yield criterion is a function that is used to predict when failure will occur in concrete and other cohesive frictional materials such as rock, soil and ceramics. This yield criterion has the functional form;

$$f(I_1, J_2, J_3) = 0 \quad (2.6)$$

Where;  $I_1$  is the first invariant of the Cauchy stress tensor and  $J_2, J_3$  are the second and third invariants of the deviatoric part of the Cauchy stress tensor. There are three material parameters ( $\sigma_c$  is the uniaxial compressive strength,  $\sigma_t$  is the uniaxial tensile strength,  $\sigma_b$  is the equibiaxial compressive strength) that have to be determined before the William-Warnke yield criterion may be applied to predict failure. In terms of  $I_1, J_2, J_3$  the William-Warnke yield criterion can be expressed as;

$$f := \sqrt{J_2} + \lambda(J_2, J_3) \left( \frac{I_1}{3} - B \right) = 0 \quad (2.7)$$

Where;  $\lambda$  is a function that depends on  $J_2, J_3$  and the three material parameters and  $B$  depends only on the material parameters. The function  $\lambda$  can be interpreted as the friction angle which depends on the Lode angle ( $\theta$ ). The quantity  $B$  is interpreted as a cohesion pressure. The William-Warnke (1975) yield criterion may therefore be viewed as a combination of the Mohr-Coulomb and the Drucker-Prager (1952) yield criteria.

Another yield criterion is Von Mises (1913) that suggests that the yielding of materials begins when the second deviatoric stress invariant  $J_2$  reaches a critical value. For this reason, it is sometimes called the  $J_{2\text{-plasticity}}$  or  $J_{2\text{flow}}$  theory. In material science and engineering the Von Mises (1913) yield criterion can be also formulated in terms of the Von Mises stress or equivalent tensile stress,  $\sigma_v$  a scalar stress value that can be computed from the Cauchy stress tensor. Mathematically the Von Mises yield criterion is expressed as;

$$J_2 = k^2 \quad (2.8)$$

Where;  $k$  is the yield stress of the material in pure shear. The magnitude of the shear yield stress in pure shear is  $\sqrt{3}$  times lower than the tensile yield stress in case of simple tension. Thus, we have:

$$k = \frac{\sigma_y}{\sqrt{3}} \quad (2.9)$$

One of the yield criterion methods is Tresca (1864) yield criterion which is also known as the maximum shear stress theory (MSST) and the Tresca-Guest (TG) criterion. In terms of the principal stresses the Tresca criterion is expressed as;

$$\frac{1}{2} \max\left(|\sigma_1 - \sigma_2|, |\sigma_2 - \sigma_3|, |\sigma_3 - \sigma_1|\right) = S_{sy} = \frac{1}{2} S_y \quad (2.10)$$

Where;  $S_{sy}$  is the yield strength in shear and  $S_y$  is the tensile yield strength.

In 1993, Hill proposed another yield criterion for plane stress problems with planary anisotropy. The Hill criterion form is;

$$\left(\frac{\sigma_1}{\sigma_0}\right)^2 + \left(\frac{\sigma_2}{\sigma_{90}}\right)^2 + \left[(p+q-c) - \frac{p \times \sigma_1 + q \times \sigma_2}{\sigma_b}\right] \left(\frac{\sigma_1 \times \sigma_2}{\sigma_0 \times \sigma_{90}}\right) = 1 \quad (2.11)$$

The most widely used criterion for soils is the Mohr-Coulomb failure criterion, which is an empirical criterion, and represents the linear envelope that is obtained from

a plot of the shear strength of a material versus the applied normal stress. Figure 2.3 illustrates an envelope of Mohr-Coulomb model.

The effective stress concept is widely accepted and at times regarded as a law (Fredlund and Rahardjo, 1993). The effective stress concept is independent of soil properties, meaning it is applicable to all types of soils (sands, silts and clays).

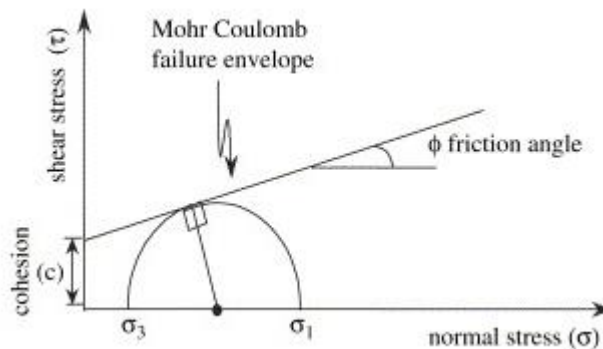


Figure 2.3. Mohr-Coulomb Failure Envelope Criterion Model  
(Source: Fredlund and Rahardjo, 1993)

### 2.6.1.2. Shear Strength Equation for Unsaturated Soils

In unsaturated soils, because of the effect of water menisci with surface tension (contractile skin), soil strength is subjected to two independent stress variables, which are; net normal stress ( $\sigma - u_a$ ) and matric suction ( $u_a - u_w$ ), (Fredlund et al., 1996). Here  $u_a$  is air pressure and  $u_w$  is pore water pressure.

Shear strength of soil is a very crucial property in geotechnical analysis and dependent of the effective stress. In classical soil mechanics, fully saturated and completely dry conditions are usually assumed in characterization of shear strength. In spite of this, almost 40% of the natural soils on the earth surface are in unsaturated state. Furthermore, unsaturated soils are also commonly encountered in civil engineering practice, such as in compaction works, construction of roads, dams and embankments.

Several failure criteria have been proposed to predict the shear strength of unsaturated soils (e.g., Alonso et al. 1990; Fredlund et al. 1996; Vanapalli et al. 1996; Sun et al. 2000; Toll and Ong 2003; Khalili et al. 2004; Tarantino 2000; Sheng et al. 2008).

Many practical problems involve assessing shear strength of unsaturated soils. Fredlund and Morgenstern (1977) have indicated that the shear strength of unsaturated soils can be described by any two of three stress state variables, namely,  $(\sigma - u_a)$ ,  $(\sigma - u_w)$ , and  $(u_a - u_w)$ , where  $u_a$  is the pore-air pressure;  $u_w$  is pore water pressure and  $\sigma$  is total stress. Fredlund et al. (1978) suggested the following equation to estimate the shear strength of unsaturated soils.

$$\tau = c' + (\sigma - u_a) \times \tan \phi' + (u_a - u_w) \times \tan \phi^b \quad (2.12)$$

The shear strength equation for an unsaturated soil (N.R. Morgenstern and R.A. Widger, 1978) is an extension of the saturated case where;

$\phi^b$  = angle indicating the rate of increase in shear strength relative to a change in matric suction,  $(u_a - u_w)$ , when using  $(\sigma_n - u_a)$  and  $(u_a - u_w)$  as the two state variables, and

$\phi'$  = angle indicating the rate of increase in shear strength with respect to the net normal stress,  $(\sigma_n - u_w)$  when using  $(\sigma_n - u_w)$  and  $(u_a - u_w)$  as the two state variables.

The effects of changes in total stress and pore water pressure are handled in an independent manner in and eqn.2.13 can be written in the following form:

$$\tau = c' + (\sigma - u_a) \times \tan \theta' + (u_a - u_w) \times \beta \times \tan \theta^b \quad (2.13)$$

Where;  $\beta = \frac{\tan \phi^b}{\tan \phi'}$ ,

$\beta$ , represents the decrease in effective stress resistance as matric suction increases.

As such,  $\beta$  varies from 1 at saturation to a low value at low water content. This means that the angle  $\phi^b$  is equal to  $\phi'$  at saturation and then reduces with matric suction. The  $\theta^b$  parameter was initially assumed to be constant for a specific soil. But recent investigations have shown that;  $\phi^b$  parameter varies with matric suction levels up to the air entry value, then it is constant and is less than  $\phi'$ . The  $\tan \phi^b$  function is currently represented by a bi-linear function with the air entry value being the inflection point (Fredlund and Rahardjo 1993). Morris, et al. (1992) has recommended that  $\phi^b = \phi' - 4^\circ$ , as a global approximation for up to the air entry value. Vanapalli, et al. (1996)

has suggested value of  $\phi^b = \phi'$ . The addition of the stress-state variables are;  $(u_a - u_w)$  and the strength parameter;  $\phi^b$ . With these two stress-state variables, the Mohr-Coulomb failure envelope becomes three-dimensional as shown in Figure 2.4. The  $(u_a - u_w)$  terms defines the third orthogonal axis.

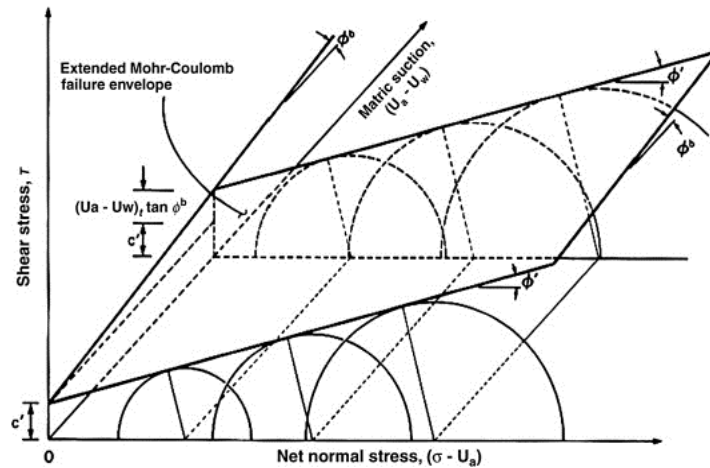


Figure 2.4. Mohr-Coulomb Failure Surface for an Unsaturated Soil  
(Source: Fredlund & Rahardjo, 1993)

## 2.7. Stages of Saturation

Unsaturated soils take place within a wide range in saturation degrees ( $S_r$ ), changing from 0 to 1. If the soil is saturated, theoretically  $S_r$  is equal to 1. Many researchers recognized that for research purposes, unsaturated soils should be divided into several stages (Wroth and Houlby 1985, Vanapalli 1994, Fredlund 1995, Fleureau, et al. 1995, Bao, et al. 1998, Cho and Santamatina 2000). The reason for the divisions is the pattern of air and water phase with respect to the form and continuity is different in each stage. The air-entry value depends on the pore size. Thus, the finer the particles are, the smaller the pore sizes and the higher is the air-entry value. Air entry generally occurs between saturation of  $S=0.9$  and  $S=1.0$ .

Changing soil boundary conditions are (e.g. changing soil suction, confining pressures etc.) shown differences at different saturation stages for unsaturated soils. Thus the research process and investigation technique may vary from one stage to another.

Unsaturated soil implies that it has a mixed fluid phase (air, water) with two percolation thresholds to be identified according to the continuity of each phase. One threshold corresponds to the formation of a continuous gas phase path. This threshold separates regimes with very different coefficients of air permeability. The other percolation threshold  $Sc$  occurs when a continuous water film forms across the particulate medium (solid particles). Electrical conduction and chemical diffusion in unsaturated media rapidly increase, when the degree of saturation exceeds  $Sc$ . Both percolation thresholds are different during drying and wetting processes. As a result, suction equalization (in terms of its value) is a distinctly slow process. Although suction in the soil is high, contribution of suction to the shear strength and stiffness are negligible, due to small portion of the wetted area. The humidity control method (rather than axis translation technique) is generally adopted for the control of suction in such soil (Liu, et al. 1993, Geiger and Durnford 2000).

## 2.8. Wetting Front and Moisture Redistribution

Wetting front and moisture redistribution are two events taking place in the saturation profile of an unsaturated soil. In the past; the wetting front approach was first developed by Green and Ampt (1911). Studies on the wetting front were continued over the years. (Lumb (1962), Bouwer (1964), Mein and Farrel (1974), Pradel and Raad (1993), Kim et al. (2006)). Some studies focused on to give a mathematical equation with explanation provide a more comprehensive explanation to the soil moisture movement, after infiltration taking place (Young, 1958, Jury, et al. 2003, Wang, et al.2003).

As illustrated in Figure 2.5, the depth of the wetting front can be related mathematically to the cumulative amount of infiltrated water,  $F$  (cm), by (Wang, et al. 2003);

$$F = Z_f (\theta_s - \theta_i) \quad (2.14)$$

Where;  $Z_f$  is wetting band thickness (cm),  $\theta_s$  (%) is the saturated moisture content and  $\theta_i$  (%) is the initial moisture content before infiltration begins.

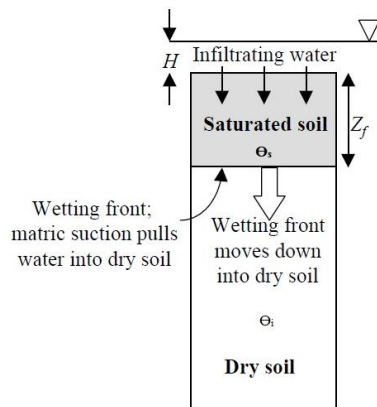


Figure 2.5. Development of Wetting Front  
(Source: Wang et al., 2003)

Wang et al. (2003) suggested that the soil below the wetting front, initially takes up moisture, following an absorption curve OA in Figure 2.6, until suction reaches the water entry value ( $W_{we}$ ) at the wetting front. Subsequently the volumetric water content increases abruptly to  $W_{we}$  (Point A) in Figure 2.6. Above the transition plane, water drains down from the soil, following a drainage curve BO in Figure 2.6. When the potential falls to the air-entry value,  $h_{ae}$  (Point C), major pores begin to empty. Hence, the difference between the water and air-entry value indicates the ability of a porous medium to hold a suspended vertical water column against gravity Figure 2.6 shows entrapment of a zone of higher water content behind the wetting front. This special moisture retention ability of a porous medium can be defined as the capillary suspension with length ( $S$ ) given by (Glass et al. (1989a);

$$S = \frac{h_{we} - h_{ae}}{\cos \beta} \quad (2.15)$$

Where;  $\beta$  is the direction (or slope) of flow with respect to gravity;  $h_{we}$  is water entry point (kPa);  $h_{ae}$  is air entry point (kPa). When  $L < S$ ,  $cm = h_{we} - h_{ae}$ , is as shown in Figure 2.6b (for  $\beta = 0$ );  $h_b$  is the matric potential at the soil surface (Point B) and  $h_a = h_{we}$  is the matric potential at the wetting front (Point A).  $L$  is the length of water infiltration. Thus, for  $L = S = h_{we} - h_{ae}$ ,  $h_b$  must be greater than the air-entry value of the soil. For  $L < S$ ,  $h_b$  must be even greater to maintain downward flow. In the early stages

following the cessation of water application,  $h_b > h_{ae}$ , the flow of water is downward and  $L$  increases. However,  $h_b$  will eventually fall to a value  $h_{ae} + (S - L)$  before  $L$  exceeds  $S$  and flow will stop, leaving the profile suspended. This situation will produce a sequence of matric potential profiles as shown Figure 2.6a. The corresponding moisture profile will be the first to form moisture redistribution as shown in Figure 2.6. When a larger amount of infiltration occurs, such that  $L > S$  (Figure 2.6); downward flow continues after water input stops, because the matric potential  $h_b$  at the surface is above the air-entry value and the matric potential head gradient across the wetted zone between the surface and the front is  $G_m = (h_{we} - h_b)/L \leq 1$ . In case, a downward flow will still occur, the surface potential is reduced below the air-entry value, because  $L > h_{we} - h_{ae}$ . Hence drainage can start from the surface. Once air enters the soil near the surface, moisture profile will trap a wetted zone of water (from Point C in the profile, where  $h = h_{ae}$  to Point A, where  $h = h_{we}$  at the wetting front). The asterisked variables indicate the maximum water content of the profile during redistribution (Peck, 1971).

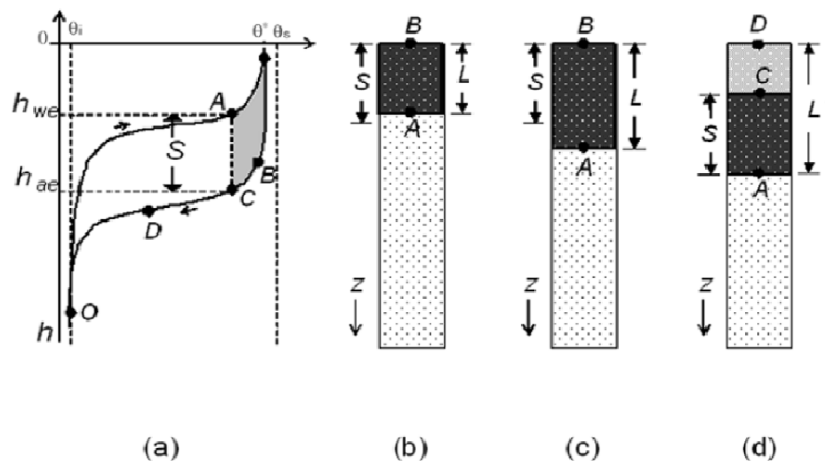


Figure 2.6 Schematics of moisture and pressure redistribution with respect to the amount of initial application: (a) hysteresis effects, (b)  $L < S$ , (c)  $L > S$ , (d) water blob at the front. (Source: Peck, 1971)

## 2.9. Wetting Band Theory by Lumb's Equation

During a steady intensity rainfall; after a few hours, soil infiltration may take place and soil stability may change. In general, soil stability is depended upon; (i) the

thickness of the saturated soil layer at the top, existing as a result of rainfall infiltration into soil and, (ii) ability (capacity) of the soil layer to drain the infiltrated rainwater. Lumb (1975) proposed the formula to predict the thickness of the water-saturated wetting band layer in time (t), caused by infiltrated rainwater amount exceeding the drain ability capacity of the soil. This has been used in addressing the issue of soil moisture and suction development in a soil mass in association with rainfall infiltration. After many field studies and observations, Lumb has derived a wetting-band equation for case of one-dimensional flow in the vertical direction as following;

$$h_w = \frac{k_s \times t}{n(S_f - S_o)} \quad (2.16)$$

Where;  $h_w$  = the depth of the unsaturated wetting front (cm)

$S_0$  = the initial degree of saturation at time t (%)

$S_f$  = the final degree of saturation at time t (%)

$k$  = the coefficient of permeability (cm/sec)

$t$  = the rainfall duration (sec)

$n$  = the porosity (no unit)

In practice; Lumb's equation is commonly used, though considers only soil permeability to water and duration of the rainfall: It does not consider rainfall intensity nor it's variability over time duration.

### **2.9.1. Wetting Band Theory by Pradel-Raad Equation**

Numerous surficial slope failures may occur at the surface of the earth's crust, during prolonged periods of heavy rains. These failures may cause enormous financial and economic damage to public and private property, including loss of lives (Campbell, 1975; Slosson-Krohn, 1979; Weber et al. 1979).

In accordance with (Build and Safety Division, County of Los Angeles, California) local codes, (e.g. Minimum Standards for Slope Stability Analysis, 1978), surficial stability is evaluated assuming the conditions of an infinite slope, where seepage into the surficial slope causing failure is more likely to occur in slopes made of

sandy or gravelly soils, rather than in those composed of clays and silts. This is supported by actual observations (Hollingsworth and Kovacs 1981).

During heavy rains, water seeps into the slope, saturating the upper layers of soil. Pore water pressures develop and reduce the shearing resistance of the soil. When the surficial soils are underlain by a more impermeable material, seepage flow parallel to the slope begins to take place (Haefeli 1948; Skempton and De Lory 1957). These conditions reduce the factor of safety of the slope and may cause surficial failures.

The minimum requirements for achieving saturation are: (1) Rainfall is intense enough to exceed the infiltration rate of the material and (2) Rainfall duration is long enough to saturate the slope up to a depth  $z_w$ .

A simple model for infiltration, based on Darcy's law, was proposed by Green and Ampt (1911). This model gives very reasonable predictions even when compared with a more rigorous approach based on unsaturated flow (Wallace 1975). A large amount of studies exist in literature on the Green-Ampt Model, for its use and capabilities. An excellent survey of studies relating to this model is contained in Brakensiek (1977). This model is based on the following assumptions: (1) The soil surface is continuously wet; (2) There is a distinct wetted front. (3) The coefficient of permeability in the wetted zone,  $k_w$ , does not change with time; and (4) There is a constant negative pressure just above the wetting front. According to Pradel-Raad model (1993), (Eqn.s 2.8 and 2.9), time necessary to saturate the soil to a depth  $z_w$  is:

$$T_w = \frac{\mu}{k_w} \left[ z_w - S \times \ln \left( \frac{S + z_w}{S} \right) \right] \quad (2.17)$$

$$k_{lim} = I_{min} \left( \frac{z_w}{z_w + S} \right) \quad (2.18)$$

Where;  $\mu$ = the wettable porosity (volume of the fillable pore space/total volume of the soil);  $z_w$ = wetting band thickness (cm);  $S$ = the wetting-front capillary suction (kPa). Also  $T_{min} = T_w$  (sec) and  $I_{min} = \text{lt/sec/m}^2$ . ;  $\theta_i = \%$

Combining the 2 equations (eqn. 2.18 and eqn. 2.19) given above;

$$k_{lim} = I_{min} \left( \frac{z_w}{z_w + S} \right) = \frac{\mu}{T_{min}} \left[ z_w - S \times \ln \left( \frac{S + z_w}{S} \right) \right] \quad (2.19)$$

Where;  $k_{lim}$  = the maximum permeability that will allow saturation to the depth  $z_w$ .

Note that the aforementioned equation does not consider the effects of runoff and evapotranspiration. Hence, soils with permeabilities well above  $k_{lim}$  may not become saturated, due to rainfall. In other words, the lower the permeability is, the higher the probability is for saturation to develop in the slope. Hence, clayey and silty materials would be more prone to develop the conditions for surficial instability, as described by Haefeli (1948) and Skempton and DeLory (1957).

Besides, various factors may affect the threshold permeability ( $k_{lim}$ ). These are; runoff quantity, evaporation and transpiration will have a significant impact on  $k_{lim}$ . In man-made slopes, there also the effects of irrigation to take into account for landscaping purposes.

Throughout the process of wetting the slope, the rainfall intensity ( $I_t$ ), is not constant and is time dependent. The intensity alters as a function of time  $t$  and may often exceed the infiltration rate of the soil,  $\theta_i$ . The excess water, ( $I_t - \theta_i$ ), will cause surface flow. During the long process of saturation, some water may actually escape the ground due to evaporation and transpiration. Such losses in soil moisture, due to evapotranspiration will depend on factors, such as; meteorological conditions, surface conditions, evaporation and transpiration from plants, though these effects can be quantified numerically (Jensen et al. 1990).

Later in this study, it will be studied that how soils with permeability greater than a certain limiting value  $k_{lim}$  may not become fully saturated and soil's saturation depth and rainfall infiltration rate could be affected by the negative pore water pressures.

Wetting-band theories are important because they are used in slope stability and landslide stability analyses.

## **CHAPTER 3**

# **DETERMINATION OF ENGINEERING PROPERTIES OF SOILS WITH LABORATORY TESTS**

### **3.1. Introduction**

For any type of soil to be used soils in civil engineering practice, the first step is to determine the engineering properties of soils. This includes laboratory testing to determine soil's physical, mechanical and chemical properties. Soil classification per the Unified Classification System (USCS) is done after performing some basic physical-property tests, including the particle size distribution and the Atterberg Limits (both liquid and plastic limits) tests. Depending on the nature of the civil engineering problem, then other required tests can be done, under either static or dynamic loading conditions.

### **3.2. Soil Classification Tests**

#### **3.2.1. Particle Size Distribution**

Soils consist of particles of various shapes and sizes. Soils' quantitative determination of the distribution of particle sizes larger than 75 micrometers (retained on the No. 200 sieve) is determined by (usually wet) sieving, while the distribution of particle sizes smaller than 76 micrometers (0.076 mm), but higher than 0.001 mm is determined, either by a sedimentation process using the hydrometer test or laser diffraction test, where the latter method has the advantage of also determining colloid range (0.001 mm > size > 0.000001 mm) particles. Figure 3.1 shows that particle distribution of the CL-ML soil used in this study.

### 3.2.1.1. Wet Sieve Analysis

This method includes a quantitative determination of the particles' size distribution in a soil upto 0.0076 mm. Application of dry sieve analysis for fine grained soils may result in wrong gradations, as for instance clay particles may lump or stick together to each other and hence cannot pass the sieve. For this reason, in practice wet sieve analysis is more preferred, compared to dry sieve analysis. At the below CL-ML (silty-clay) soils size distibution curve is shown (ASTM C 136).

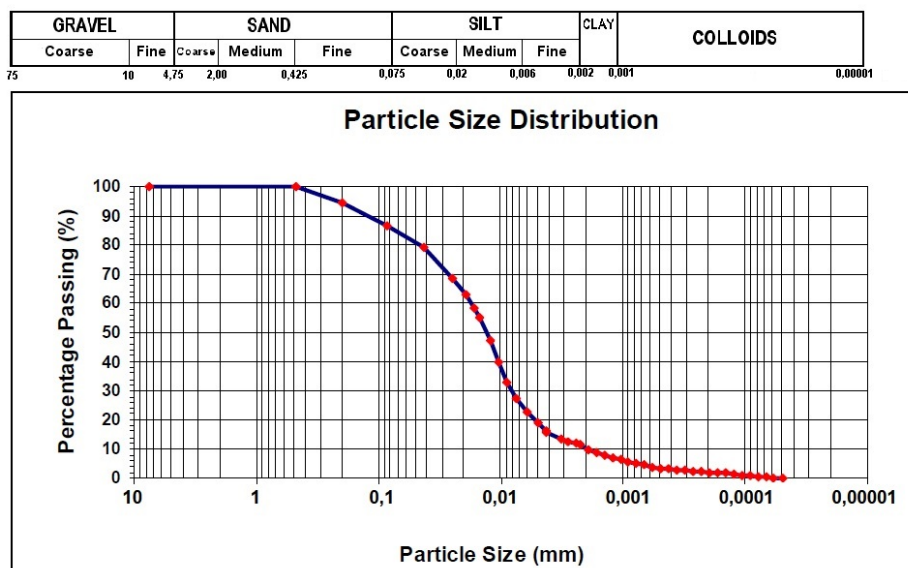


Figure 3.1. Particle Size Distribution Graph of CL-ML Soil used in this Study

### 3.2.1.2. Hydrometer Test

Hydrometer analysis is a widely used method of obtaining an estimate of the distribution of soil particle sizes between the No. 200 sieve (0.076 mm) and 0.01 mm. The data is presented on a semi-log graph, where the percent finer is plotted against the particle diameter (in mm) and may be combined with the data from the (wet) sieve analysis of the material retained on the No.200 sieve. (ASTM D422 – 63(2007)) The principal value of the hydrometer analysis appears to be obtaining the clay fraction (generally accepted as the percent finer than 0.002 mm). Figure 3.2 shows CL-ML soil type's hydrometer analysis illustration photo.



Figure 3.2. Hydrometer Tests Performed in this study

Hydrometer analysis is based on the “Stokes’ Law”, which gives the relationship among the velocity of fall of spheres in a fluid, the diameter of the sphere, specific weights of the sphere and of the fluid, and the fluid viscosity. In equation form of this relationship is;

$$v = \frac{2}{9} \times \frac{G_s - G_f}{\eta} \times \left(\frac{D}{2}\right)^2 \quad (3.1)$$

Where,  $v$  = Falling velocity of spheres (cm/sec)

$G_s$  = Specific gravity of sphere

$G_f$  = Specific gravity of (suspension) fluid (varies with temperature)

$\eta$  = Absolute or dynamic viscosity of the fluid (g/(cm\*sec))

$D$  = Diameter of the sphere (cm)

To solve for  $D$  and using the specific gravity of water,  $G_w$  in equation 3.1 gives;

$$D = \sqrt{18\eta v \div (G_s - G_w)} \quad (3.2)$$

$$V = \frac{L}{T} \quad (3.3)$$

$$A = \sqrt{18\eta \div (G_s - G_w)} \quad (3.4)$$

$$D = A\sqrt{L(cm) \div t(min)} \quad (3.5)$$

Where; size D ranges between:  $0.002 \text{ mm} \leq D \leq 0.2 \text{ mm}$

### 3.2.1.3. Laser Diffraction Method

Laser diffraction method (LDM) is modern, convenient and the most widely used method for determining the particle size distribution (ISO 13320). In LDM, a representative cloud or ensemble of particles passes through a broadened beam of laser light which scatters the incident light onto some Fourier lens as shown in Figure 3.3. Laser diffraction based particle size analysis relies on the fact that particles passing through a laser beam will scatter light beams at an angle that is directly related to their size. As the particle size decrease, the observed scattering angle increases logarithmically. Scattering intensity is also dependent on the particle size, which diminishes with increasing particle volume. Large particles will scatter light at narrow angles with high intensity, whereas small particles will scatter light at wider angles with low intensity. In this method the lens focus the scattered light onto a detector array and using an inversion algorithm, a particle size distribution is obtained from the collected diffracted light data. Sizing particles using this technique depends upon availability of an accurate, reproducible, high resolution light scatter measurements to ensure full characterization of the sample for a particle size distribution to be made.

Laser diffraction is a non-destructive, non-invasive method that can be used for either dry or wet samples. As it derives particle size data using some fundamental scientific principles, there is no need for external calibration, in addition to a wide dynamic measuring range with particles in the size range of 0.02 to 2000 microns. (Figure 3.4) (Source: [www.chemie.de/articles/e/61205](http://www.chemie.de/articles/e/61205)).

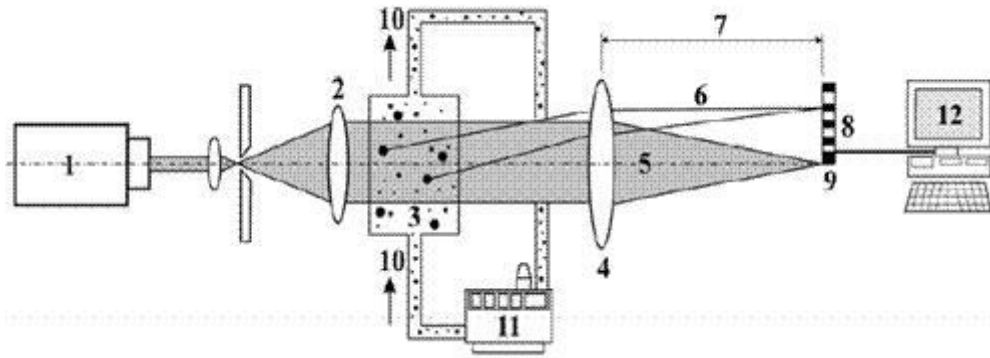


Figure 3.3. Illustration of Laser Diffraction Test Method  
(Source: ISO 13320)

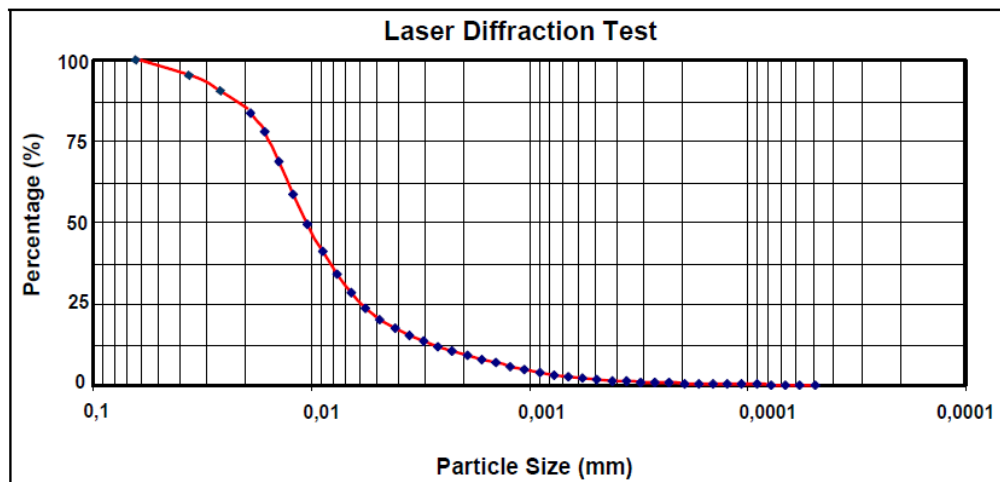


Figure 3.4. Typical Test Graph of the LDM Equipment used  
(Source: ISO 13320)

### 3.2.2. Atterberg Limits Tests

Atterberg Limits tests (ASTM D4318 – 10), which includes the liquid limit, plastic limit, shrinkage limit tests and determination of the plasticity index as the difference between the first two tests, are widely used in the Unified Soils Classification System (USCS). These values are used extensively, either individually or together with other soil properties to correlate with engineering behavior of soils, including consolidation and compressibility, hydraulic conductivity (unsaturated soil) and permeability (saturated soils), compaction, shrink-swell and shear strength behavior etc.

The liquid and plastic limits of a soil and its water content can be used to express its relative consistency or liquidity index. In addition, the plasticity index and the percentage finer than 2- $\mu\text{m}$  particle size can be used to determine its activity number.

Defined boundaries of four states in terms of limits in each Atterberg Limit tests are as follows:

- Liquid limit (LL) : The boundary between the liquid and plastic states;
- Plastic limit (PL): The boundary between the plastic and semi-solid states;
- Shrinkage limit (SL): The boundary between the semi-solid and solid states.

These limits have since been more definitely defined by Casagrande as the water contents, which exist under the following conditions: (ASTM D4318 – 10)

- Liquid limit (LL): The water content at which the soil has such small shear strength that it flows to close a Groove of standard width, when jarred in a specified manner.
- Plastic limit (PL): The water content at which the soil begins to crumble, when rolled into threads of a specified size.
- Shrinkage limit (SL): The water content that is just sufficient to fill the pores, when the soil is at the minimum volume it will attain by drying.

The amount of water which must be added to change a soil from its plastic limit to its liquid limit is an indication of the plasticity of the soil. This plasticity is measured by the plasticity index, which is equal to the liquid limit minus the plastic limit, ( $PI=LL - PL$ ).

### **3.2.2.1. Liquid Limit Test**

Liquid Limit (LL) test (ASTM D4318-10) is performed to determine the water content (%) at which amount of soil in a standard cup and cut by a groove in the Casagrande Apparatus (Figure 3.5) closes after 25 blows. Dimension of the groove; depth: 13 mm (1/2 in.) is subjected to 25 blows from cup being dropped 10 mm. This method is more widely used and its termed as a multipoint liquid limit test. LL test result of the used soil is 48. (Figure 3.6)

Another method to determine liquid limit (LL) is termed as the one-point test (ASTM D 423-66). In this method, a falling cone needle type penetration device and stopwatch is used for 5 seconds. Cone penetration needle has a weight of 80 grams and Direct Shear Test Results of the (%50 CL - ML+%50 SP) soil sample at the relative Compaction of 45 %. Penetrate into soil. This procedure is repeated for different water contents and the water content corresponding to 20 mm penetration is the liquid limit (LL) of the soil.



Figure 3.5. Casagrande Apparatus used for the Multi-Point Liquid Limit Test

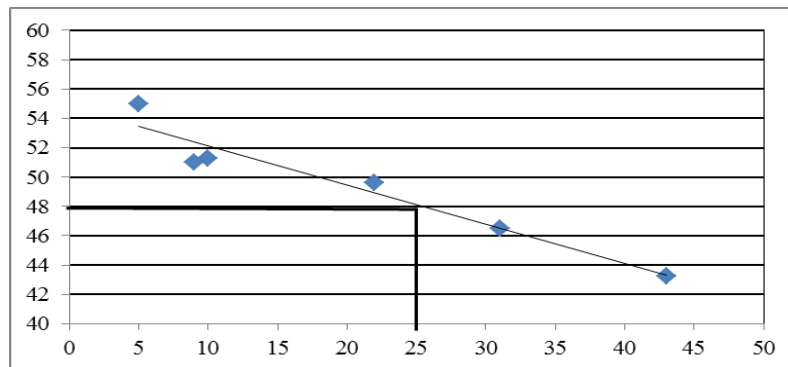


Figure 3.6. Liquid Limit Test Plot of the CL-ML Soil

### 3.2.2.2. Plastic Limit Test

Plastic limit (PL) test (ASTM D4318-10) is also widely performed. It's the lowest water content (%) at which soil acts like a plastic material without any tiny cracks. Process of this method is that soil specimen is dried by airing. Then the soil sample is shaped by rolling it into threads on a glass surface beneath the fingers of one hand with backward and forward movement, until its shape thickness reaches 3 mm. If

the soil does not have any hairline cracks or crumble, then its oven-dry water content is determined as standard procedure (must be kept in the oven at 105 °C for 24 hours to determine plastic limit (PL) of the sample. The differences between LL and PL are the Plasticity Index (PI) of the sample (Figure 3.7).



Figure 3.7. The Plastic Limit (PL) Test Equipment

In summary; average of six LL tests indicated that the value of the liquid limit is 47%. In the same way; Plastic limit is 41%, thus  $PI = 7\%$ . With these test results, soil classification using the Unified Soil Classification System (USCS) can be made as the soil being as type of CL-ML (Figure 3.8).

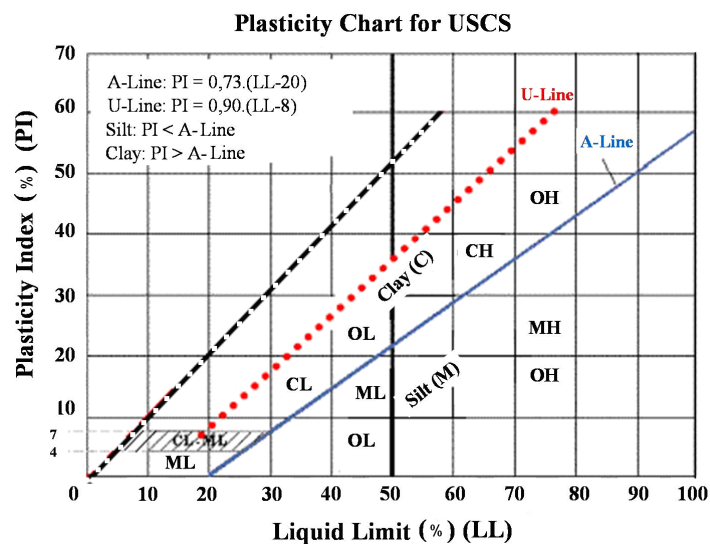


Figure 3.8. The Unified Soil Classification System (USCS)'s Plasticity Chart (Source: Casagrande, 1948)

### 3.2.2.3. Specific Gravity of the Soil

The specific gravity ( $G_s$ ) of a soil is used in the phase relationship of air, water, and solids in a given volume of the soil. It is a non-dimensional parameter. The process of the method is defined by the standard ASTM D 854-02.

The specific gravity of soil solids is used to figure out the density of the soil solids. This is done by multiplying its specific gravity by density of water at the proper temperature. Figure 3.9 shows specific gravity test set-up for CL-ML soils.

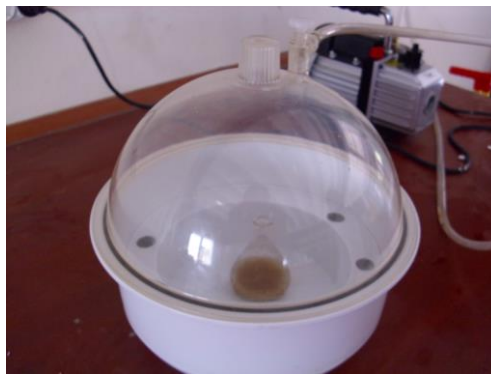


Figure 3.9. Specific Gravity Test Equipment

Process of the test method is that; firstly, the weight of the empty clean and dry pycnometer,  $W_p$  is recorded. Then, 10 gr of a dry soil sample (passing through 4.75 mm (No. 4) sieve is placed in the pycnometer. Next, the total weight of the pycnometer including the dry soil,  $W_{ps}$  is recorded. Later, some distilled water is added to fill almost half to three-fourth of the pycnometer-vacuum above the soil sample, and then is both stirred and vacuumed for 10 minutes, to remove the air out of the soil sample. Next step is to stop vacuuming and carefully removing the vacuum pump from the pycnometer. Afterwards, the pycnometer is filled with some distilled water upto the mark and the external surface of the pycnometer is cleaned with a clean, dry cloth. Next step is to determine the weight of the pycnometer with its contents,  $W_B$ . Later, the pycnometer is emptied, cleaned-up with distilled water and dried with clean cloth. In The pycnometer weight with the distilled water is  $W_A$ .

Determination of the specific gravity,  $G_s$  of soil solids is found from the following formula;

$$G_s = \frac{W_0}{W_0 + (W_A - W_B)} \quad (3.6)$$

Where;  $W_0$  = weight of sample of oven-dry soil,

$W_A$  = weight of pycnometer filled with water,

$W_B$  = weight of pycnometer filled with water and soil

Since in the experiments two types of tests were used, specific gravity ( $G_s$ ) of the CL-ML soil is found as 2.69 and for the SP soil, it is found as 2.65.

### **3.3. Standard Proctor Compaction Test for Soils**

In construction of highway embankments, foundation mats, road bases and in many other engineering structures, soil compaction is done to increase the shear strength of soils. The unit weight of soils increases up to a point and then decreases, depending on the soil's water content. The Standard Proctor type compaction test procedure (ASTM D 698–12) was first developed by Proctor in 1933. In the Standard Proctor Test, the soil is compacted by a 2.5 kg hammer, which falls a distance of 30.5 cm onto a soil filled steel mold. The mold is filled and subsequently compacted in three stages with three equally thick layers of soil and each layer is subjected to 25 drops of the hammer. The Modified Proctor Test (ASTM D 1557) is identical to the Standard Proctor Test, except that it uses a 4.5 kg hammer falling a distance of 45.7 cm and uses five equally thick layers of the soil instead of three. Standard Proctor Test's steel mold is 4 inches in diameter and has a volume of about 944 cm<sup>3</sup>, whereas the Modified Proctor test's steel mold is 6 inches in diameter and has a volume of about 2123 cm<sup>3</sup> (Figure 3.10).



Figure 3.10. Standard Proctor Compaction Test

Both the Modified Proctor compaction test and the Standard Proctor compaction test is generally used for fine grained or cohesive soils. An objective of any soil compaction process is to satisfy two fundamental principles;

- Compaction increases soil's shear strength, which in turn increases the bearing capacity of foundations constructed over them
- Compaction also decreases the amount of settlement of structures and increases the stability of embankment slopes.

By using compaction, air content may decrease up to a minimum level and soils particles become closer and denser. The compaction test result of the soil specimen used in the tests is reported by plotting the relationship between the moisture content change and the dry density change of the soil specimen. In this study the Standard Proctor compaction test was used. A 6-point Standard Proctor compaction test result of the CL-ML soil used in the 2-D experiments of this study is shown in Figure 3.11 below.

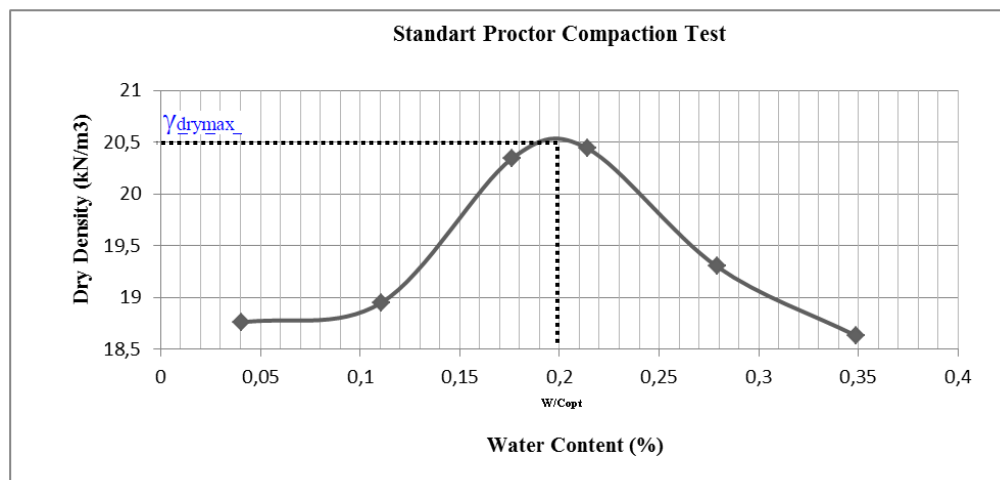


Figure 3.11. Result of Standard Proctor Test of the CL-ML soil in this study

As water it is considered as incompressible inside a soil sample, but air voids are, controlling soil's water content to be at or near the optimum water content corresponding to the highest dry unit weight is the most efficient way to decrease air voids' volume by the Proctor Compaction method. By increasing soil's water content in small increments, soil's dry unit weight, ( $\gamma_{dry}$ ) first increases up to a maximum level and then decreases. Soil's dry density at the maximum level is called the maximum dry density and the corresponding water content is called the optimum water content. Ratio of the soil's density to its maximum dry density obtained from any Proctor compaction test is called relative degree of compaction, RC, (%), which is mostly used for fine grained/cohesive soils. On the other hand, for granular soils, the term relative density, RD (%) is used and is given by the following formula;

$$R_D = \frac{\frac{1}{(\gamma_d)_{min}} - \frac{1}{(\gamma_d)}}{\frac{1}{(\gamma_d)_{min}} - \frac{1}{(\gamma_d)_{max}}} \quad (3.7)$$

Where;  $\gamma_{dry}$  = Granular soils' dry density in field ( $\text{kN/m}^3$ ),

$\gamma_{dry(min)}$  = Minimum dry density of granular soil obtained in laboratory ( $\text{kN/m}^3$ ),

$\gamma_{dry(max.)}$  = Maximum dry density of granular soil obtained in laboratory ( $\text{kN/m}^3$ ),

The last two values are determined using the vibration-table test method (ASTM D 4253/4254).

### 3.3.1. (Static) Direct Shear Tests for Various Soils Used

A simple test (ASTM D6528-07) for finding the shear strength of a soil is the Direct Shear Test (DST), in which a shearing force is applied laterally to the upper half of a soil sample having a certain normal stress and placed in cylindrical or cubic boxes, whereby soils resistance to shearing is measured in the lower half. DST can be performed at certain water content as an either drained or un-drained test, after consolidating the sample before shearing. Otherwise an undisturbed sample can be used.

It's noted that sample must be saturated at the end of consolidation stage and before shearing stage. Disadvantages of the test are pre-determined shearing plane (which may not be the weakest soil plane) and limited horizontal displacement, which may not be enough for soil to develop its shear strength. For granular soils, such drawbacks are minimal and DST gives good and reliable result for soils' shear strength. DST's basic concept and stresses are given in Figure 3.12 and in equations 3.8-3.9, whereby; the normal stress ( $\sigma_n$ ) is due to the applied vertical load  $P_v$  over soil sample's area at time (t) and the shearing stress ( $\tau$ ) is due to the applied horizontal load ( $P_h$ ) over soil sample's area at time (t). Equations for the normal and shear stress are given below;

$$\sigma_n = \frac{P_v}{A} \quad (3.8)$$

$$\tau = \frac{P_h}{A} \quad (3.9)$$

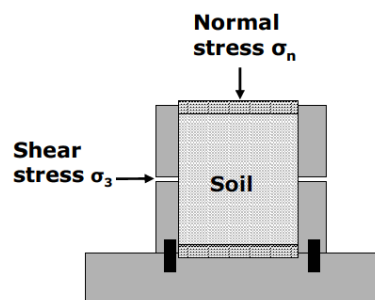


Figure 3.12. Direct Shear Test (DST) concept

The (static) Direct Shear Test (DST) is an inexpensive, fast and simple test, particularly for granular soils. Static means constant (not variable) stress applied during testing (static). DST results of various soils used and obtained from the tests conducted during this study at the Geotechnical Laboratory of the Ege University are given in Figure 3.13 to Figure 3.21 and are summarized in Table 3.1.

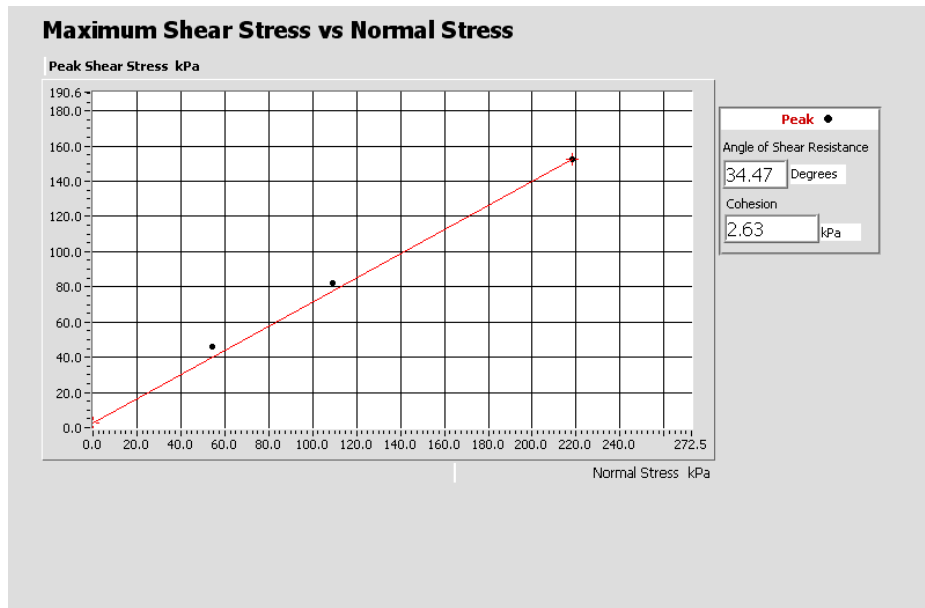


Figure 3.13. Direct Shear Test Results of the 100% SP Soil Sample at the Relative Compaction of 45%

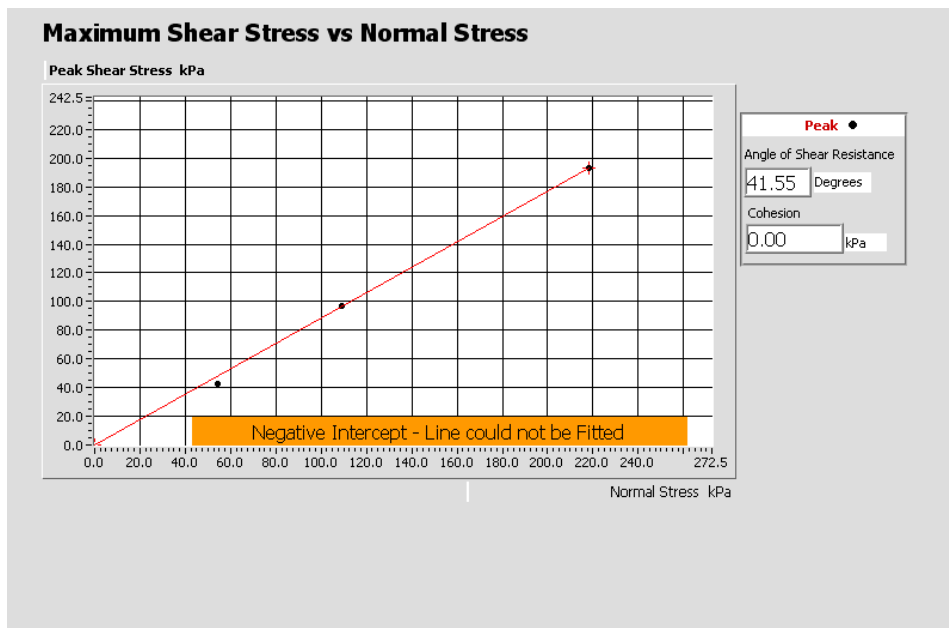


Figure 3.14. Direct Shear Test Results of the 100% SP Soil Sample at the Relative Compaction of 90%

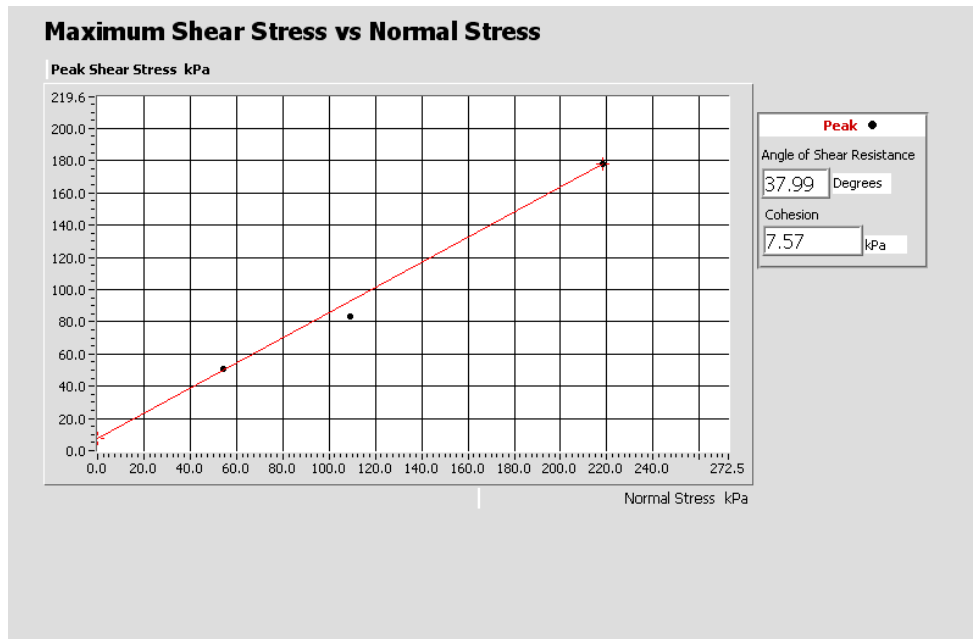


Figure 3.15. Direct Shear Test Results of the (%25 CL - ML+%75 SP) Soil Sample at the Relative Compaction of 45%

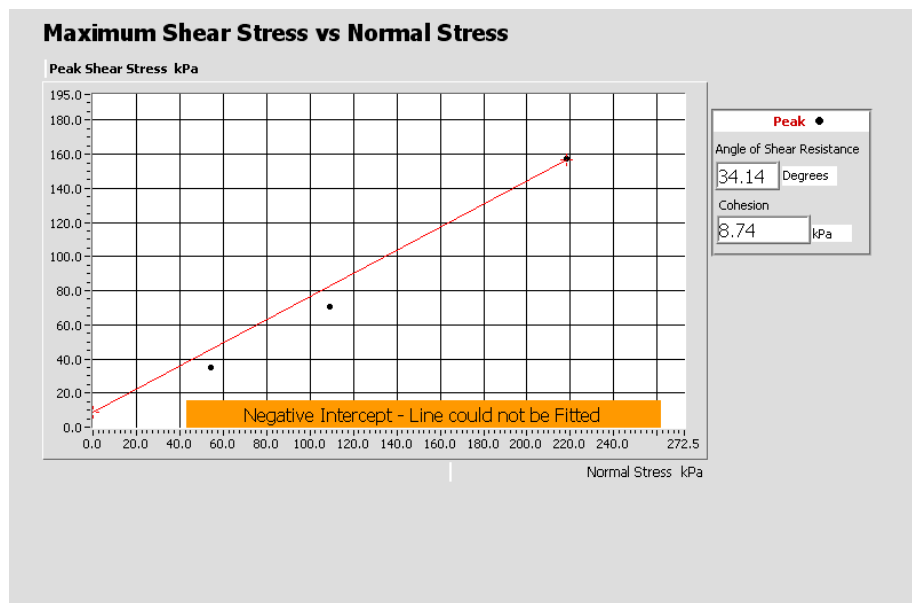


Figure 3.16. Direct Shear Test Results of the (%25 CL - ML+%75 SP) Soil Sample at the relative Compaction of 90%

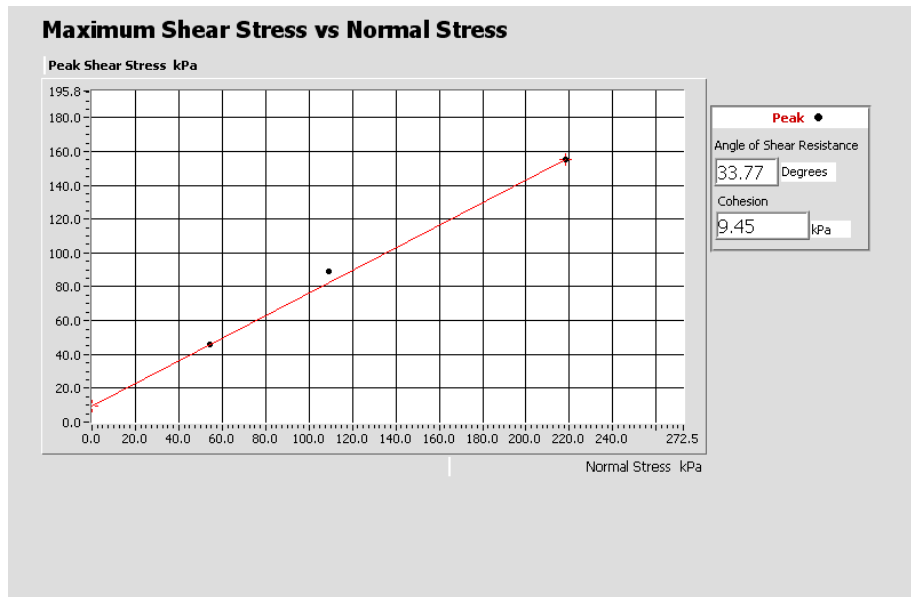


Figure 3.17. Direct Shear Test Results of the (%50 CL - ML+%50 SP) Soil Sample at the Relative Compaction of 45%

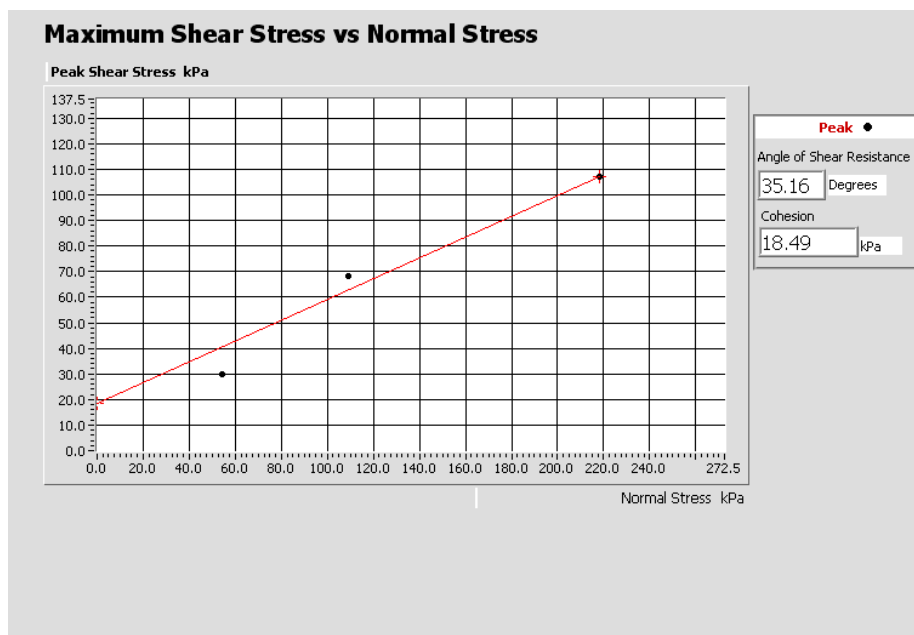


Figure 3.18. Direct Shear Test Results of the 100 % CL-ML Soil Sample at the Relative Compaction of 90%

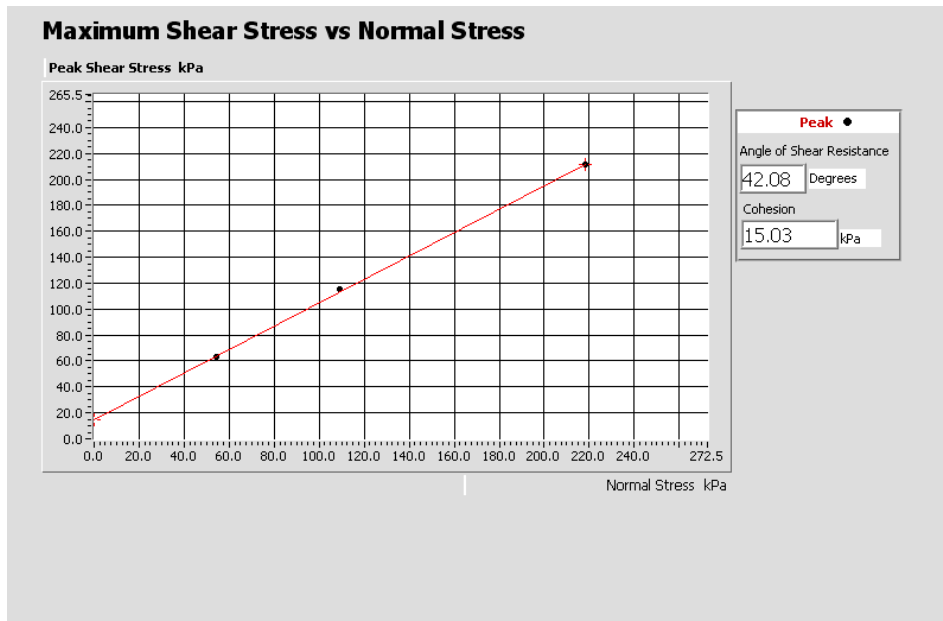


Figure 3.19. Direct Shear Test Results of the (%50 CL - ML+%50 SP) Soil Sample at the Relative Compaction of 90%

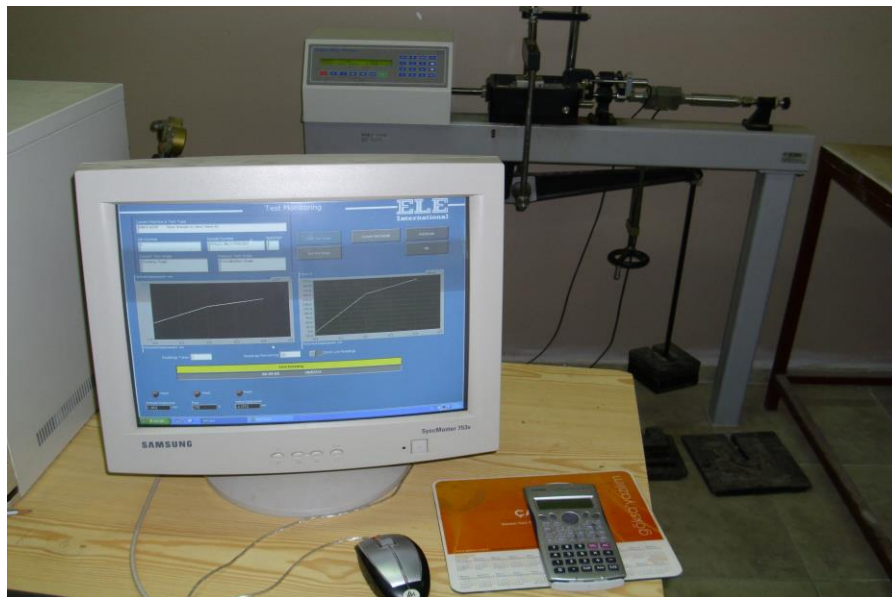


Figure 3.20. Automatic Static-Direct Shear Test Set-up Used (Ege University Geotechnical Laboratory)

Table 3.1. Summary of DST Results

Test No	Type of Soil	Relative Density $R_D$ (%)	Friction Angle $\Theta$ (°)	Cohesion $c$ (kPa)
1	100%SP	45	34,47	2,63
2	100%SP	90	41,55	0
3	25%CL-ML+75%SP	45	37,99	7,57
4	25%CL-ML+75%SP	90	34,14	8,74
5	50%CL-ML+50%SP	45	33,77	9,45
6	50%CL-ML+50%SP	90	42,08	15,03
7	100%SP	90	35,16	18,49

### 3.3.2. (Static) Triaxial CU Test for the CL-ML Soil Used

This test (ASTM D4767-11) is first developed and extensively used by A.W. Bishop of Imperial College (University of London)-Civil Engineering Department's Soil Mechanics Laboratory (Bishop, 1961). It's a drainage controlled test, when load is subjected to the soil specimen in 3-dimensions. The test is called triaxial for the reason that three principal stresses are assumed to be applied and controlled. During initial saturation stage, all three principal stresses are equal to each other, which is also equal to the chamber fluid pressure applied and this stage involves saturating the sample under isotropic (the same) triaxial stresses. During shearing (the second stage), the major stress,  $\sigma_1$  is equal to the applied load divided by the area and is termed as the axial stress and is added to the chamber pressure,  $\sigma_3$ . The applied axial stress minus the chamber pressure,  $\sigma_1 - \sigma_3$  is named as the "principal stress difference" or the "deviator stress". The triaxial test is the most common method used in geotechnical testing and research laboratories for finding shear strength of a soil. Conventional (static) triaxial test involves subjecting a cylindrical soil sample to radial stress (confining pressure) under controlled axial stresses and axial displacements. The cylindrical soil specimen has generally the dimension of 37.5 mm in diameter and 75 mm in height. The height to diameter ratio is usually two. The soil specimen is placed inside the rubber membrane vertically. Ends of the specimen are covered by porous plate at the top and bottom to allow for drainage at the top (if required) and to permit pore water pressure measurements (again, if required). Soil specimens can be extruded from a field obtained

100 mm diameter thin-walled “Shelby Tube” or prepared from a completely remolded sample (to eliminate any structure effect) and sheared in the second stage, after consolidating (CU-test) or un-consolidating (UU-test) it in the first stage. During consolidating and saturation reaching (i.e. the first) stage, drainage line could be opened. But if the drainage line is opened during the shearing (i.e. the second) stage, the test is called as a drained (CD-test), where no pore water pressures, but only volume changes (sample’s overall volume change and drainage line volume change is measured under a certain constantly kept cell and back pressures, difference of which indicates effective consolidation pressure. If sample is saturated, ( $S=1$  and  $B=1$ ) both volume changes, measured as described above, should be equal to each other. It’s noted that just  $B=1$  (pore pressure coefficient) alone may not mean full saturation, especially during the unloading stages (Egeli,İ., 1981) .(Figure 3.21)



Figure 3.21. Automatic (Static) Triaxial CU-Test set-up used by (Ege University Geotechnical laboratory) (Source: Pulat, H.F, 2009)

Depending on the combination of static (constantly kept loading) and drainage stages, there are three (3) main types of triaxial tests;

1. Unconsolidated-Undrained (UU) test (ASTM D2850- 03a (2007)), in which test drainage is not permitted and consolidation is not performed. This is a very quick test and also referred the Q-test. When this test is performed, all drainage valves are closed during the test duration. Axial stress is loaded to the sample with a fast but constant strain rate, after the chamber pressure  $\sigma_3$  is applied. UU test is not applicable, if the rate of construction is slow, which allows consolidation of soil to take place. This test is usually performed in clayey soils.

2. Consolidated-Undrained (CU) test (ASTM D4767-11), which is also named as the R-test. Complete consolidation of the test specimen is permitted under the static (constantly applied) confining pressure, but no-drainage is permitted during the

(second) shearing stage A minimum of three tests is required to define the Mohr-Coulomb strength parameters;  $c'$  and  $\phi'$ . Specimens must be completely saturated, before application of the deviatoric stress in the second (shearing) stage, during when pore water pressures are also measured. By using effective stress law and effective stress plots, the effective stress parameters  $c'$  and  $\phi'$  are obtained. If pore water pressure measurements are not performed in the CU-test, then total stress parameters of  $c$  and  $\phi$  are found, in which  $c$  is called “apparent cohesion (kPa) and  $\phi$  is called “angle of shearing resistance”.

3. Consolidated-Drained (CD) test (ASTM D7181-11), which is also called as the slow or S-test. In this test, complete consolidation of the test specimen is permitted under a constant confining stress and drainage is permitted during the second and slow shearing stage. Slow rate of strain is applied, in order to avoid any build-up of pore water pressures inside the specimen. A minimum of three tests are required for the effective Mohr-Coulomb parameters (ie.  $c'$  and  $\phi'$  determinations). CD tests are generally performed on granular well-draining (e.g. sandy) soils. For slow draining soils, several weeks may be needed to perform any CD test.

Only 1 set (under 3 consolidation pressures) triaxial CU-tests were performed for the CL-ML soil used in the 2-D tests of this study. This test was performed by Pulat, H.F, 2009 (who also used the same soil) at the Ege University-Civil Engineering Department’s Geotechnical Laboratory. No other triaxial tests were thought to be needed, as numerous DSTs already performed for various soils would suffice for study purposes. Static triaxial CU-test results of the CL-ML soil is given as  $c' = 8,65$  kPa and  $\phi' = 29,65^\circ$  as shown in Figure 3.22.

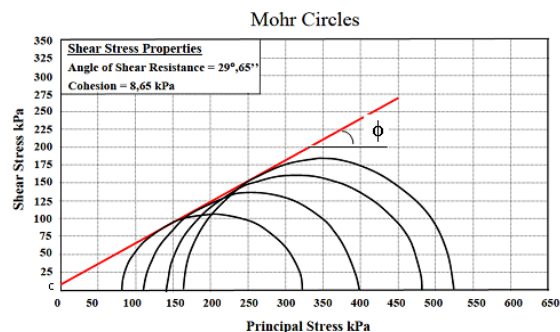


Figure 3.22. (Static) Triaxial CU-Test results of the CL-ML Soil Used (Ege University Geotechnical laboratory) (Source: Pulat, 2009)

### 3.4. Permeability Tests for Saturated Soils

Permeability test (for saturated soils) is a measure of the ease with which water flows through soils or rocks. It is an important parameter so each type of soil has different water transmission characteristics. Permeability is a quite important property, because it may cause structural instability like seepage under a dam, liquefaction, landslides, tunnel collapse etc. The permeability of soils dependent upon size of soil grains, properties of pore fluids (air, water), void ratio of soil, shapes and arrangement of soil pores, degree of saturation. Ranges of permeability for various soils are given in below. Table 3.2

Table 3.2. Range of Permeability for Various Soils

Soil Type	Coeff. of Permeability. (k) (cm/sec)	Degree of Permeability
Gravel	$k > 10^{-1}$	Very high
Sandy gravel, clean sand, fine sand	$10^{-1} > k > 10^{-3}$	High to medium
Sand, silty sand	$10^{-3} > k > 10^{-5}$	Low
Silt, silty clay	$10^{-5} > k > 10^{-7}$	Very low
Clay	$k < 10^{-7}$	Virtually impermeable

Some soils are pervious, some are relatively impervious. Permeability concept is related to the Darcy's Law, which establishes empirically that the flux of water through a permeable formation is proportional to the distance between the top and bottom of the soil column. The discharge velocity ( $v$ ) is proportional to the hydraulic gradient ( $i$ ), which gives the relationship known as the Darcy's law:

$$v = k \times i \quad (3.10)$$

Where; the coefficient of proportionality,  $k$ , has been called as the "Darcy's coefficient of permeability", "coefficient of permeability", or simply "permeability". The term "hydraulic conductivity" is mostly used for unsaturated soils, while "permeability" is used for saturated soils. Coefficient of permeability,  $k$  is commonly

expressed in cm/s or in m/s, m/day, m/hour. In geotechnical engineering practice; soils are either low permeable soils (clays, silts) or high permeable soils (gravels, sands). For the former group, falling head permeability test, while for the latter group constant head permeability test is used. Details of these tests are given below Table 3.3

### 3.4.1. Falling Head Permeability Test

This test is used to determine the coefficient of permeability of a fine-grained soil, such as; silts and clays. Intermediate or low permeability soil's laboratory test is the falling head permeability test. This test is applied also to undisturbed soil specimens. Before starting the test and flow measurements, soil sample must be saturated and standpipes must be filled with de-aired water up to a given level. The test is performed, when the stand pipes reaches the set limit. When test starts, a constant water flow is obtained from the soil container. The time required for water in the standpipe to drop from the upper level to the lower level is recorded. Test is repeated a couple of times, until recorded time is roughly the same using standards; AS1289.6.7.2-2001 or ASTM D5856. The same set can be used for both falling and constant head tests (Figure 3.23).



Figure 3.23. Falling Head and Constant Head Permeability Test-Equipment

The Coefficient of Permeability is then calculated using the following formula;

$$k = \frac{a * L}{A * t} \ln \frac{h_0}{h_1} \quad (3.11)$$

Where;  $k$  is coefficient of permeability (cm/sec)  $a$  is area of the burette (cm<sup>2</sup>)  $L$  is length of soil column (cm),  $A$  is area of the soil column (cm<sup>2</sup>),  $h_0$  is initial height of water (cm),  $h_1$  is equal to (final height of water)  $h_0 - \Delta h$  (cm),  $t$  is time required to get head drop of  $\Delta h$  (sec).

### 3.4.2. Constant Head Permeability Test

The constant head permeability test is a common laboratory testing method used to determine the permeability of granular soils like sands and gravels. This method is used to calculate of seepage through earth dams, seepage into tunnels dug in permeable soils, embankments of canals, under sheet pile walls etc. Standards used are; ASTM D 2434 or AS1289.6.7.1-2001. Table 3.3 shows results of CL-ML and SP soils permeability test.

The Coefficient of Permeability is calculated using the following formula;

$$k = \frac{V \times L}{A \times h \times t} \quad (3.12)$$

Where;  $k$  is coefficient of permeability (cm/sec),  $V$  is collected volume of water (cm<sup>3</sup>),  $L$  is length of soil column (13.65) (cm),  $A$  is area of the soil column (31.65 cm<sup>2</sup>),  $h$  is head difference (34.3 cm),  $t$  is time required to get  $V$  volume (sec).

Table 3.3. Results of Falling and Constant Head Permeability Tests Conducted During This Study

Test No	Type of Soil	Permeability (k) (cm/sec)
1	SP	0,0224
2	CL-ML	0,000041

## CHAPTER 4

# LITERATURE REVIEW OF STUDIES ON UNSATURATED SOIL'S HYDRAULIC PROPERTIES

### 4.1. Introduction

Soils are particulate materials, thus, their properties are governed by interparticle forces. In unsaturated soils, negative pore-water pressure in menisci at particle contacts increases the interparticle forces. The behavior of water in unsaturated particulate materials is related to phenomena such as vapor pressure, evaporation, suction and cavitation. A theoretical frame work for unsaturated soil mechanics has been established over the past four decades. The measurement of soil parameters for the unsaturated soil constitutive models, however, demands laboratory process. Laboratory studies have shown that there is a relationship between the soil-water characteristic curve for a particular soil and the properties of the unsaturated soil (Fredlund and Rahardjo, 1993b). Previously it has become an acceptable procedure to predict empirically the permeability function for an unsaturated soil by using the saturated coefficient of permeability and the soil water characteristic curve is used as the basis for the prediction other unsaturated soil parameters, such as permeability and shear strength functions, it is important to have a reasonably accurate characterization of the soil water characteristic curve.

The soil-water characteristic curve (SWCC) for an unsaturated soil is defined as the relationship between water content and suction for the soil (Fredlund, D.G, 1995). SWCC shows variation between the degree of saturation and matric suction as shown in Figure 4.1.

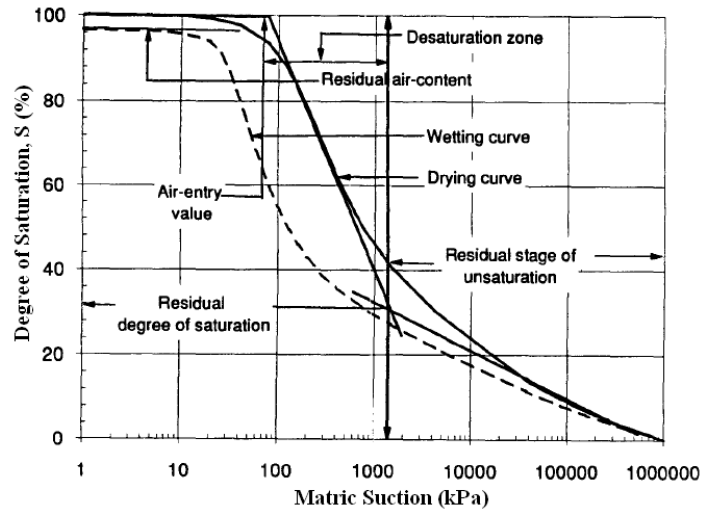


Figure 4.1 A Typical Soil-Water Characteristic (SWC) Curve  
(Source: Fredlund, D.G, 1995a)

Soil hydraulic properties are important parameters affecting water flow in unsaturated soils. Richard (1931) has proposed following equation 4.1 to represent water flow in the vadose zone;

$$\frac{\partial \phi}{\partial t} = \frac{\partial}{\partial z} \left[ K(\phi) \times \left( \frac{\partial \psi}{\partial z} + 1 \right) \right] \quad (4.1)$$

Where;  $\phi$  = the volumetric water content  $\phi$  ( $L^3/L^3$ ),

$K$  = the hydraulic head  $H$  [L],

$z$  = elevation  $z$  (L),

$T$  = time (sec),

$k_u$  = unsaturated hydraulic conductivity function (L/T), expressed as a function of suction  $\Psi$  or of  $\Theta$ .

In order to solve eqn.4.1, the  $k$  function needs to be defined. Several techniques have been developed to measure the unsaturated hydraulic conductivity  $k_u$  in laboratory or in the field (Klute and Dirksen 1989). These techniques can be time-consuming and expensive. For that purpose, Water Retention Curve (WRC) is often used (Green and Corey 1971; Mualem 1976, 1986; Leong and Rahardjo, 1997). WRC describes the amount of water retained in a soil (express as mass or volume content,  $\Theta_m$  or  $\Theta_v$ ) under equilibrium at a given matric potential. The curve showing the relationship between soil

water suction and soil water content for a soil is called the Water-Retention Curve (WRC) as shown in Figure 4.2 below.

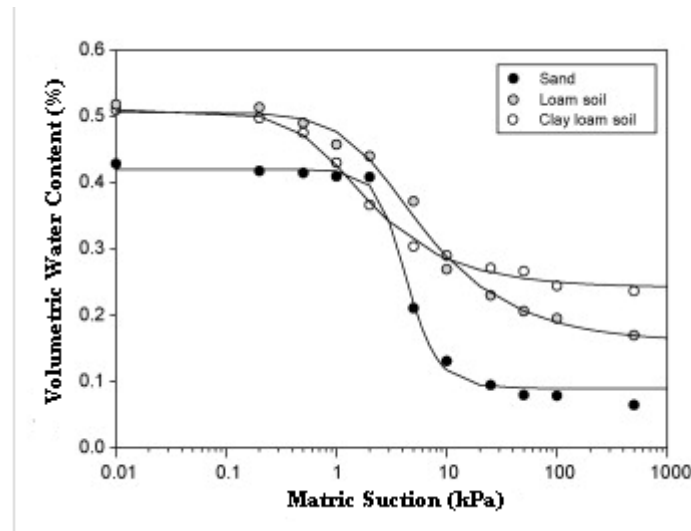


Figure 4.2. Typical Water-Retention Curve of Some Soils  
(Source: Moret-F, D. et al. 2008)

The difference between SWCC and WRC is that the first one uses changes in the degree of saturation ( $S$ ) against matric suction, and the second one uses changes in volumetric water content against the matric suction. Since  $S$  is indirectly measured but water content is directly measured, WRC is more widely used recently and gives more reliable results, compared to SWCC.

## 4.2. Suction

Water in soil voids below ground water table (GWT) is normally continuous. Soil may be saturated ( $S=1$ ), with voids full of water. Pore pressures at depths below GWT are derived from a combination of the weights, lying above the given elevation and the drainage conditions below. Pore pressure normally has a positive value and can be measured using a (saturated) piezometer with a porous filter that is making intimate contact with the water in the soil.

If the water contained in the voids of a soil is subjected to no other force than gravity, the soil lying above GWT is completely dry. However, powerful molecular and

physico-chemical forces acting at the boundary between soil particles and water may cause water to rise by capillarity mechanism. Water menisci separate air, water sides and pressures. The attraction that the soil exerts on the water is termed soil suction.

Soil suctions can be found in all ground that lies above the water table. This may be natural ground surface or slopes, fill materials and other earth structures that are constructed above the GWT. Soil suctions will also be present in samples that have been recovered from a ground investigation. Laboratory measurements of suction can be very useful for assessing soil's shear strength, slope stability, sample quality, estimating in-situ effective stress and detecting the presence of desiccation.

#### 4.2.1. Total Suction

Total soil suction is defined in terms of the free energy or the relative vapor pressure or humidity of the soil moisture and is given by eqn.4.2 below (D.G. Fredlund and H.Rahardjo, 1993)

$$\psi = -\frac{R \times T}{v_{w0} \times \varpi_v} \ln \left( \frac{u_v}{u_{v0}} \right) \quad (4.2)$$

Where;  $\Psi$  is (in kPa).

The total suction ( $\Psi$ ) consists of two components, matric suction and osmotic suctions and given by the eqn.4.3 below. (D.G. Fredlund and H.Rahardjo, 1993)

$$\psi = (u_a - u_w) + \pi \quad (4.3)$$

Where;  $u_a$  : pore air pressure (kPa)

$u_w$  : pore water pressure (kPa)

$(u_a - u_w)$  : Matric Suction (kPa)

$\pi$  : Osmotic Suction (kPa)

#### 4.2.1.1. Matric Suction

Matric suction is an important parameter of unsaturated soils, because it affects the strength of the soil. A meniscus forms at the soil-air-water interface due to surface tension, resulting in reduced pore water pressure, compared to that in air. It's noted that there are 3 kinds of water in pore water. The first two of them contributes to matric suction and the last one contributes to osmotic suction. These are; free (non-adsorbed) water, dissolved air in water (vapor water) and film (adsorbed) water by the soil particles. The first two also contribute to water rising by the capillary mechanism (Egeli, 1981). As pressure in water decreases and may become negative, matric suction pressure increases. While this happens, the radius of curvature of the meniscus and soil pore sizes decreases, due to surface tension forces' pulling effects. If soil's degree of saturation decreases below the optimum water content, soil's matric suction tend to increase, due to increasing air, but decreasing water pressures. Above the optimum water content, menisci reduce and air bubbles form, due to water pressure increase. Near full saturation ( $S=1$ ) all air in air bubbles gradually dissolve in pore water in accordance with Henry's Law (Eqn.4.4) below (Egeli, 1992);

$$P = k_h \times c \quad (4.4)$$

Where; P: partial pressure of gas above the solution (in atm)

$k_h$ : constant of dimensions of pressure divided by concentration

c: concentration of the solute (in mol/L)

#### 4.2.1.2. Osmotic Suction

Osmotic suction is caused by adsorbed (film) water and ion concentration in that water. Increased ion concentration also increases osmotic suction, which can be a significant portion of the total suction. Figure 4.3 can be used to illustrate osmotic suction (D.G. Fredlund and H.Rahardjo, 1993).

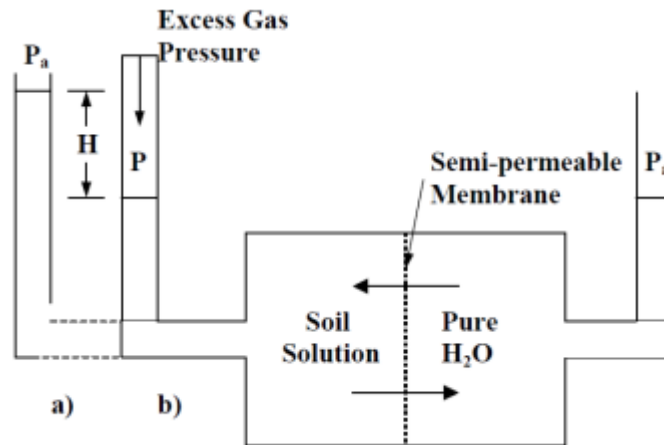


Figure 4.3. Osmotic Suction Illustration  
(Source: D.G. Fredlund and H.Rahardjo, 1993)

In Fig. 4.3;

- a) Water flows through the membrane into the solution due to the osmotic suction in the solution.
- b) Water flows through the membrane into the pure water due to the application of pressure on the solution.

The pressure on the solution, required to equalize flow of water from the solution to the pure water, is equal to the osmotic pressure of the solution (Tindall, J.A, and Kunkel, J.R., 1999).

## 4.2.2. Total Suction Measurements

Researchers use psychrometers, filter papers and hanging column to study total suction. Each of equipment has a measuring range. Also the reliability of measurements change, depending on the test situations.

### 4.2.2.1. Psychrometers

These are used to measure total suction (ASTM D7664-10). Principle of operation relies on the temperature difference between an evaporating and non-evaporating surface is dependent on the relative humidity. A very small current causes

the temperature to increase and decrease at the junctions of a thermocouple (Peltier Effects). Condensation and subsequent evaporation will occur at the junction that is cooled to the dew point. Evaporation will cause a cooling of the junction. Sensor capabilities of psychrometers, are between 100 and 8000 kPa (D.G. Fredlund and H.Rahardjo, 1993)

#### **4.2.2.2. Filter Papers**

Primarily dry filter paper of prescribed mass (and size) is calibrated to measure both matric and total suctions indirectly (ASTM D5298). Measurement is achieved as follows;

Dry filter paper is placed in contact with the soil (for matric suction measurement) or suspended above the soil (for total suction measurement) in a closed container and allowed to come to equilibrium with the soil water or vapor pressure. The water content of the filter paper at equilibrium (usually takes 7 days) is an indication of the suction pressure. If sensor capabilities are used, rather than manometers or gages, then measure high suction pressures upto,  $(-) 10^4$  or  $(-) 10^5$  kPa (10-100 MPa) can be possible. Though this is a very wide range covering the range beyond the plant available free water's permanent wilting point at -1.5MPa, filter paper method is most suited to be used for the range between the tensiometers' maximum range of  $(-)100$ kPa, upto the permanent wilting point at  $(-) 1.5$  MPa (Hyprop User Manual p14, 2011).

#### **4.2.3. Matric Suction Measurements**

Direct measurements of negative pore-water pressures are limited to negative one atmosphere, due to the cavitation of water in the measuring system. An indirect method of measuring matric suctions is based on thermal properties (ASTM D7664-10).

##### **4.2.3.1. Direct Measurement of Matric Suction**

By using high air-entry ceramic porous stones it is possible to directly measure pore water pressure (less than atmospheric) using a pressure gauge or transducer.

#### **4.2.3.1.1. Tensiometers**

Pressure of water contained in a high air-entry porous stone will come to equilibrium with soil's pore water pressure making it possible to measure negative pore water pressure (ASTM D3404-91 (2003)). For this, a small ceramic is attached to a tube filled with de-aired water, which is connected to a pressure measuring device, such as; pressure gage, manometer or transducer (tensiometer). Before using a tensiometer, firstly it should be saturated by filling the ceramic tip with its tubing tip with water and applying a vacuum to the tubing. Next, the ceramic tip is allowed to dry to reduce the water pressure in the sensor and any air bubbles that appear are removed. Then the sensor is installed to the ceramic tip, which will be in direct contact with soil and any remaining air bubbles as they appear in the tubing are removed. The tensiometers used in the İYTE laboratory are factory calibrated. They do not require a re-calibration as such, except doing a small procedure of correction for the difference in elevation head of the pressure gauge and the ceramic tip for  $u_a = 0$ , meaning that air pressure initially is equal to atmospheric pressure conditions in the laboratory, where ambient temperature is constant (at 21°) and no air currents should be present. Correction for elevation head is checked as follows;

$$(u_a - u_w)_{soil} = -u_w + \gamma_w \times x \quad (4.5)$$

Where;  $\chi$ = the differences in elevation head, which is the vertical distance between the transducer and the ceramic tip. Another expression for matric suction ( $u_a - u_w$ ) is given as below;

$$u_a - u_w = \frac{2T}{r} \quad (4.6)$$

Where; T= tension forces in meniscus (kN/m)

r= radius of curvature of the curvature (m)

Tensiometers have 2 kPa graduations between 0 to 100 kPa (1 bar). If sensor has air inside, it will result in wrong (incorrect) measurements of the pore water pressure.

Air can accumulate because of;

Air comes out of solution as the water pressures decrease

Air in soil can diffuse through the ceramic material;

Water vaporizes (cavitation) as the soil water pressure approaches the vapor pressure of water at the ambient temperature.

User manual of the Hyprop test set-up (UMS, 2011) used in our laboratory tests on 3 undisturbed and unsaturated soil samples recommends that; for the most cases seen in practice, suction range for the plant-available (free) water varies between 0 to -1.5 MPa, which is called as the 'Permanent Wilting Point'. (This is a point of permanent dryness and no chance to return to suction range <irreversibility point of dryness> for the plant). The permanent wilting point is the water content of a soil when most plants (corn, wheat, sunflowers) growing in that soil wilt and fail to recover their turgor upon rewetting. The matric potential at this soil moisture condition is commonly estimated at -15 bars. Most agricultural plants will generally show signs of wilting long before this moisture potential or water content is reached (more typically at around -2 to -5 bars) because the rate of water movement to the roots decreases and the stomata tend to lose their turgor pressure and begin to restrict transpiration. This water is strongly retained and trapped in the smaller pores and does not readily flow. The volumetric soil moisture content at the wilting point will have dropped to around 5 to 10% for sandy soils, 10 to 15% in loam soils, and 15 to 20% in clay soils.(G.J. Bouyoucos, 1936) In between this range, Hyprop and other tensiometers give excellent accuracy between 0 to (-)100kPa. Whereas; Pressure Plate method described below, give good accuracy between (-) 50kPa to (-)1 MPa, meaning that it's better suited to be used for the purposes of irrigation-water management and ecological studies, rather than for plant-available-water studies. In other words, using pressure plate in plant-available-water studies for the suction range between 0 to (-) 50 kPa, is not recommended Further details of the Hyprop test set-up is given in the next Chapter (5).

#### ***4.2.3.1.2. Pressure Plate Extractor***

Uses an indirect measurement method with the axis-translation technique (ASTM D6836-02(2008)e2), which reverses the reference air pressure from atmospheric to above atmospheric, causing the pore water pressure to change, as it comes to equilibrium with the pore air pressure.

In a closed system, the air pressure is varied and the soil's pore water pressure is varied by the same magnitude, so that the matric suction remains constant. No water flow occurs. This behavior is used to verify that the axis-translation technique is valid.

In an open system, high pore air pressure forces pore water to flow from the soil to the ceramic disk, until the soil's pore water pressure, which is equal to the pressure in the disk, comes to equilibrium with the soil's pore air pressure. The procedure is as follows; Start by first saturating a ceramic plate and putting it on a soil sample placed on the ceramic plate and allow the soil to reach a desired state of equilibrium. Vary the air pressure in the pressure cell, until equilibrium is reached. For plant-available - water studies (such as ours), calibration capacity of pressure plate method should be up to the 'permanent wilting point' at 15 bars (1.5 MPa).

### **4.3. Evaporation Method**

Measurement of the hydraulic properties of soils in the dry range of the optimum water content is hard to realize, as the direct measurement of the hydraulic properties is generally difficult due to limited matric suction measuring capabilities. On the other hand, measurement of the hydraulic properties of soils in the wet range of the optimum water content is possible to realize, as the direct measurement of the hydraulic properties is easy with matric suction measuring methods.

Many laboratory and field methods exist to determine soil hydraulic properties, especially for the unsaturated soil's hydraulic conductivity (Klute and Dirksen, 1986; Green et al., 1986). Most methods are time consuming, costly, and are often limited to relatively narrow ranges of water content. The method goes back to the work of Wind (1966), who had the idea to use evaporation experiments to simultaneously compute the unsaturated hydraulic conductivity and the water-retention functions from the weight changes of a soil sample and tension changes in the sample, which are recorded by tensiometers. These methods allow an accurate characterization of the water-retention

properties by use of a porous system, from saturation to the measurement limit of the tensiometers or upto the point where significant hydraulic gradient occurs in the unsaturated hydraulic conductivity of the sample (Schindler and Müller, 2006; Peters and Durner, 2006a). Various modifications of these methods exist (Becher, 1970; Schindler, 1980; Plagge, 1991; Wendroth et al., 1993; Schindler and Müller, 2006).

The method of Schindler (1980) is a simplified set-up using the evaporation method, taking into account the total soil sample's weight changes during drying after saturation and measured matric suctions (water tensions, or absolute value of the matric potential is expressed as a positive quantity,  $\Psi$  in kPa). According to previous research; Peters and Durner (2006a) explained that in spite of the larger spatial distance of the tensiometers, effects of spatial and temporal nonlinearity are negligible in the data evaluation and that the method leads to precise and unbiased results, provided that the usual assumption of water flow according to Richard's (1931) equation 4.6, depending on existence of local equilibrium between water content and matric pressure, is valid (Durner and Flühler, 2005).

$$\frac{\partial \phi}{\partial t} = \frac{\partial}{\partial z} \times \left[ K(\theta) \times \left( \frac{\partial \Psi}{\partial z} + 1 \right) \right] \quad (4.7)$$

Where; K: Hydraulic Conductivity (mm/sec)

$\Psi$ : Pressure Head (kPa)

z: Elevation above a vertical datum (m)

$\Theta$ : Water content (%)

t: Time (sec)

Equation 4.6 represents the movement of water in unsaturated soils. All present methodic alternatives of the evaporation method suffer from the range limitation that is given by the measurement range of the tensiometers on the dry end. To get retention-curve values at higher tensions, the pressure plate extractor (Dane and Hopmans, 2002) can be used. This has significant disadvantages, since it involves methodical differences (measurement procedure, sample size, disturbed soil in pressure plate extractor), as it's time and cost consuming method and yields no information about the hydraulic-conductivity function between 0-50 KPa and higher than 1.5 MPa tension range (Hyprop using manual , 2011, Peters and Durner, 2006b).

### **4.3.1. Tensiometer Use on Wet End in a Soil Drying from Saturation**

The prerequisite for extending the measurement range with “high quality” tensiometers consist of three basic interconnected components: a) a semi-permeable porous cup, b) a water reservoir and c) measurement gauge or pressure transducer. Pressure equilibrium between the water in the tensiometer and the surrounding soil is achieved through water movement across the porous tensiometer cup.

If the tension of the soil-water exceeds the air-entry pressure, the cup drains and becomes air-permeable, which is water-tension measurement becomes incorrect. Air enters into the tensiometer and its internal tension drops off. Ceramic cup material of the tensiometer is therefore configured to ensure that its air-entry pressure is larger than the highest soil-water tension to be measured. As the classical measurement limit is normally yielded by the vapor pressure of the water inside the cup, the air-entry value for most tensiometer cup materials is greater than 100 kPa.

The dynamics of a tensiometric measurement in a drying soil from saturation by evaporation can be separated in three distinct stages. In first stage, the measured tension reflects the matric potential of the surrounding soil. Most of tensiometers’ upper limit is 80 kPa (Young and Sisson, 2002). For the optimal performance, water inside the tensiometers should be free of any dissolved gas in water. If dissolved gas exists, then a small gas bubble will form that swells continually during the drying stage and yields to a retarded and incorrect tensiometric measurement (Durner and Or, 2005). This must be precluded, which can be done by visual checking the tensiometer’s water lines and by using proper implementation measures, as described in Schindler et al. (2010).

The second stage is the vapor-pressure stage. If absolute soil water pressure is decreased below the liquid’s vapor pressure, then water inside the tensiometer starts to boil. The pressure inside the tensiometers equilibrates to the vapor pressure, which is closed to vacuum. Water in contact with the porous cup will flow through the cup into the surrounding soil, while the vapor bubble inside the cup expands continually. As a result, the soil in the immediate vicinity of the porous cup will be less dry (lower tension) than it would be, without the presence of the tensiometer. The tensiometer readings in this stage are no longer representative of the soil-water matric potential. The beginning of stage 2 can be retarded if boiling retardation occurs. With a suitable tensiometer design, reliable tension values upto and greater than 400 kPa can be

measured, before cavitation occurs, when the pressure inside the tensiometer collapses to the liquid's vapor pressure (Schindler et al., 2010). The third and final stage can be titled "air-entry stage". It occurs when the tension in the surrounding soil exceeds the air-entry pressure of the ceramic material. The largest continuous pores of the ceramic drains from the soil to the tensiometer; where air inserts. At this moment, the measured tension falls towards to zero (0), which is means tensiometer are no longer valid.

#### 4.4. Principle of the Extension of the Measurements

The basic idea for extending the measurement range is to use the ceramic's air-entry pressure at the well-defined moment of the tension collapse, (i.e. at the initiation of stage three) as additional measurement of the soil's matric potential. If this assumption is valid, an interpolation of the tension from the last reliable values of stage 1 to the initiation point of stage 3 can be performed (Figure 4.4). Any smooth function with higher-order continuity, such as polynomial functions or Hermitian spline interpolation can be used for interpolation with relatively small uncertainty. Applying this procedure to both tensiometers extends the data evaluation into the dry range (Uwe Schindler<sup>1</sup>, Wolfgang Durner<sup>2</sup>, G.von Unold<sup>3</sup>, L. Mueller<sup>1</sup> & R. Wieland<sup>1</sup>)

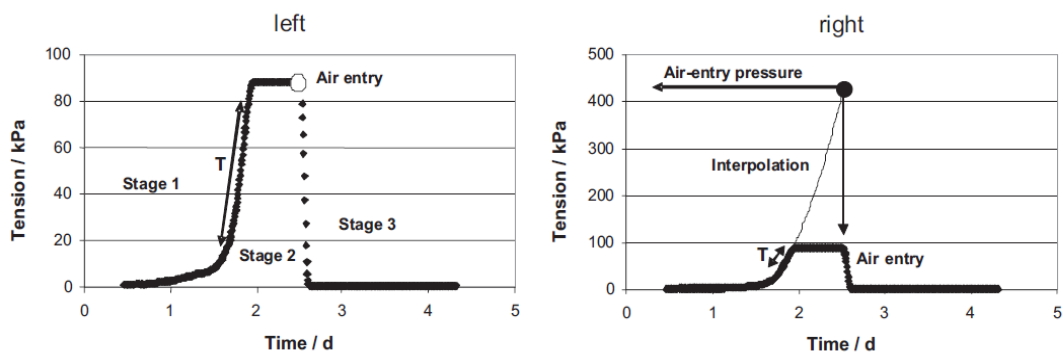


Figure 4.4. Tension Dynamics during Evaporation (left) and Interpolation to Air-Entry Pressure (right) for Clay Soil

#### 4.5. Material and Methods

The validity of the proposed evaporation method, which depends on the general precondition that the matric potential of the tensiometer cup is in equilibrium with the soil in contact, relies on the following points: (1) the air entry pressure of the ceramic cup is much higher than 100 kPa, (2) the air entry pressure is well defined and reproducible, (3) the water loss from the tensiometer to the surrounding soil during stage 2 does not affect the soil's tension at the begin of stage 3. The first and second assumptions can be tested empirically by repeatedly determining the air-entry pressure of the tensiometer cup material. The third assumption depends on a variety of factors. Most important amongst them are (1) the speed of drying of the soil, (2) the unsaturated hydraulic conductivity of the surrounding soil material, (3) the size of the contact area between the tensiometer cup and soil, (4) the amount of water-loss from inside the tensiometer into the surrounding soil. To investigate the bias in the tension measurements, due to water loss from the tensiometer, we have numerically simulated the drying process of the soil with an embedded tensiometer using HYPROP, which is a commercial apparatus having vertically aligned tensiometers that is optimized to perform evaporation measurements.

#### **4.5.1. Evaporation Method According to Schindler**

Soil cores should be taken from undisturbed bulk or Shelby-Tube soil samples by use of Hyprop's stainless-steel sampling cylinders, which have a sharpened leading edge on one side to minimize soil disturbance during insertion. Then the protective cap is removed from the upper side of the sample (the side with the straight rim, without the cutting edge) and the mesh fabric is placed on the sample.

Next, the perforated saturation attachment is attached to the clamp the cloth. Then around the sample is turned around and its second plastic cap is removed. After the dish is filled with water and the sample is place in the dish, standing on the perforated attachment. The water level should be 1 cm below the upper rim of the sampling ring. The cutting edge shows upwards, so the sample is saturated from the reverse side. Most crucial moment is the point, where the sample ring is slightly lift-up and tilt, during the saturation stage, when the sampling ring with saturation attachment inside the water filled saturation bowl. Proper handling will prevent air bubbles to be

trapped between the soil samples and the mesh fabric. Hence, this process should be carefully done, so that no soil particles are flushed out.

Other step is degassing of the syringes, tensiometers and the sensor unit. For this the reservoir syringe with the short rubber tube is taken and into it, 10 ml of deionized or distilled water is sucked in. End of the tube is plugged with a finger while the syringe is pulled-up. This causes vacuum inside the syringe and dissolved gas is released. Next, the syringe is rotated to collect all bubbles from the walls of the syringe. Then the syringe is held upright while emptying water with air bubbles. This procedure is repeated, until no bubbles are visible to exist.

For degassing ceramic tip of tensiometers following steps are used. 1) Insert the ceramic tip into the tube as far as possible with the ceramic tip pointing downward. The cup's tip should be close to the syringe nozzle. The syringe is pulled up just a little, while the syringe is held downwards and tapped on it to loosen any air bubbles. Then the tube is taken from the syringe, while leaving the shaft inside the tube. Next, air is removed from the syringe and the ceramic. After, 10 ml deionized/distilled water is withdrawn into the syringe and it's degassed as described before. Then the threaded side of the Tensiometer shaft is completely inserted into the tube of the vacuum syringe and the O-ring is rolled-up so the shaft is securely fixed. Next is to pull up the vacuum syringe, until both spacers snap in and then turned around to collect all the bubbles. Then the spacers are released and water is allowed to flow into the shaft. The same procedure is repeated, until no air bubbles remain in the tube. Next is to reattach the vacuum syringe and pull it up, until the spacers clamp.

Also sensor unit should be degassed. For this, the acrylic sensor head attachment is placed onto the sensor head. The sensor head should sit firmly on the O-Ring. Then the acrylic attachment is filled with deionized/distilled water using the droplet syringe and the tube and the vacuum syringe is attached, by making sure that no air bubbles exist in the line. Afterwards, tensiometer shafts are inserted and the syringes are removed from the tensiometer shafts. Each hole on the sensor unit is marked by a groove. The long shaft is inserted where the long groove is, and the short shaft is put, where the short groove is. Next, a drop of water is added on top of the shaft with the droplet syringe, so that the meniscus is convex. Then, the sensor unit with the adapter cable and USB-converter is connected to out to PC socket and tensioVIEW is started

and first “Refilling”, after “Refilling window” is opened. Figure 4.5 shows refilling section of HYPROP.

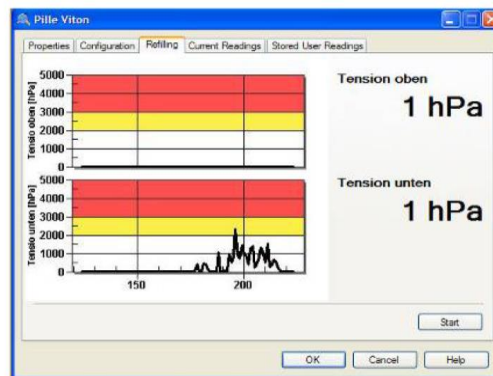


Figure 4.5. Refilling Window View of Hyprop Test  
(Source: Hyprop Manual, 2011)

Noted that while the shaft is carefully screwed into the sensor unit, the pressure must not be exceed 1 bar (100 kPa). In case the pressure rises too high, then stop the turning-in should be stopped or some time should be allowed for the pressure to drop (Figure 4.6).



Figure 4.6. Assembly of the Tensiometer  
(Source: Hyprop Manual, 2011)

The undisturbed soil sample (whose initial void ratio, degree of saturation is already determined) is placed into the dish to reach saturation for at least 24 hours. Afterwards, the soil sample is taken out of the saturation dish and the auger positioning tool is placed onto the sampling ring. Next, the test-set provided auger is used to drill 2

holes in the sample. Then sensor unit with 2 probes are inserted into the drilled holes in the soil sample (Figure 4.7).



Figure 4.7. Soil Sample with Two Shaft Holes  
(Source: Hyprop Manual, 2011)

An O-ring on the sensor unit is pushed each of the shafts to the very bottom. The rings will keep dirt out, once the Tensiometer shafts are installed. Close the clips to fix sampling ring to the sensor unit. Thus the soil sample assembly is completed. Hyprop testing will start automatically, when the soil sample assembly is placed onto the electronic scale provided. Note the surface of soil sample should be moist and not dry. If dried, then some water should be dripped onto the soil surface to create even starting conditions. (Figure 4.8)

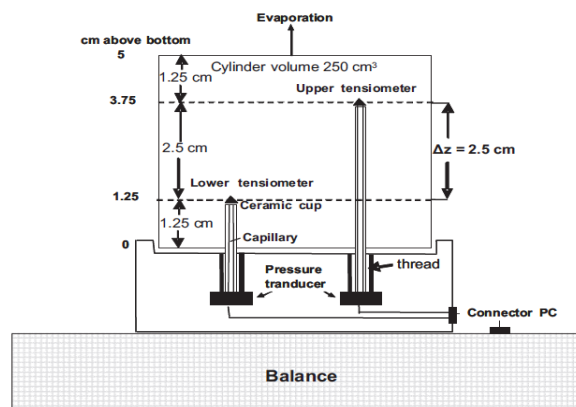


Figure 4.8. The Schematic Illustration of Hyprop Measurement Device  
(Source: Hyprop Manual, 2011)

A measuring test normally ends, if one of the tensiometers reaches the end of its measuring range (-100 kPa). The test does not stop automatically but must be stopped

by the user. Readings between the start and stop lines are used for the evaluation. Start and stop lines should be set by the user. The software recognizes the drop out of the tensiometer beyond the measuring range limit and sets the stop line at that point. The drop out of a tensiometer can easily be seen on both graphs of the tensiometer readings. Alternatively, measurements during a test can also be stopped manually. When the test ends, the whole sample assembly is held over a bowl or dish to assure that no soil material is lost, while the fastener clips are unlocked. Then gently the soil sampling ring is taken take off from the sensor head. Lastly, the final water contents and final sample weights should be determined for further calculations by the oven-drying method, by taking care of not to lose any soil material during the final (dismantling) stages. For this purpose, the soil sample is placed into a bowl whose weight is known. Both is placed in a drying oven at 105 °C for 24 hours and then is weighted again. The difference in weight is the exact dry weight of the sample which is entered in the field ‘Soil dry weight’.

#### 4.5.2. Discrete Data for Retention and Conductivity Relation

At different points of time  $t^i$ , the water tensions  $h_1^i$  and  $h_2^i$  (in kPa) of both depths are measured, as well as the weight of the sample (in grams  $\cong$  cm<sup>3</sup>). The analytic procedure is based on the assumption that water tension and water content distribute linear through the column and that water tension and sample weight changes are linear between the two evaluation points at ceramic tips.

The initial water content is determined from the total loss of water (i.e. evaporation + water loss by oven drying).

The average water content,  $\Theta^i$  (%), derived from initial water content and loss of weight, and the medial water tension,  $h^i$  give a discrete value  $\Theta^i(h^i)$  (kPa) of the retention function at any time  $t^i$ (sec). For calculation of conductivity function, it is assumed that between two time points  $t^{i-1}$  and  $t^i$ , the water flow quantity through the cross section between the 2 tensiometers (and therefore exactly at the column centre) is;

$$q^i = 1/2 \times \left( \frac{\Delta V^i}{\Delta t^i \times A} \right) \quad (4.8)$$

Where;  $q^i$ : Water flow between both tensiometers,

$\Delta V^i$ : is the water loss in  $\text{cm}^3$  determined by weight changes,

$\Delta t^i$ : is the interval between two evaluation points,

A: the cross section area (in  $\text{cm}^2$ ) of the column.

The data for the hydraulic conductivity function are determined by inverting the Darcy Equation:

$$K^i(h^i) = -\frac{q^i}{\Delta h^i / \Delta z + 1} \quad (4.9)$$

Where;  $K^i(h^i)$ = Hydraulic conductivity function as determined by the Darcy-Equation 4.6 ( $\text{cmh}^{-1} \times \text{kPa}$ ).

$h^i = \frac{1}{4}(h_1^{i-1} + h_2^{i-1} + h_1^i + h_2^i)$  is the medial water tension between two evaluation points,

$K^i$  is the related hydraulic conductivity (in  $\text{cm h}^{-1}$ ).

$\Delta h^i = \frac{1}{2}((h_2^{i-1} - h_1^{i-1}) + (h_2^i - h_1^i))$  is the medial difference of the water tension between both tensiometers (kPa).

$\Delta z = z_2 - z_1$  is the distance between both tensiometers (in cm).

Unreliable  $K(h)$  data sets close to saturation are filtered, depending on the measuring accuracy of the tensiometers. In order to obtain enough number of data points for the hydraulic function even with relatively long intervals, both the tension curve and the weight curve between two evaluation points are interpolated with the hermitian splines (Peters and Durner, 2008). For achieving this, relatively short evaluation intervals are selected.

## 4.6. Retention and Conductivity Functions

In general hydraulic characteristics are termed by parametric functions for  $\Theta(h)$  and  $K(h)$ . In HYPROP test set-up, three models can be chosen. These models can be adapted to measure the data via a robust and non-linear optimizing procedure.

#### 4.6.1. Van Genuchten/Mualem Model

In this model, the effective saturation  $S_e = (\theta - \theta_r) / (\theta_s - \theta_r)$  and the unsaturated conductivity,  $K$  in relation to the matric potential,  $h$  are predetermined by the following equation formula (van Genuchten, 1980):

$$S_e(h) = \left(1 + (\alpha|h|)^n\right)^{1/n-1} \quad (4.10)$$

$$K(h) = K_s \left(1 + (\alpha|h|)^n\right)^{\tau(1/n-1)} \left[1 - (\alpha|h|)^{n-1} \left[1 + (\alpha|h|)^n\right]^{1/n-1}\right]^2 \quad (4.11)$$

Here the residual water content,  $\Theta_r$  (%) the water content at saturation,  $\Theta_s$ ; the inverse value of the bubble point potential,  $\alpha$  [cm<sup>-1</sup>] and the pore size distribution,  $n$  [-] are the fitting parameters for the retention function. Also, the tortuosity parameter  $\tau$  [-] and the saturated conductivity  $K_s$  (mm/sec) are fitted to get the conductivity function.

#### 4.6.2. The Bimodal Van Genuchten/Mualem Model

This model proposed by Durner (1994) explains the retention and conductivity function by overlapping of two individual van Genuchten functions (Priesack and Durner, 2006).

$$S_e(h) = \sum_{j=1}^2 \omega_j \left(1 + (\alpha_j|h|)^{n_j}\right)^{1/n_j-1} \quad (4.12)$$

$$K(h) = K_s \left[ \sum_{j=1}^2 \omega_j \left[1 + (\alpha_j|h|)^{n_j}\right]^{1/n_j-1} \right]^{\tau} \left[ \frac{\sum_{j=1}^2 \omega_j \times \alpha_j \left\{1 - (\alpha_j|h|)^{n_j-1} \left[1 + (\alpha_j|h|)^{n_j}\right]^{1/n_j-1}\right\}}{\sum_{j=1}^2 \omega_j \times \alpha_j} \right]^2 \quad (4.13)$$

Where; the  $j$  is indexes for the parameters of each Van Genuchten function, and  $\omega_j$  are the weights of both partial functions. The following restriction applies:  $0 < \omega_j < 1$  and  $\sum \omega_j = 1$ ,  $\omega$  is tortuosity weight parameter related to soil type.

### 4.6.3. The Brooks and Corey Model

In the Brooks & Corey (1964) model the retention and conductivity function are defined as:

$$S_e(h) = \begin{cases} 1 & \text{for } h > \alpha^{-1} \\ (\alpha|h|)^{-\lambda} & \text{for } h < \alpha^{-1} \end{cases} \quad (4.14)$$

$$(4.15)$$

$\lambda$  [-] and  $\tau$  [-] are two fitting parameters which correspond to the pore size distribution, respectively with the tortuosity.

## CHAPTER 5

# LABORATORY TESTS ON WATER-INFILTRATION INTO UNSATURATED FINE-GRAINED SOIL SLOPES

### 5.1. Introduction

Numerous shallow landslides and surface slope failures occur every year in many parts of Turkey and around the world. Shallow landslides usually are triggered by heavy rainfalls. During heavy rains, water seeps into the ground, saturating the upper layers of soil. Pore-water pressures develop, which reduce the shearing resistance of the soil. Flow activity of prolonged (sustained) rainfall influences stability of landslides or slopes indirectly. There have been many approaches in literature studying unsaturated granular-soil slope stability, but they can have some uncertainties and deficiencies (Fredlund-Rahardjo, 1993).

In order to overcome this uncertainty, one way for the engineers and researchers to generate the needed data, is to use modeling, which can save time and costs incurred, as modeling provides the ability to do analysis quickly and efficiently. Also we can change modeling and design scenarios. This way results for various options can be compared.

This chapter studies validity of wetting-band (infiltration) phenomena in granular unsaturated soils in two parts. In the first part; a specially developed (2-D) test set-up at the İYTE-Geotechnical laboratory, which was previously used in angular soil slope experiments (Pulat, 2009) was re-used this time for few horizontal ground-surfaced infiltration tests in unsaturated granular soils to verify validity of Pradel&Raad, 1993 and Lumb, 1975 theories. To better understand the infiltration phenomena and to avoid complication which may have been otherwise introduced by the slope angle, flat (i.e. horizontal) ground-surfaced shallow slopes were chosen for the experimental studies. In the second part, similar experiments were conducted using a specially designed (1-D) test set-up at the İYTE-Geotechnics laboratory for additional horizontal ground-surfaced infiltration tests again to verify validity of Pradel and Raad, 1993 and Lumb, 1975 theories. Numerical results obtained from these 2 theories (in

both 2-D and 1-D tests) were compared with the actual observations made during these tests.

## 5.2. Soil Container

Part of the (İYTE-Geotechnical laboratory designed) special rainfall infiltration modeling system is a soil container, which is a rectangular box with dimensions of 2 m in length, 1.5 m in width and 0.4 m in height. Side and top views of the soil container are shown in Figure 5.1. All 4 sides are made of 8 mm thick plexiglass to observe rainfall infiltration and strong enough to resist the lateral earth pressure, while the bottom surface is covered with 5 mm thick and 100 mm wide metal plates, leaving in between 50 mm wide permeable bands of very fine-mesh sieving strips, placed at 100 mm intervals Figure 5.2, so that no soil, but only the percolated infiltrating water can pass thru' it to the bottom tank. Soil container has been designed to have a maximum of 20 kN carrying capacity.

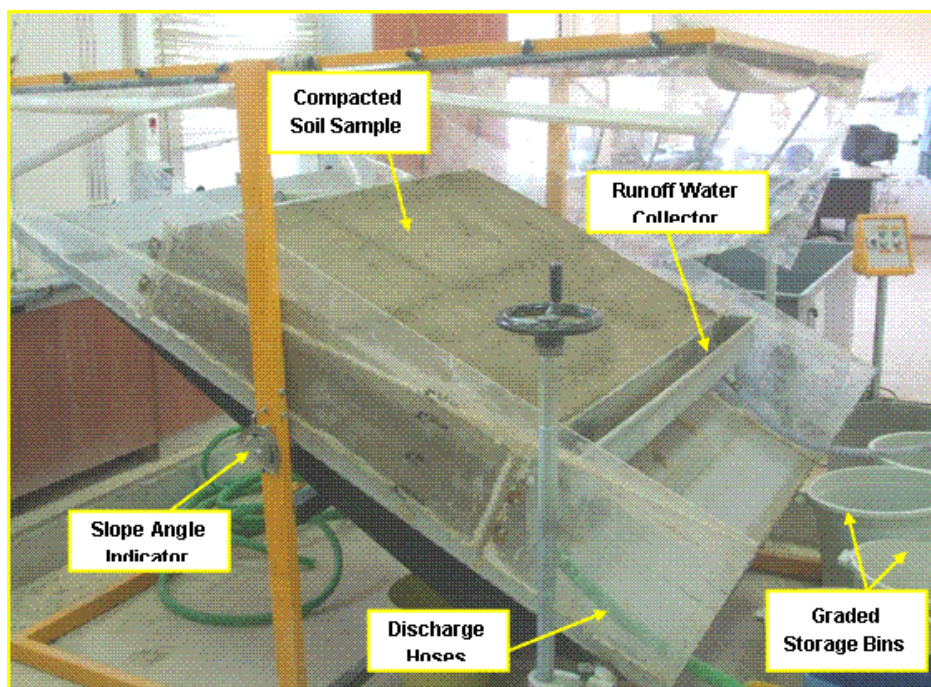


Figure 5.1. Sloped Soil Container View during the Previous Slope Stability Study  
[Source: Pulat, 2009]

Lateral surface of the soil container was designed from 8 mm thick plexiglass, enabling observations of soil displacement and water-infiltration into soil to be made during the experiments. Another important reason of using plexiglass is minimizing the friction along the sidewalls of the soil container, so that plane-strain conditions are closely approximated with low friction surface along the sides of the container.

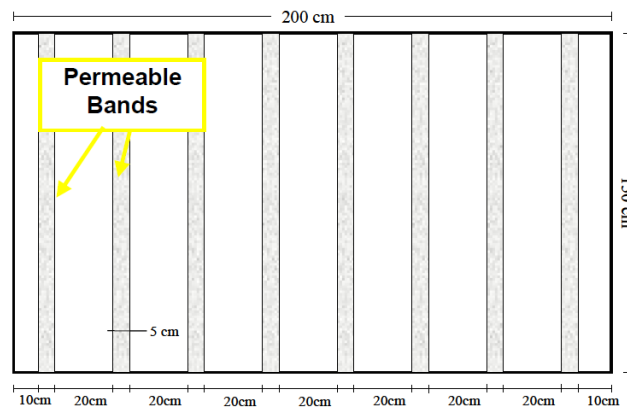


Figure 5.2. Top View of the Soil Container's Bottom

An important problem of this enormously heavy system was to design a sustainable support frame, without causing any overturning or collapse. Soil container was carried by two rectangular sectioned steel box profiles with dimension of 60 mm x 40 mm and a wall thickness of 4 mm. In addition to these box profiles, two supplementary support elements made of stainless steel with height adjustable features are attached to the support frame. General view of test set-up with horizontal empty soil container is shown Figure 5.3.

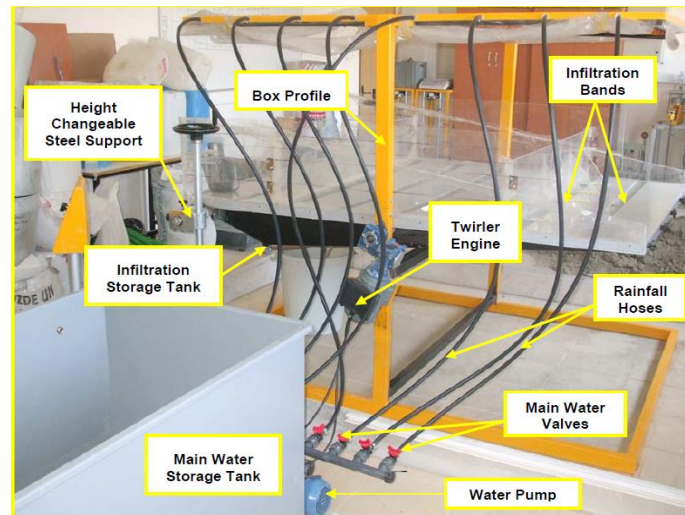


Figure 5.3. General View of the Test Set-Up with Horizontal Empty Soil Container  
(Source: Pulat, 2009)

## 5.2.1. Artificial Rainfall System

Rainfall is artificially produced using a specially designed sprinkler system. The artificial rainfall system is used to produce uniform and adjustable (intensity, duration) rainfall simulation. The artificial rainfall system consists of the main water storage tank, water pump, main water supply valves, rainfall hoses and sprinklers.

### 5.2.1.1. Main Water Storage Tank

In order to determine the intensity of rainfall to be supplied from the artificial rainfall system, a water storage tank (a water-rectangular tank made of sheet metal and holds upto 800 liters of water) is manufactured to provide the water supply (Figure 5.4). Thus intensity and volume of the generated rainfall through fine spray nozzles connected to the water pump and water container via rubber pipes could be measured. Infiltration water is discharged from the soil storage tank with the aid of discharge hoses to the graduated plastic storage bins for volume measurement. The main water storage tank is formed from metal plates which has wall thicknesses of 3 mm. Graduate indicator is used to determine the amounts of total water and consumed water during the tests.

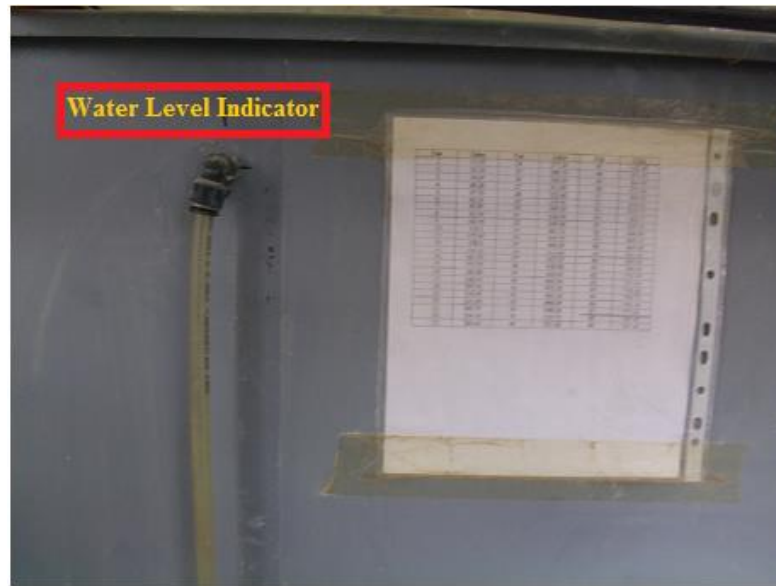


Figure 5.4. Lateral View of the Water Storage Tank

### 5.2.1.2. Water Pump

Task of the water pump (Figure 5.5) is to convey water from the main storage tank to the soil container. Most appropriate pump with model no. is PR100, manufactured by the Best Science and Technology co. of U.K. was used. Capacity of the pump is 45 lt/hr and its power rating is 1 HP with 0.75 Kw. Maximum height water can be pumped is 74 m.

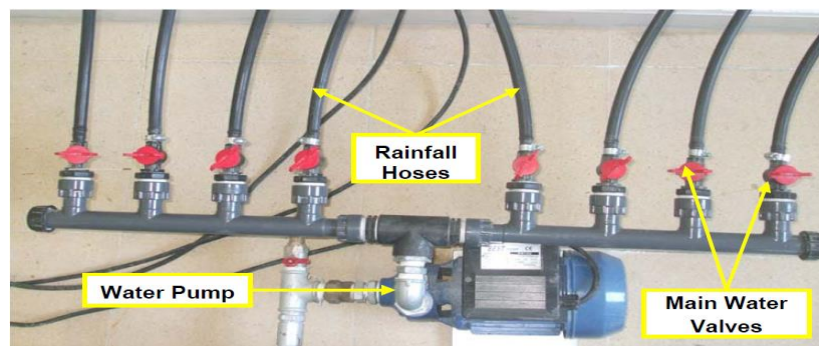


Figure 5.5. Water Pump, Rainfall Hoses and Main Water Valves

### **5.2.1.3. Rainfall Hoses and Sprinklers**

The most fundamental task of the artificial rainfall system is undertaken by hoses and sprinklers. The system was constructed with 1 cm diameter PVC pipings and a simple frame to hold the sprinklers above the soil container. Sprinkler frame has an 8 rows and each row has 12 nozzles (Figure 5.6).

### **5.2.2. Infiltration Bands and the Discharge System**

The purpose of the test set-up is to observe rainfall infiltration into the granular soil with a horizontal ground surface, while checking soil's matric suctions (i.e. differences between air and pore water pressures) at various places, depths and seeing its effect on the slope stability. Though tensiometers can also measure small positive pore water pressures, if there is no air in soil pores, this condition only happens after a prolonged (sustained) rainfall, when a moving wetting-band develops between the ground surface and a certain soil depth observable from the transparent sides of the soil container. If matric suctions decrease and pore water pressures increase, soil's shear strength decrease (due to effective strength principle) and slope failures in the form of large displacements can take place with occurrence of some shallow landslides. Rainwater can infiltrate into the granular soil with the effect of the gravity and the capillary forces. As rainwater infiltrates through the soil layer and reaches to the steel bottom plate, fine-meshed percolation bands prevent soils, but let water to pass thru' to the bottom water tank underneath the soil container. Gathered percolated water in the infiltration storage tank can be discharged to the graduated plastic bins placed underneath, with the help of 2 numbers of each 2 m long and 30 mm in diameter discharge hoses. Other vital observation is the surface runoff water discharge system, where the quantity of the surface runoff water can be measured. When the rainwater reaches to the soil surface, part of the rainfall starts to infiltrate into soil and the other part may flow at the ground surface of the slope as 'the surface runoff'. If the slope angle is steep, surface runoff can reach high speeds, which may cause great deformations on the slope surface. To determine how much rainwater starts to flow on the slope surface, runoff collector is used. Surface water first reaches to the runoff

collector and afterwards it is discharged by using the discharge-hoses. Amounts of runoff water can be measured using the graduated storage bins made of plastic. Graduated water collection bin and discharge hose under the soil container is shown in Figure 5.6, Figure 5.7 and Figure 5.8



Figure 5.6. Filled Soil Container and Placed-in Tensiometers to Measure Soil-Suction



Figure 5.7. Another View of The Filled Soil Container and Placed-in Tensiometers

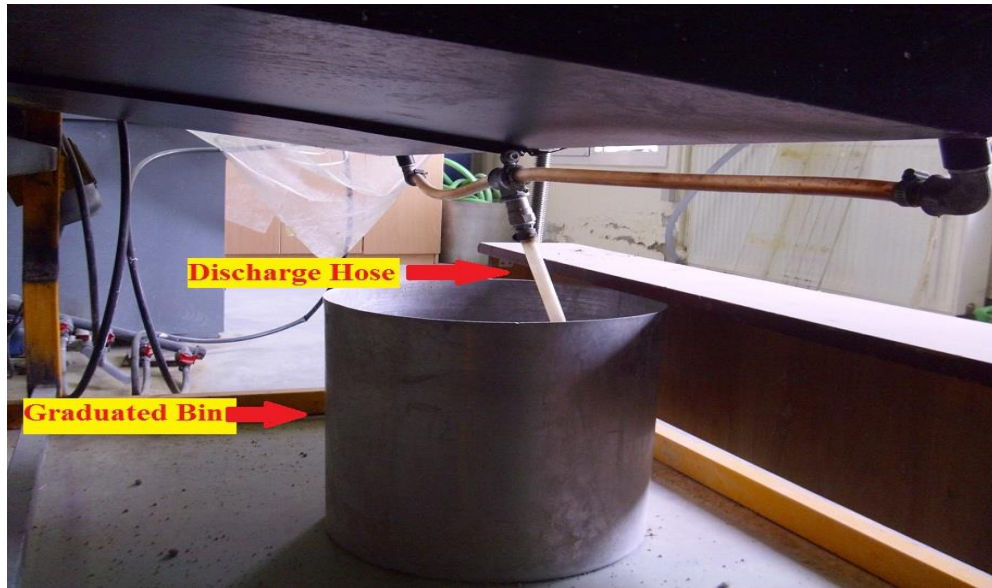


Figure 5.8. Discharge Water Collection Bin Under the Soil Container

### 5.3. 2-D Infiltration Study Experiments

These tests are included into two groups; each is given in sections 5.3.1 and 5.3.2 below.

#### 5.3.1. Previously Conducted 2-D Experiments

As discussed comprehensively in the previous sections, twelve main experiments were performed at the İzmir Institute of Technology (IYTE)'s–Soil Mechanics Laboratory by a previous researcher (Pulat, 2009). Twelve experiments had a soil thickness of 25 cm. Additional 3 tests were performed by this researcher with a soil thickness of 30 cm. There were three variables in these tests, which were; soil densities (no. of blows/layer), initial water content and type of soils used. Other data, such as; amounts of surface runoff, infiltrated water (into soil) or infiltrated-through (passing thru' soil) water, adsorbed water, infiltration depth, eroding soil heights, wetting-band (infiltration) depth along the slope etc. In addition to the collected data, lots of observations were also made about the failure mechanisms occurring during the experiments, such as; any translational sliding or not, deformation types, any surface settlements or not etc. Testing data and the results were given in Table 5.1, Table 5.2

and Table 5.3. Main observation was that, the vast majority of the total rainwater received by the granular slope, flowed down the slope as the surface runoff. Another important conclusion was that; in granular slopes having low initial density (10 blows/layer) and low initial water contents (14%), the amounts of infiltrated water was small or non-existent, due to soils developing big initial suctions, which allowed a slower infiltration rate of water into the slope. On the other hand, in granular slopes having high initial density (30 blows/layer) and high initial water contents (30%), the amounts of infiltrated water was large, due to soils reach saturation quicker, which allowed a faster infiltration rate. Additionally, wetting-band thicknesses (i.e. infiltration depths) were also observed as shown in Figure 5.9.



Figure 5.9. Infiltration (wetting band) Depth Measurement after the Experiment

Table 5.1. Basic Data of the Previously Performed 12 Tests  
(Source: Pulat, 2009)

No	Number of Blows	Initial $W_c$ (%)	Total (lt) Water $Q_T$	Absorbed Water (lt) $Q_M$	Infiltrated Water (lt) $Q_i$
1	10 Blows	14	400	295,4	72
2	10 Blows	30	400	286,96	87,55
3	25 Blows	14	400	315,2	52,4
4	25 Blows	30	400	307	57
5	10 Blows	14	400	353	0
6*	10 Blows	30	400	302	80
7	25 Blows	14	400	361	0
8*	10 Blows	30	400	294,5	80,7
9	10 Blows	14	400	330	24
10	10 Blows	30	400	364	0
11	25 Blows	14	400	376	0
12	25 Blows	30	400	382	0

(\*): Soil Sample consist of 90%CL-ML and 10%SP

Table 5.1 gives the summary of previously are performed 12 tests with a rainfall intensity of  $0.18\text{lt/sec/m}^2$ , including the density of soil and the date of experiments. The weight of soil is related to the compaction effort directly. The weight of CL-ML and SP soils ranged between 5.05 kN, which equals to 505 kg and 5.62 kN, which equals to 562 kg. The date of experiments was organized at the beginning of the thesis, because the amounts of soil used in these 12 experiments were substantial. Thus in order to control the initial water content precisely, soil materials was first air-dried and then re-used again in another experiment. For example; for the 14% initial water content, soil material was used and then soil material was left to dry, whose water content was checked at frequent intervals. When the soil reached to the desired water content (e.g. 1%), the soil was ready to be used in any experiment.

Table 5.2. Detailed Data of the Previously Performed 12 Tests  
(Source: Pulat, 2009)

No	Angle of Slope	Number of Blows	Initial $W_c$ (%)	Weight of Soil (kN)	Volume of Soil ( $\text{m}^3$ )	Density of Soil ( $\text{kN/m}^3$ )	Soil Type
1	15°	10 Blows	14	5,11	0,375	13,60	CL-ML
2	15°	10 Blows	30	5,05	0,375	13,40	CL-ML
3	15°	25 Blows	14	5,45	0,375	14,50	CL-ML
4	15°	25 Blows	30	5,32	0,375	14,20	CL-ML
5	25°	10 Blows	14	5,15	0,375	13,70	CL-ML
6*	25°	10 Blows	30	5,62	0,375	15,00	90% (CL-ML) + 10% (SP)
7	25°	25 Blows	14	5,27	0,375	14,10	CL-ML
8*	15°	10 Blows	30	5,52	0,375	14,70	90% (CL-ML) + 10% (SP)
9	35°	10 Blows	14	5,22	0,375	13,90	CL-ML
10	35°	10 Blows	30	5,18	0,375	13,80	CL-ML
11	35°	25 Blows	14	5,41	0,375	14,40	CL-ML
12	35°	25 Blows	30	5,17	0,375	13,80	CL-ML

Slope failure in shallow landslides of non-cohesive soils are mostly triggered by high intensity and relative short duration rainfall up to few hours, where rainwater infiltrates into soil and destroys inter-granular friction and effective stresses changes due to stress state changes occurring in soil during and after rainfall. Final degrees of saturation were all above 95%. Various slope angles under constant high intensity (0,18 lt/sec/m<sup>2</sup>) and duration (1500 sec. or 25 min.) of rainfall. The overall correlation of tests was observed wetting band depths ( $h_{\text{obser}}$ ) with the calculated wetting band depths from the Lumb's Equation ( $h_{\text{LE}}^*$ )

Table 5.3. Previously Conducted 12 Test Results (\*) with Initial-Final Conditions and Comparison of Average Observed Wetting-Band Depths ( $h_{\text{obser}}$ ) with Results from the Lumb's Equation ( $h_{\text{LE}}$ ) (Source: Pulat, 2009)

Test No	$W_{\text{cf}}$ (%)	$\gamma_{\text{dry(max)}} (\text{g/cm}^3)$	$e_f$	$S_f$ (%)	$k_f$ (cm/s)	$n_f$	$W_{\text{ci}}$ (%)	$S_i$ (%)	$h_{\text{Lumb}} (\text{cm})^*$	$h_{\text{obser}}$ (cm)
1	0,35	1,35	0,93	0,98	0,000045	0,48	0,14	0,46	0,27	25
2	0,38	1,31	0,99	1,00	0,000055	0,50	0,14	0,46	0,31	25
3	0,34	1,36	0,92	0,97	0,000044	0,48	0,14	0,46	0,27	19,4
4	0,33	1,38	0,89	0,97	0,000041	0,47	0,14	0,46	0,26	18,8
5	0,37	1,31	0,99	0,97	0,000055	0,50	0,14	0,46	0,32	25
6	0,34	1,36	0,92	0,97	0,000044	0,48	0,14	0,46	0,27	18,4
7	0,38	1,31	0,99	1,00	0,000055	0,50	0,50	0,95	3,35	25
8	0,37	1,31	0,99	0,97	0,000055	0,50	0,50	0,95	7,16	25
9	0,38	1,31	0,99	1,00	0,000055	0,50	0,50	0,95	3,35	25
10	0,39	1,29	1,00	0,99	0,000057	0,51	0,50	0,95	3,78	25
11	0,38	1,31	0,99	1,00	0,000055	0,50	0,50	0,95	3,35	17,6
12	0,37	1,31	0,99	0,97	0,000055	0,50	0,50	0,95	7,16	17,7

(Notes:  $t=1500$  seconds,  $G_s=2,61$ ,  $I = 0,18$  lt/sec/m<sup>2</sup>; (\*) calculated during this study by researcher)

After rainfall was stopped, a 40 cm long 'Shelby Tube' type thin-walled soil sampler was used to obtain undisturbed samples in order to determine the final void ratio, degree of saturation, specific gravity and final water content (Figure 5.10).



Figure 5.10. Shelby Tube used to obtain Undisturbed Soil Samples after Rainfall.  
(Source: Pulat, 2009)

Twelve previously conducted 25 cm deep soil experiments were to check the validity of the calculated (Lumb, 1975) wetting-band thickness equation, against the made observations. During this study, additional 3 experiments conducted by this researcher. In these tests, soils in the container were all 30 cm deep and these tests were done to check the validity of the calculated wetting-band depths using the Pradel-Raad, 1993 theory, against the observations made. Since Pradel-Raad, (1993) equation includes average matric-suction calculation, tensiometers needed to be used to determine suction measurements at 3 levels of the 30 cm high soil-columns. Tensiometers are inserted with 10 cm intervals also 2-D system, corresponding to depths of 5cm, 15cm and 25cm from the surface of soil-column. Wetting-band observations of the previous twelve main experiments were done by Pulat, who did not use any tensiometer measurements and hence his 12-test main experiment data cannot be used to check the validity of the Pradel-Raad, (1993) theory. But this can be checked in the additional 2-D and 1-D tests done during this study, where tensiometers are used. Thus with these additional tests, computations can be made to check the validity of both Lumb's, (1975) equation and Pradel-Raad, (1993) equation to determine the wetting-band thicknesses. But compared to the earlier done 12 main experiments, a lower rainfall intensity ( $0.05 \text{ lt/sec/m}^2$ ) was applied (to allow for higher suctions to develop) in these additional 2-D and 1-D tests, though the rainfall duration was kept as the same (25 mins or 1500 sec.). Results of 2-D additional tests are given in Table 5.4 below.

Table 5.4. Summary of the 2-D additional tests conducted with initial, final conditions and comparison of observed wetting band depths ( $h_{\text{obser}}$ ) against ( $h_{\text{P-R}}$ ) and  $h_{\text{lumb}}$  values.

Test No	$W_{\text{cf}}$ (%)	$\gamma_{\text{drymax}}$ ( $\text{g}/\text{cm}^3$ )	$e_{\text{f}}$	$S_{\text{f}}$ (%)	$k_{\text{f}}$ (cm/s)	$n_{\text{f}}$	$W_{\text{c}_i}$ (%)
1	0,34	1,34	0,89	0,98	0,0224	0,47	0,14
2	0,35	1,38	0,99	0,97	0,000044	0,50	0,14
3	0,33	1,35	0,92	0,97	0,000055	0,48	0,14

$W_{\text{cf}}$ =final water content,  $e_{\text{f}}$ =final void ratio,  $n_{\text{f}}$ = final porosity,  $S_{\text{f}}$ =final degree of saturation

Table 5.4. (Continues)

$S_{\text{i}}$ (%)	Matric Suction (cbar)	$h_{\text{P-R}}$ (cm)	$h_{\text{lumb}}$ (cm)	$h_{\text{obser}}$ (cm)	Type of Soil
0,46	30	1,28	137,48	30	100%SP
0,46	62	0,55	0,26	14,4	100%CL-ML
0,46	54	0,56	0,34	23,3	50%SP+50%CL-ML

(NOTE:  $S_{\text{i}}$ =initial degree of saturation,  $h_{\text{p\&R,Lumb,Obser.}}$ =wetting band thickness)

## 5.4. 1-D Infiltration Study Experiments

Since 2-D main (previous) tests and 2-D additional tests gave poor comparisons with the observations (see section 5.5 below) it was imperative to do additional 1-D tests, which were easier and quicker to do. Variables are rainfall intensity, soil type, soil density, initial water content, initial void ratio, initial degree of saturation. Rainfall intensity was kept same as the additional 2-D tests ( $5,24 \times 10^{-4} \text{lt}/\text{sec}/\text{m}^2$ ).

### 5.4.1. Materials and Test Procedure Used

#### 5.4.1.1. Soil Plexiglas Cylinder

Soil Plexiglas Cylinder is formed two parts. First part is for 40 cm high soil column with a water-permeable steel wire mesh (made of no.200 US sieve mesh) and

the second part is 20 cm high water-infiltrating reservoir cup with a valve at the bottom. Although the above part is 40 cm high, our tested soil-column was only 30 cm high in this study. Both top and bottom parts have the same diameter of 20 cm. The total height of the Plexiglas soil cylinder is 60 cm and its thickness is 5 cm. Since the band has very fine mesh sieving stripes, no soil, but only the infiltrating water can pass through the band to bottom reservoir. The reason of choosing transparent Plexiglas material is to observe the wetting band thicknesses. Figure 5.11 shows 1-D test set-ups.



Figure 5.11. 1-D Test Equipment

#### **5.4.1.2. Artificial Rainfall Supply**

3 cm diameter hose is used to generate artificial rainfall. Hose has head which is able to adjust intensity and flow rate of water. Length of hose is 5 m. It is made of flexible material. During test hose was adjusted “mist” for the reason that mist is closer the real rainfall and it is intensity. Intensity of test is  $(5,24 \times 10^{-4} \text{lt/sec/m}^2)$ . 1-D tests take average 25 minutes to apply artificial rainfall in each test. Figure 5.12 shows artificial rainfall supplier.



Figure 5.12. Artificial Rainfall Supplier

### 5.4.1.3. Matric Suction Measuring Tensiometer Devices

Matric suction is the difference pore air and pore water pressures, which are differentiated by the soil meniscus and affects the shear strength. Each type of soil has different matric suction measurement range. For instance; amount of colloid content increase or decrease matric suction. During rainfall shear strength is decreased depends on increase pore water pressure and degree of saturation of soils. There have been several methods to calculate matric suction so we have used ceramic head devices which are called tensiometers (T5-2100F).

Three tensiometers are placed per 10 cm of 1-D test set-up. These tensiometers are consisted of three parts. (Figure 5.14) First part is body of tensiometer which has distilled water in it. Second part is lid which is covered the tensiometer body. Which avoid leaking out air to tensiometer body. Third and most important part is ceramic head. Ceramic head leads water into the tensiometer but it does not permit air to enter until the air-entry matric suction is reached. Therefore we can calculate matric suction of soils. Figure 5.13 shows placing tensiometer in the 1-D system.



Figure 5.13. To Assembly a Tensiometer in 1-D Test Set-Up



Figure 5.14. Parts of the used Tensiometers (Model:T5-2100F)

#### **5.4.1.4. Type of Soils, Compaction Method, Rainfall Intensity Used in 1-D Tests**

In this study, two different soils were used to build 1-D test models. One of the soil types was SP (uniform sand) and the other was CL-ML (silty-clay). Same rainfall intensity was applied to 1-D test set-up as in 2-D additional tests ( $0,05\text{lt}/\text{sec}/\text{m}^2$ , but reduced in proportion to the surface area). Also to have variation in this study; 100% SP was by weight and every new test we have increased fine-grained soils weight by 5% percent until 50% CL-ML+50% SP test was set up. Also each soil mixture layer was subjected to four types of different soil compactions by the 2 kg weight used (ie. loose, 5 blows, 10 blows, 20 blows per layer) (Figure 5.15).



Figure 5.15. 1-D Experiments - Soil Compaction via 2 kg Weight/10cm Soil Layer

Rainfall intensity was modified in accordance with the 1-D test response. Each mixture of soil has different negative pore water pressures. Thus, 32 main experiments were performed at water contents between: 1 to 3%. These experiments took three months to finish completely. Tensiometers (dial gauges) are needed to be calibrated frequently after the tests for the accuracy of readings. On the other hand in 1-D tests, actually applied rainfall intensity was  $5,24 \times 10^{-4} \text{lt}/\text{sec}/\text{m}^2$ , due to proportional reduction of the surface areas (from that of the soil container to that of the Plexiglas cylinder, which is  $314,16 \text{cm}^2$ ) in order to consider the size effect.

#### **5.4.2. 1-D Experimental Results**

A total of 32 numbers of 1-D tests were conducted to compare wetting-band thicknesses obtained from The Paradel-Raad, (1993) theory and Lumb's, (1975) theory

against the actual observations made during the tests. 1-D test results are given in Table 5.5.

Table 5.5. Summary of the 1-D Tests and comparison of average observed wetting band Depths ( $h_{\text{observed}}$ ) vs. results obtained from the Pradel-Raad, 1993 ( $h_{\text{P-R}}$ ) and Lumb's, 1975 ( $h_{\text{lumb}}$ ) Equations.

Test No	$W_{cf}$ (%)	$\gamma_{\text{drymsx}}$ g/cm <sup>3</sup>	Number of Blows	$S_f$ (%)	$k_f$ (cm/sec)	$W_{ci}$ (%)	$h_{\text{P-R}}$ (cm)	$h_{\text{observed}}$ (cm)	$h_{\text{lumb}}$ (cm)	Type of Soil
1	0,34	1,35	Loose	0,98	0,0224	0,010	1,58	30	201,9	100%SP
2	0,38	1,34	5 blows	0,98	0,0226	0,012	1,65	30	184,6	100%SP
3	0,36	1,35	10 blows	0,99	0,0224	0,010	1,88	30	201,9	100%SP
4	0,34	1,33	20 blows	0,97	0,0224	0,011	2,20	30	212,52	100%SP
5	0,37	1,35	Loose	0,98	0,0202	0,013	2,31	30	161,85	10%CL-ML +90%SP
6	0,35	1,34	5 blows	0,98	0,0201	0,011	1,46	30	165,66	10%CL-ML +90%SP
7	0,33	1,34	10 blows	0,99	0,0221	0,010	1,95	30	193,18	10%CL-ML +90%SP
8	0,38	1,36	20 blows	0,98	0,0237	0,010	1,99	30	209,61	10%CL-ML +90%SP
9	0,37	1,33	Loose	0,98	0,0189	0,012	1,44	30	155,77	20%CL-ML +80%SP
10	0,35	1,34	5 blows	0,97	0,0182	0,013	2,29	30	148,69	20%CL-ML +80%SP
11	0,34	1,36	10 blows	0,99	0,0197	0,012	1,89	30	168,95	20%CL-ML +80%SP
12	0,37	1,32	20 blows	0,98	0,0211	0,010	1,93	30	190,20	20%CL-ML +80%SP
13	0,34	1,37	Loose	0,97	0,0157	0,011	2	30	124,80	30%CL-ML +70%SP
14	0,33	1,38	5 blows	0,98	0,0160	0,010	1,29	30	127,19	30%CL-ML +70%SP
15	0,35	1,35	10 blows	0,97	0,0173	0,010	1,45	30	145,38	30%CL-ML +70%SP
16	0,38	1,37	20 blows	0,98	0,0184	0,011	1,97	30	156,11	30%CL-ML +70%SP
17	0,36	1,36	Loose	0,99	0,0135	0,012	1,24	30	97,97	40%CL-ML+SP

18	0,33	1,37	5 blows	0,98	0,0137	0,011	1,73	30	106,81	40%CL-ML+60%SP
19	0,34	1,38	10 blows	0,97	0,0148	0,010	1,87	30	116,35	40%CL-ML+60%SP
20	0,37	1,37	20 blows	0,97	0,0158	0,011	1,51	30	135,43	40%CL-ML+60%SP
21	0,35	1,33	Loose	0,99	0,0112	0,012	1,01	30	79,77	50%CL-ML+50%SP
22	0,38	1,35	5 blows	0,98	0,0114	0,013	1,03	30	86,54	50%CL-ML+50%SP
23	0,34	1,34	10 blows	0,97	0,0124	0,010	1,18	30	98,57	50%CL-ML+50%SP
24	0,33	1,34	20 blows	0,99	0,0132	0,012	1,46	30	108,79	50%CL-ML+50%SP
25	0,37	1,36	Loose	0,99	0,0213	0,012	2,03	30	172,24	95%SP+5%CL-ML
26	0,38	1,37	5 blows	0,99	0,0217	0,013	1,57	30	182,66	95%SP+5%CL-ML
27	0,39	1,37	10 blows	0,99	0,0240	0,012	1,97	30	212,26	95%SP+5%CL-ML
28	0,38	1,38	20 blows	0,98	0,0250	0,011	2,19	30	228,24	95%SP+5%CL-ML
29	0,37	1,32	Loose	0,97	0,0168	0,013	1,54	30	134,62	75%SP+25%CL-ML
30	0,35	1,31	5 blows	0,98	0,0171	0,012	1,70	30	143,70	75%SP+25%CL-ML
31	0,38	1,31	10 blows	0,97	0,0185	0,010	2,05	30	160,03	75%SP+25%CL-ML
32	0,34	1,32	20 blows	0,98	0,0197	0,10	2,56	30	177,58	75%SP+25%CL-ML

( $W_{cf}$ =final water content,  $\gamma_{drymax}$ . = max.dry unit weight,  $S_f$ = final degree of saturation,  $k_f$ = permeability of soils)

## 5.5. Conclusion on the Combined Results of 1-D and 2-D Experiments

Wetting-band theories are important because they are used in slope stability and landslide stability analyses. As discussed previously, twelve main experiments were

performed by Pulat (2009) but checking his observations against the Lumb's, (1975) wetting band theory was performed during this study, during which time additional three 2-D main experiments were performed. In order to determine wetting band thicknesses against these two theories, additional 32 numbers of 1-D main experiments were performed at the Geotechnical Laboratory of İzmir Institute of Technology. In the previous 12 numbers of 2-D main experiments, variables were; two types of soils, initial water contents and soil densities. Comparison of wetting-band thicknesses calculated now from the Lumb's, (1975) theory and Pulat's, (2009) observations did not match closely. Lumb's theory gave much lower results (between 1,08% - 40,5%) of the actually observed wetting band thicknesses (Table 5.3). Original 12 numbers of 2-D results could not be used to check the validity of the Pradel-Raad, (1993) theory, as soil's (matric) suction measurements were not done then. That's why additional 3 numbers of 2-D main experiments were done during this study with the tensiometers to have soil's (matric) suction measurements. Results of the three additional 2-D main experiments are shown, together with Pradel-Raad, (1993) calculation results vs. observed wetting band thicknesses in which indicates poor correlations. Pradel-Raad's theory again gave much lower results (between 2,4% – 4,3%) of the actually observed wetting band thicknesses.

On the other hand; results of 32 numbers of 1-D tests and calculations against Pradel-Raad's (1993) and Lumb's, (1975) theories are given in Table 5.5. Results show poor correlations between the theories and actual observations. Theoretical which results obtained from the both theories ranged between 3,37% - 8,53% of the actual observations. This means that both theories need modifications, which could be the subject of detailed future and further studies.

## CHAPTER 6

# TESTING UNSATURATED FINE-GRAINED SOIL FOR ITS HYDRAULIC PROPERTIES

### 6.1. Introduction: Review of Suction and Hydraulic Conductivity Measurements in Unsaturated Soils

Soil suction is an important parameter describing moisture content, affecting engineering behavior of unsaturated soils. Soil suction is expressed as a pressure term that is a measure of the pulling force (tension) exerted on water and matric suction is the difference between air pressure and pore water pressure. Total suction is the sum of matric and osmotic suctions. Matric suction affects shear strength and hydraulic conductivity of an unsaturated soil. Matric suction is also closely related to capillarity, mineral structure and adsorptive surface forces whereas pore fluid osmotic suction is related to dissolve salt content in pore water, which affects swelling properties. Hence rather than total suction, matric suction is an important parameter to use in engineering practice to predict the behavior of an unsaturated soil. Although, filter paper method is the simplest technique for measuring both total and matric suctions, tensiometers are quicker and give more accurate results for measuring matric suction and therefore could be preferred.

Matric suction is an important parameter, not only for determining water-holding capacity, but also for determining the engineering behavior of unsaturated soils. Although factors affecting the soil suction changes are important, the aim here is limited to determining how matric suction and other basic soil properties can affect unsaturated fine-grained soil's hydraulic properties, such as, the maximum water-retention capacity and the maximum hydraulic conductivity capacity, especially for clays with low (<10%) to medium (10-30%) colloid contents. This is because of the fact that such ranges are quite commonly encountered in practice with clays having inorganic colloids.

## **6.2. Hyprop Testing Technique for Unsaturated Soil's Water Retention and Hydraulic Conductivity Properties**

Previously it was known that hydraulic conductivity decreases by several orders of magnitude, when an unsaturated soil's matric suction increases (D.G. Fredlund and A. Xing, 1994). There are several methods to determine hydraulic properties (hydraulic conductivity,  $h_c$  and water retention curve, wrc) in literature. Many of these methods (including pressure plate test, filter paper test and hanging column etc.) not only are ambiguous, but also don't have continuous measuring intervals over small (few kPa) to medium (100 kPa) and to very high ranges (1000 kPa) of matric suctions, covering a complete range from full saturation to drying. In engineering practice, the most important ranges (for practical purposes) are the first 2 ranges mentioned above. A recently developed equipment called HYPROP (**H**ydraulic **P**roperty **A**nalyzer) covers these 2 ranges by using the evaporation method (ASTM D3404-91(2013)). The test set gives automatic plotted results during continuous testing period graphically. Thus, schematic and visual drawings make observations easy and clear.

### **6.2.1. Sample Preparation**

Before testing starts, the protective cap from the upper side of the sample (the side with the straight rim without cutting edge) is removed and the undisturbed sample is extruded from the "Shelby-Tube" by the provided sampler ring and mesh fabric, which is placed on the sample. Then the perforated attachment cap and its clamp is attached. Dish is filled with de-aired/de-ionized water, before sample is placed with the perforated attachment for reaching full saturation. The water level should be 1 cm below the upper rim of the sampling ring. The sampler ring's cutting edge shows upward and the sample is weighted and its degree of saturation is continually checked until full saturation ( $S=1$ ) is reached (Figure 6.1).



Figure 6.1. Dish with Water and Sample during The Initial Saturation Process.

Then the set up progress continues with degassing syringe, tensiometers and sensor unit. To achieve this, the ceramic tip is inserted into the tube as far as possible with the ceramic pointing down toward the syringe. The cup's tip should be close to the syringe nozzle. Next, the syringe is pulled upright to get rid of all air bubbles in the syringe and in the ceramic tip. Degas sensor unit is critical and needs caring. The acrylic caps onto the sensor head is attached, after filling-up the acrylic attachment with de-aired/de-ionized water using the droplet syringe. When the tensiometers are filled with de-aired water, they are placed onto the sensor unit with silicone caps on, which is then inserted into sample after opening their placed inside the sample via help of a same diameter screw-driver provided with the set. Note that while screwing in the tensiometer shafts into the soil, care is placed not to exceed 1 bar pressure for avoiding soil disturbance. Then the soil sample is taken out of the saturation dish and is the sensor unit assembly is placed onto the sampling ring containing the soil sample (Figure 6.2). Next is to place the silicone disk over the tensiometers and close the clips to fix sampling ring and the sensor unit to make a tightly clad assembly. Figure 6.3 shows then placing the assembly unit onto the weighing scale starts the evaporation process and the test automatically.



Figure 6.2. Assembling the Hyprop's Sensor Unit with the Sampler Ring

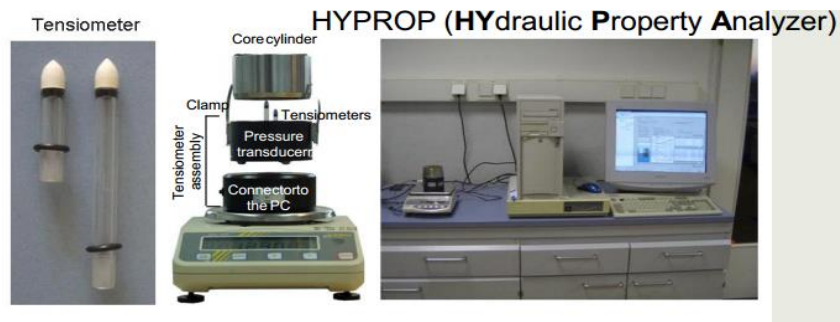


Figure 6.3. Test Set-up of the HYPROP Equipment

### 6.3. Hyprop Testing Theory Using the Evaporation Method

Soil sampling ring has two tensiometers, which is installed in a soil sample at two depths ( $z_1$  and  $z_2$ ). The middle point between the sensing tips of the tensiometers is at the center of the soil sample. To begin with the testing, the undisturbed soil sample is obtained by slowly pushing-in of the coring cylinder into the "Shelby-Tube". This sub-sample obtained, is made saturated before the test, by placing its closed side on the Hyprop scale. The upper side of the sample is open to atmosphere so that soil can lose its moisture by slow evaporation at the constant laboratory temperature (with no fast blowing winds/air-currents in the laboratory, which causes fast evaporation to occur). While soil sample's degree of saturation reduces from full saturation ( $S=1$ ) by losing its moisture thru' evaporation, the soil's water-tension [kPa], causing an average matric-potential and a hydraulic gradient is automatically calculated at the mid-point of the sample, using linear regression. The mass difference, measured by the scale, is used to calculate the volumetric water-content and the water's flow rate. Measuring process, which starts automatically, when the sampler ring is placed onto the scale, will last until one of the tensiometers runs dry or the mass changes becomes marginal or near zero. The remaining final moisture content is determined by the oven drying of the sample at  $105^\circ\text{C}$  for 24 hours. With these values, the water-retention curve and the unsaturated hydraulic conductivity is found by intermittent points [upto (-) 100 kPa] and beyond [upto (-) 1000 kPa] by the built-in software's extrapolation.

### 6.3.1. Discrete Data for Retention and Conductivity Relation

At different points of time  $t^i$  the water tensions  $(h_1)^i$  and  $(h_2)^i$  (in hPa) of both depths are measured as well as the weight of the sample (in grams =  $\text{cm}^3$ ). The analytic procedure is based on the assumption that water tension and water content distribute linear through the column and that water tension and sample weight changes are linear between two evaluation points.

The initial water content is determined from the total loss of water (i.e. evaporation+ water loss by oven drying). The average water content  $\Theta^i$  derived from initial water content and loss of weight, and the medial water tension  $h^i$  give a discrete value  $\Theta^i(h^i)$  of the retention function at any time  $t^i$ .

For the calculation of the conductivity function it is assumed that between two time points  $t^{i-1}$  and  $t^i$  the water flow through the cross section situated exactly between both tensiometers and therefore exactly at column center  $q^i = \frac{1}{2}(\Delta V^i / \Delta t^i A) \Delta V^i$  is the water loss in  $\text{cm}^3$  determined by weight changes,  $\Delta t^i$ , is the interval between two evaluation points and A the cross section area (in  $\text{cm}^2$ ) of the column. The data for the hydraulic conductivity function are determined by inverting the Darcy Equation.

$$K^i(h^i) = -\left(q^i\right) \left(\Delta h^i / \Delta z + 1\right) \quad (6.1)$$

Where;

$(h^i) = 1/4[(h^{i-1})_1 + (h^{i-1})_2 + (h^i)_1 + (h^i)_2]$  is the medial water-tension between two evaluation points, with  $K^i$  as the related hydraulic conductivity (in  $\text{cm h}^{-1}$ ).

$\Delta h^i = \frac{1}{2}[(h^{i-1})_2 - (h^{i-1})_1 + (h^i)_2 - (h^i)_1]$  is the medial difference of the water-tension between both tensiometers, whereas  $\Delta z = z_2 - z_1$  is the distance between both tensiometers (in cm).

Unreliable  $K(h)$  data-sets close to saturation are filtered depending to the measuring accuracy of the tensiometers. To get sufficient number of data points for the hydraulic function, even with relatively long intervals, both the tension curve and the weight curve between the two evaluation points are interpolated with hermitian splines method. On this basis relatively short evaluation intervals are utilized.

## 6.3.2. Water Retention and Hydraulic Conductivity Functions

Normally hydraulic characteristics are described by parametric functions for  $\Theta(h)$  and  $K(h)$ . With the HYPROP, either of three models can be chosen. These models can be adapted to measure data via a robust and non-linear optimizing procedure. In our study, the Van Genuchten/Mualem model was chosen to determine the hydraulic properties of the tested soil samples materials with the Hyprop testing equipment.

### 6.3.2.1. Van Genuchten/Mualem Method

In this model, the effective saturation  $S_e = (\Theta - \Theta_r) / (\Theta_s - \Theta_r)$  and the unsaturated conductivity  $K$ , in relation to the matric potential  $h$ , are predetermined by the following equation formula.

$$S_e(h) = \left(1 + (\alpha|h|)^n\right)^{1/(n-1)} \quad (6.2)$$

$$K(h) = K_s \left(1 + (\alpha|h|)^n\right)^{\tau(1/(n-1))} \left[1 - (\alpha|h|)^{n-1} \left[1 + (\alpha|h|)^n\right]^{1/(n-1)}\right]^2 \quad (6.3)$$

Where;  $\alpha$  = air-entry point

$n$  = porosity

$\tau$  = tortuosity parameter

In the above equations:6.2-6.3, the residual water content is  $\Theta_r$ , the water content at saturation is  $\Theta_s$ , the inverse value of the bubble point potential is  $\alpha$  [ $\text{cm}^{-1}$ ] and the pore size distribution is  $n$  [-] are the fitting parameters for the water-retention function. Furthermore; the tortuosity parameter,  $\tau$  [-] and the saturated hydraulic-conductivity,  $K_s$  are also fitted to get the conductivity function. Figure 6.4 and Figure 6.5 shows experimental process of Hyprop tests in İYTE Geotechnical Laboratory.



Figure 6.4. Experimental Sets-up of the Hyprop Tests



Figure 6.5. A Hyprop Test is in Progress

### 6.3.3. Optimization of the Parameters

The  $\Theta(h)$  and  $K(h)$  functions are adapted simultaneously to the data points by the built-in software. Adaptation is accomplished by non-linear regression. However, the assumption that the water content is spread out linearly over the soil column is not always fulfilled in coarse-pored or structured soil samples. Therefore, the so called ‘‘integral fit’’ applied for the adaption of the retention function overcomes such problems.

## 6.4. Testing Materials and Laboratory Tests on the Samples

In this study only three 3 unsaturated clayey-soil samples with varying degrees of plasticity index (PI, %) and colloid contents (c, %) were used. The soil types of these samples per the USCS or USCSM classifications were ML, OL and CH types. Sub-samples were obtained from the undisturbed Shelby tube samples, obtained from the nearby Tahtalı Lake's bottom sediments in İzmir. Laboratory index tests (for soil classification purposes) of the samples were done at the Ege Zemin and İYTE Lab's in İzmir and the Laser Diffraction Tests (LDT) were done at the Gazi University's Technical Education Faculty-Geotechnical Lab. in Ankara, where the same regression equation and correlation coefficient were used for the tests with the same testing instrument in testing both -0.002 mm and 0.001 mm sizes.

It's noted that the (-) sign denotes the % passing (or finer than) the mentioned sizes. The results are shown in Figure 6.6.

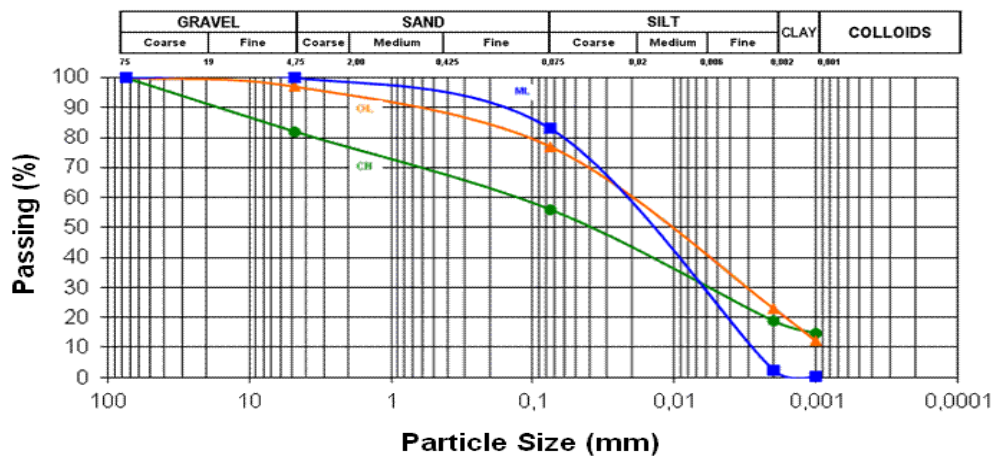


Figure 6.6. Particle Size Distributions of 3 Undisturbed Soil Samples

Table 6.1. Comparing the laboratory test results of the 3 undisturbed soil samples

Soil Type by USCS	$w_i$ (%)	$G_s$	$S_i$ (%)	$e_i$	LL (%)	PL (%)	PI (%)	Sieve Analysis (%)			Hydrometer Analysis (%)	
								<0.076 (mm)	Sand size	Gravel size	<0.0076 (mm)	$2 \cdot 10^{-3}$ (mm)
CH	29	2.76	91	0.88	52	22	30	56	26	18	56	31
OL	31	2.72	93	0.91	45	25	20	77	20	3	77	38
ML	32	2.69	94	0.92	33	28	5	83	17	0	83	4

(Table 6.1 continues next page)

Table 6.1 (cont.)

Lazar Diffraction Analysis (%)		Hydraulic Conductivity (mm/day)
<0.002 mm	<0.001 mm	
18.8	14.7	0.02818
23	12	0.001
2.4	0.1	0.0631

It can be seen that Lazer Diffraction test gives lower and about 60% of hydrometer test results. This may be interpreted as hydrometer test overestimating the fines in suspension by about 40% (i.e. for the -0.002 mm of the fine fraction). This is due to the fact that the hydrometer theory is derived from the sedimentation theory, which depends on the Stokes law, as it may give only approximate results [Ozer, M., 2006], as shown in Table 6.1. Lazer diffraction method is also used to determine -0.001 mm of the fine fraction, which shows the % finer than the maximum colloid size of 0.001 mm Table 6.1. Note that the hydraulic conductivity values reported in Table 6.1 are the values corresponding to the samples' maximum matric suction point during the Hyprop tests. Results are shown in below.

## 6.5. Hyprop Test Results

### 6.5.1. Matric Suction vs. Time

For all the 3 samples tested, matric suction continued to increase gradually over time up to a maximum point, after which it decreased also gradually (Figure 6.7, Figure 6.8 and Figure 6.9).

#### 6.5.1.1. ML Soil Sample

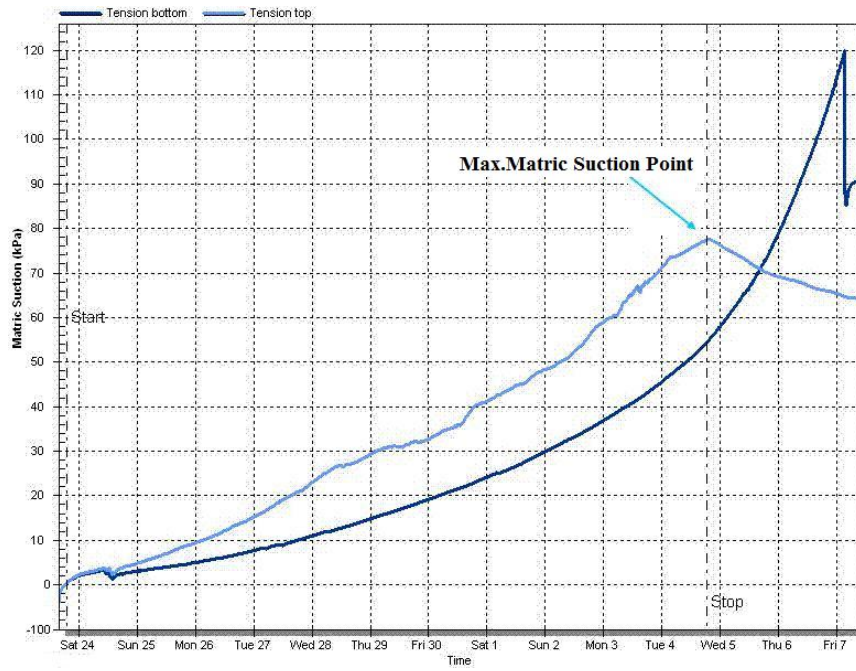


Figure 6.7. Variation of Matric Suction with Time for the ML Soil Sample

### 6.5.1.2. CH Soil Sample

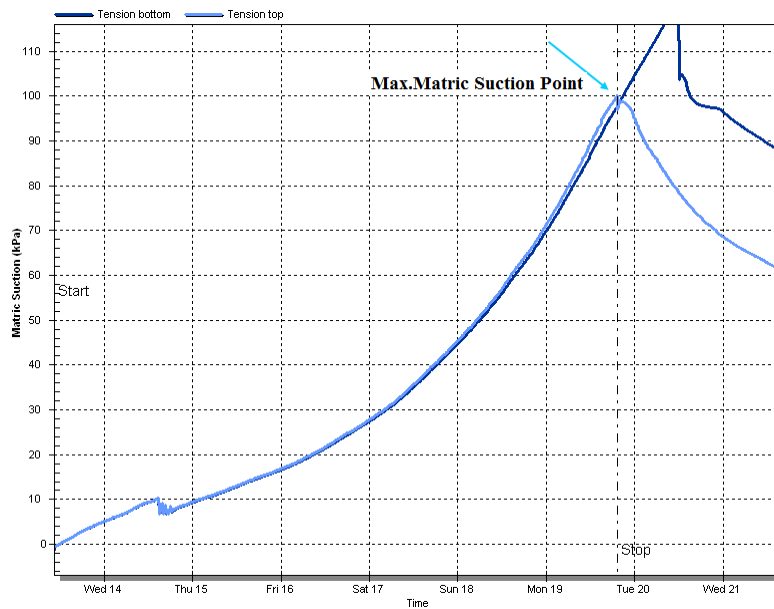


Figure 6.8. Variation of Matric Suction with Time for the CH Soil Sample

### 6.5.1.3.OL Soil Sample

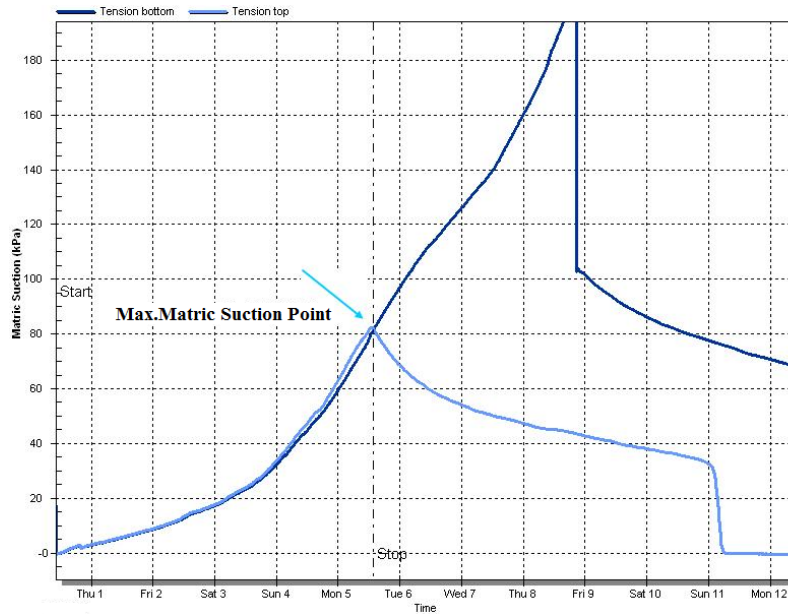


Figure 6.9. Variation of Matric Suction with Time for the OL Soil Sample

Figure 6.10 shows the combined graph of for variation of matric suction with time of the 3 undisturbed soil samples used.

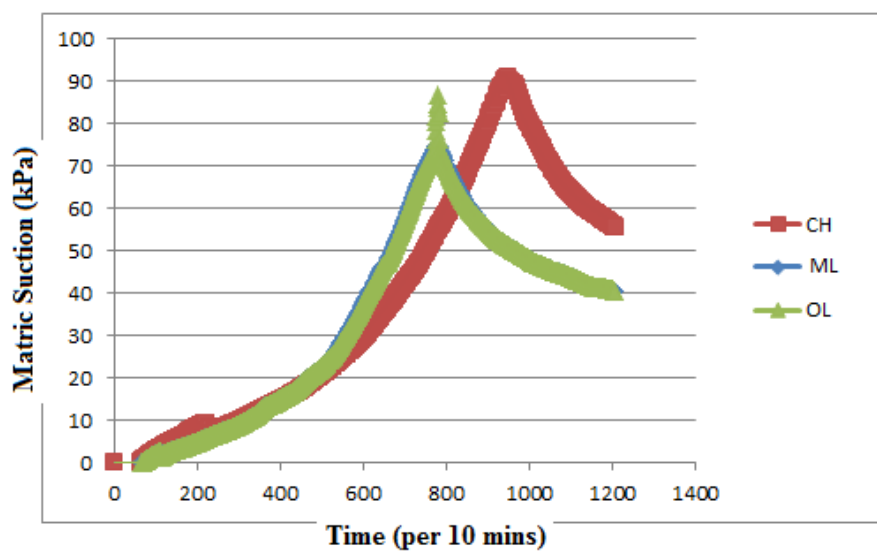


Figure 6.10. Variation of Matric Suction with Time of 3 Soil Samples used

## 6.5.2. Hydraulic Conductivity vs. Matric Suction

The results from Figure 6.11, Figure 6.12 and Figure 6.13 show the obtained plots of the Hyprop's built-in software. These show that with increasing matric suction, hydraulic conductivity gradually decreased up to (-) 10 kPa, after which it decreased almost linearly at constant rate up to about (-) 100 kPa. The actual automatic readings at small time intervals by the Hyprop tensiometers are shown in faint bubbles up to about (-) 100 kPa. Linear line for higher matric suctions between (-) 100 kPa and (-) 1000 kPa is the result of automatic curve fitting process by the built-in Hyprop software. This is because of sample fast losing water content initially, but in later stages water content loss is slowing down and hydraulic conductivity changes accordingly, until test stops at the air-entry point.

### 6.5.2.1. ML Soil Sample

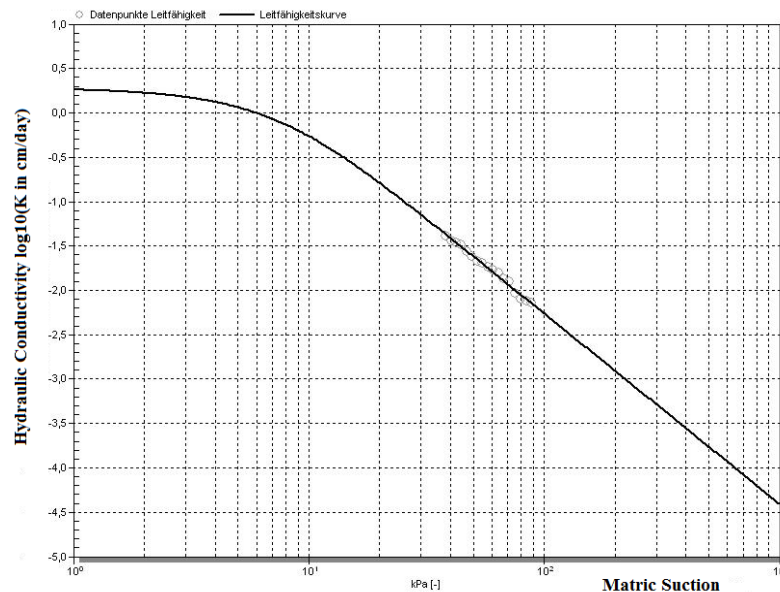


Figure 6.11. Variation of Hydraulic Conductivity with Matric Suction for the ML Soil Sample

### 6.5.2.2. CH Soil Sample

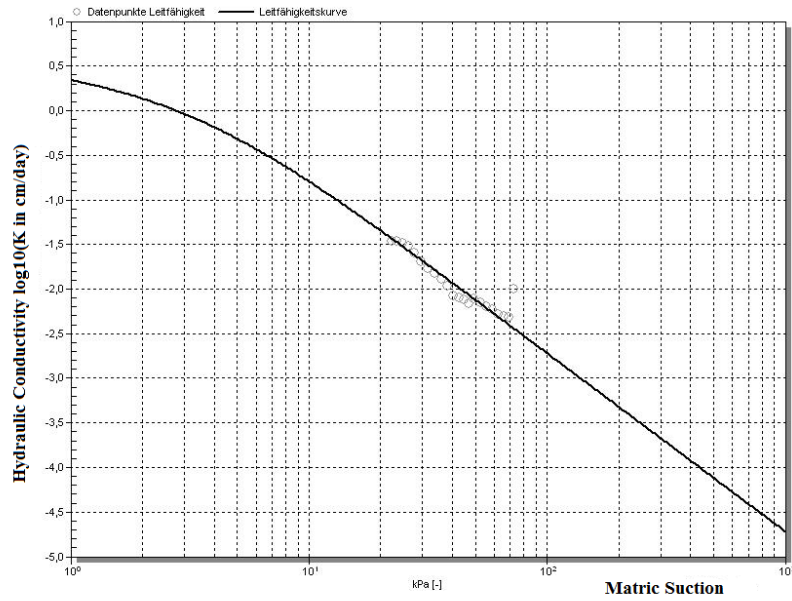


Figure 6.12. Variation of Hydraulic Conductivity with Matric Suction for the CH Soil Sample

### 6.5.2.3. OL Soil Sample

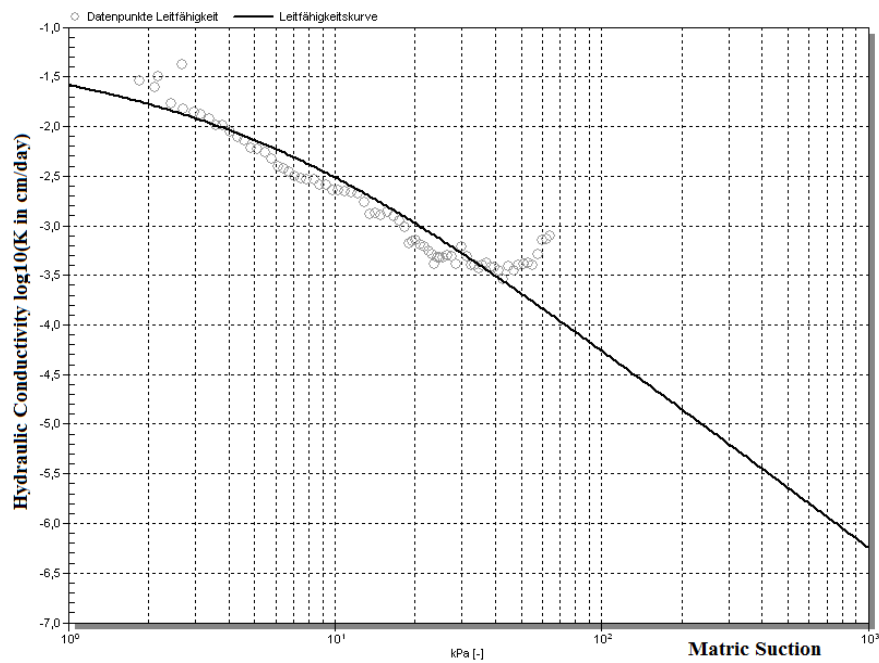


Figure 6.13. Variation of Hydraulic Conductivity with Matric Suction for the OL Soil Sample

Figure 6.14 shows the combined graph for variation of hydraulic conductivity with matric suction of the 3 undisturbed soil samples used.

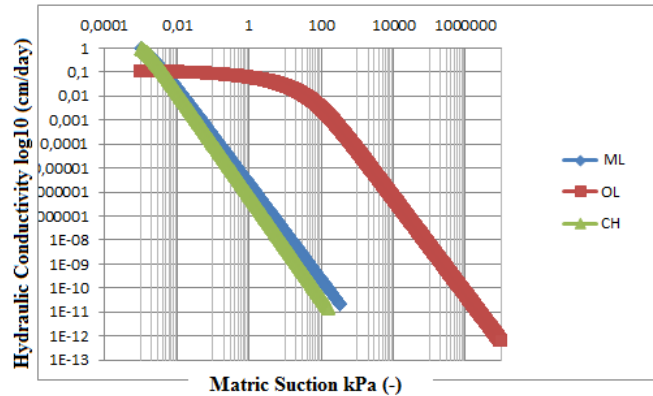


Figure 6.14. Variation of Hydraulic Conductivity with Matric Suction of 3 Soil Samples Used

### 6.5.3. Volumetric Water Content vs. Matric Suction

Initial water contents of the sub-samples obtained from the ‘‘Shelby Tube’’ is determined precisely by the oven drying method, before the Hyprop tests (Table 6.1).

Weighing scale uses this actual as input and calculates the volumetric value approximately at each automatic measurement point thru’ its weighing scale, considering Hyprop assembly is nearly saturated and using the known quantities, which are the sample’s volume, sample’s weight with the sensor assembly unit, which is automatically deducted by the built-in software. As the evaporation method considers that the capillary water filling all the soil pores and no adsorbed (or film) water presence, the calculated porosity (or void ratio) becomes equals to saturated water content,  $\Theta_s$ . This results-in having only approximate values during the tests. Hence, the water content is called the volumetric water content. Similar to hydraulic conductivity above, results show that with increasing matric suction, volumetric water content also gradually decreases with slow rate up to (-) 10 kPa, after which it decreased almost linearly at constant rate up to about (-) 100 kPa. The actual automatic readings at small time intervals by the Hyprop tensiometers are shown in faint bubbles. Dark line beyond (-) 100 kPa and up to about (-) 1000 kPa is the result of automatic curve fitting process by the built-in Hyprop software (Figure 6.15, Figure 6.16, Figure 6.17). This is because

of sample fast losing water content initially, but in later stages water content loss is slowing down, until test stops at the air-entry point.

### 6.5.3.1. ML Soil Sample

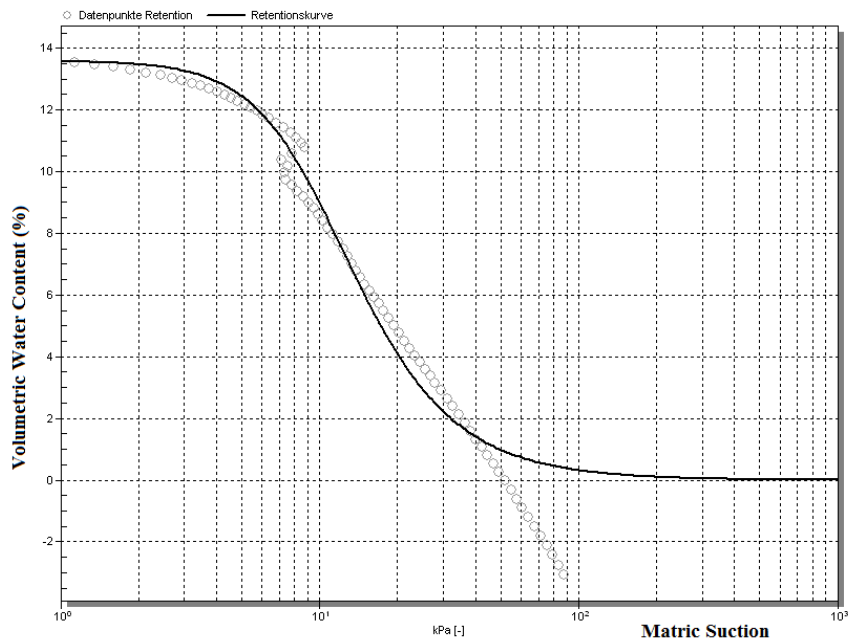


Figure 6.15. Variation of Volumetric Water Content with Matric Suction for the ML Soil Sample

### 6.5.3.2. CH Soil Sample

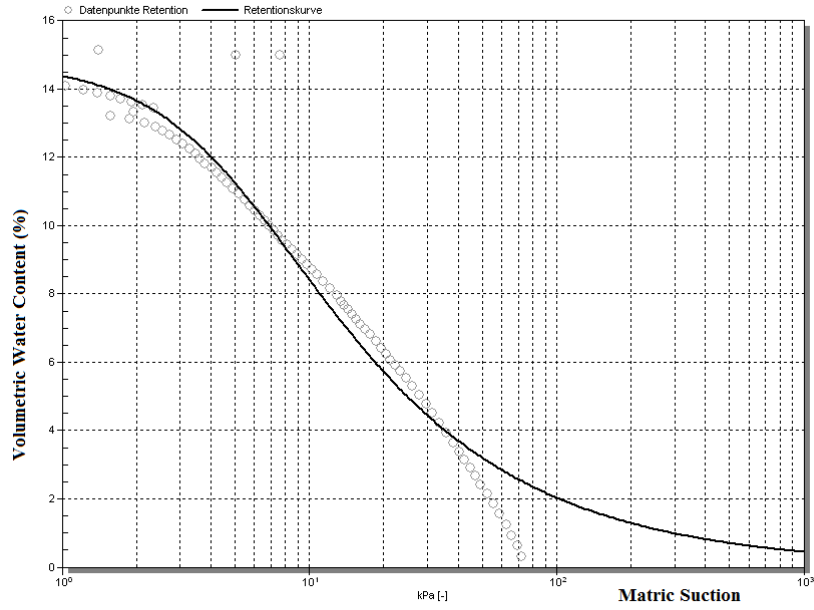


Figure 6.16. Variation of Volumetric Water Content with Matric Suction for the CH Soil Sample

### 6.5.3.3.OL Soil Sample

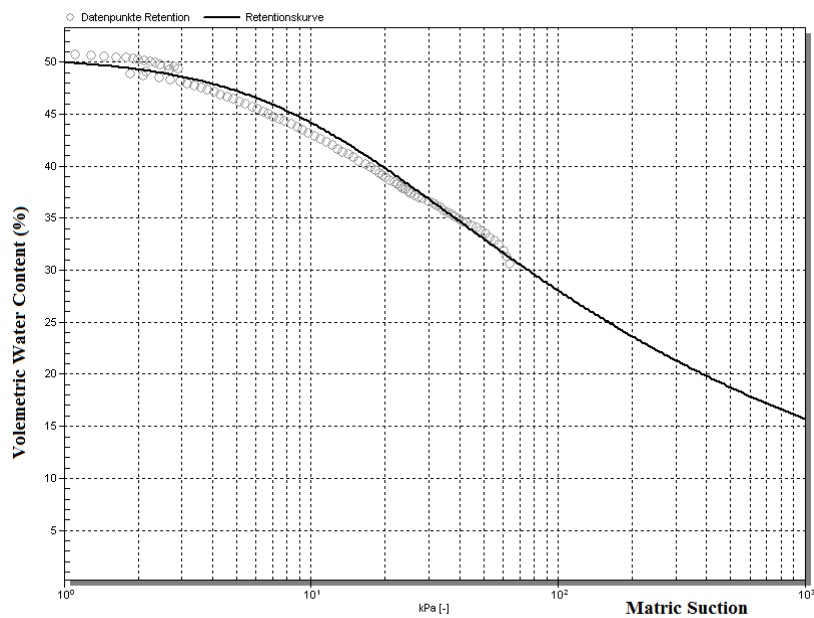


Figure 6.17. Variation of Volumetric Water Content with Matric Suction for the OL Soil Sample

Figure 6.18 shows that combined three undisturbed soils volumetric water content versus matric suction tests results.

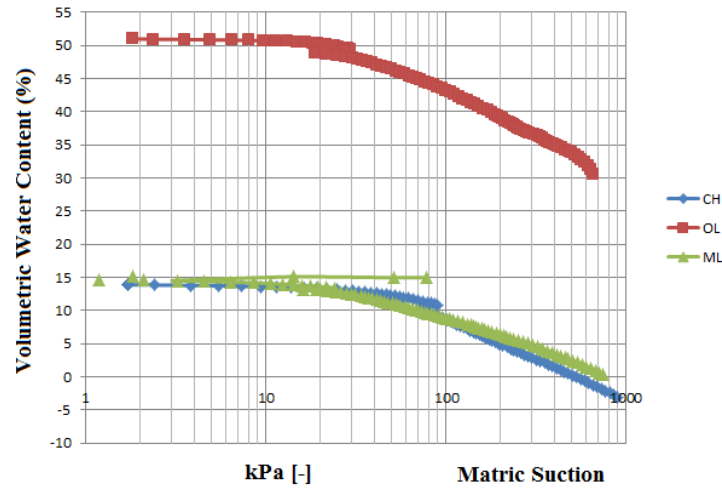


Figure 6.18. 3 Undisturbed Soils Water-Retention (WRC) Tests Results by using HYPROP

#### 6.5.4. Correlations with the Hyprop Test Results

Following correlations were made using the Hyprop test-results presented above.

##### 6.5.4.1. Plasticity Index vs. Time to Reach the Maximum Matric Suction

Time it took (in days) to reach the values of the maximum matric suction (in kPa) obtained in the above presented Hyprop test result graphs were plotted against the plasticity indices (PI, %) of the 3 samples, whose properties were tabulated in Table 6.1. The general trend of the results was that, as PI decreases (from 30 or 20 to 5), sample becomes more granular in nature and time to reach the maximum matric suction increases, provided that sample had greater initial void ratio. The difference between 20 and 30 was not so apparent and perhaps could be ignored. Low PI (ML) material had larger initial void ratio, yielding to larger pore sizes filled with larger air bubbles

(compared to the other 2 samples), meaning that it takes more time to reach pressure equalization thru' diffusion process (Egeli, 1981), between air bubbles and to reach the point of maximum matric suction. The correlation coefficient ( $R^2$ ) is medium (0.8429), but the general trend is nearly apparent (Figure 6.19).

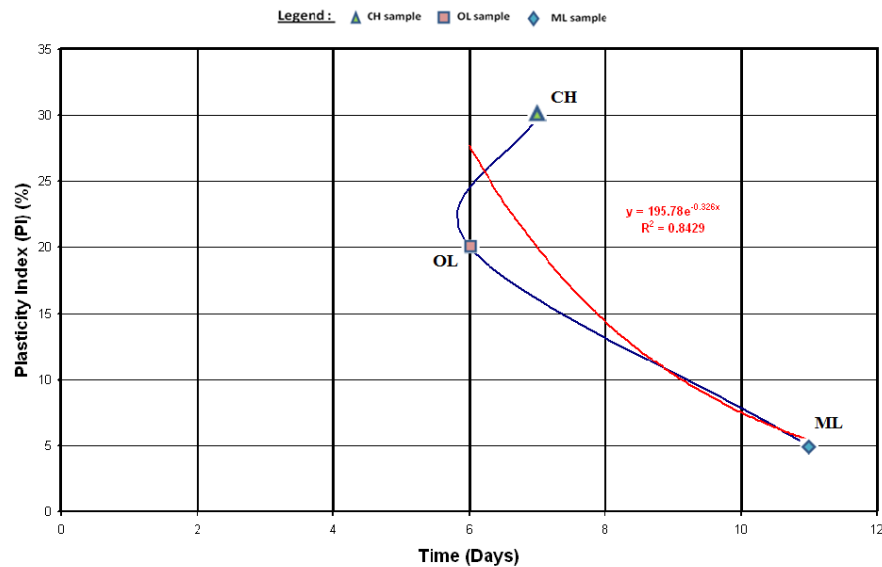


Figure 6.19. Variation of Plasticity Index against Time To reach the Maximum Matric Suction

#### 6.5.4.2. Colloid Content vs. Time to Reach the Maximum Matric Suction

Plotting time (in days) it took to reach the maximum matric suction (kPa) obtained in the Hyprop test-result graphs against the colloid contents (c, %) of the 3 samples used (second column from the last in Table 6.1 show that as the colloid content decreases (from 15 or 12 to 0.1), time to reach the maximum matric suction increases. The difference between 12 and 15 was not so apparent and perhaps could be ignored. Compared to the other 2 samples, low colloid content (ML) material had larger initial void ratio, meaning larger pores filled with larger air bubbles. It takes more time to reach pressure equalization between air bubbles thru' diffusion process and to the point of maximum matric suction (Egeli, 1981). The correlation coefficient is high (0.9498), but the general trend is nearly apparent (Figure 6.20).

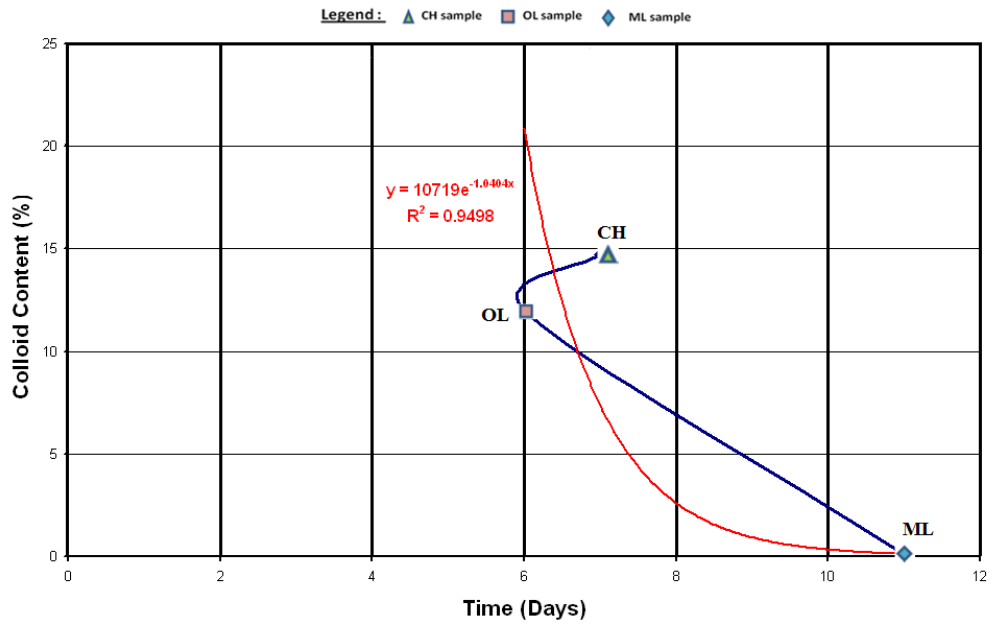


Figure 6.20. Variation of Colloid Content against Time To Reach the Maximum Matric Suction

### 6.5.4.3. Plasticity Index vs. the Maximum Matric Suction

The values of the maximum matric suction in (kPa) obtained in the above presented Hyprop test-result graphs were plotted against the plasticity indices (PI, %) of the 3 samples used, whose properties were tabulated in Table 6.1. Results show that as PI increases, the maximum matric suction also increases. Though the correlation coefficient ( $R^2$ ) is medium (0.7699), the general trend is nearly apparent (Figure 6.21).

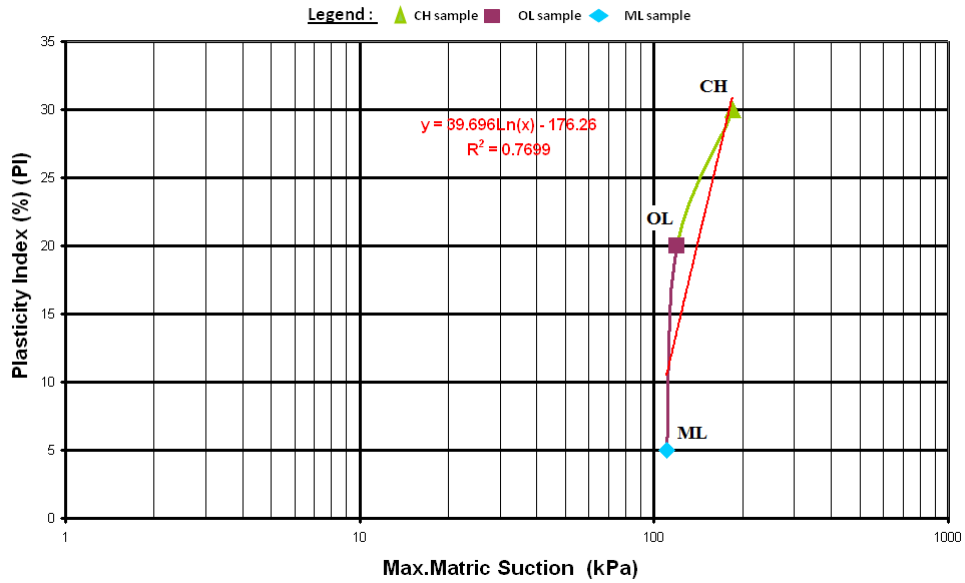


Figure 6.21. Variation of Plasticity Index against The Maximum Matrix Suction

#### 6.5.4.4. Colloid Content vs. the Maximum Matrix Suction

Similar to above by plotting the values of the maximum matrix suction (in kPa) obtained in the Hyprop test-result graphs (presented above) against the colloid content (c, %) of the 3 samples used (second column from the last in Table 6.1 show that as the colloid content increases, the maximum matrix suction also increases. Though the correlation coefficient is low, the general trends still clear (Figure 6.22).

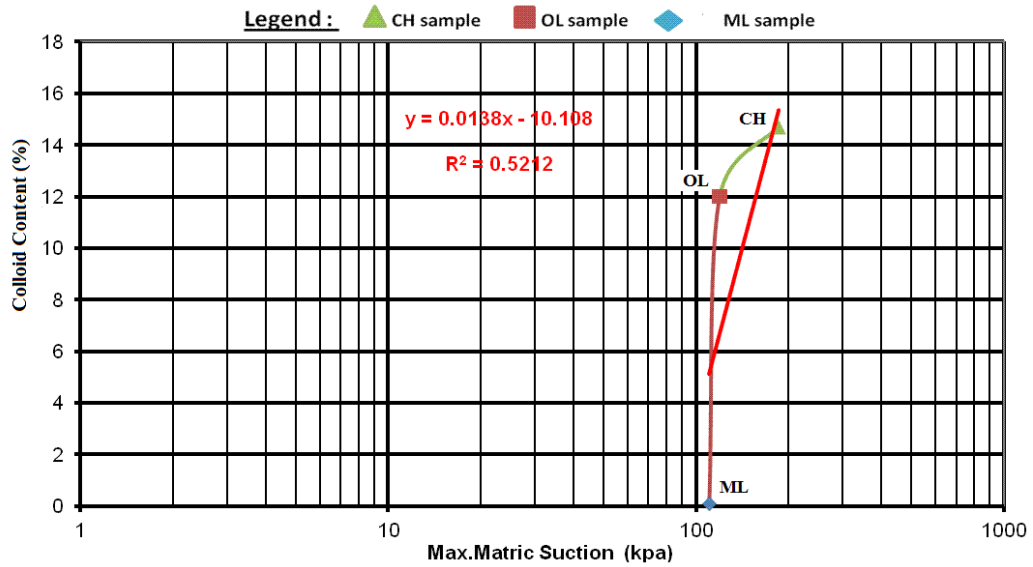


Figure 6.22. Variation of Colloid Content against The Maximum Matrix Suction

#### 6.5.4.5. Hydraulic Conductivity vs. the Maximum Matrix Suction

As noted earlier, hydraulic conductivity values listed in the last column of Table 6.1 are the values (in mm/day) corresponding to the maximum matrix suction values (in kPa), obtained in the Hyprop tests conducted on the 3 samples used. Unfortunately no clear trend has existed. Because of three samples having near maximum matrix suctions (MMS). Various soils could be selected giving different MMS so that their hydraulic conductivity at MMS variation could be better observed. This needed further study (Figure 6.23).

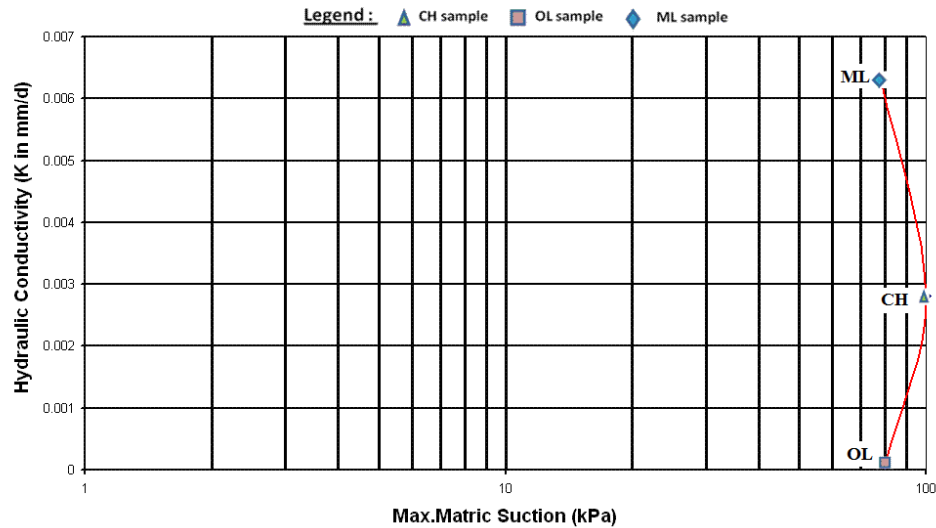


Figure 6.23. Variation of Hydraulic Conductivities at the Maximum Matric Suction against the Maximum Matric Suction

#### 6.5.4.6. Hydraulic Conductivity at the Maximum Matric Suction against the Plasticity Index (PI)

Values of the hydraulic conductivity (in mm/day) corresponding to the maximum matric suction (in kPa) obtained in the Hyprop test-results graphs presented above were plotted against the Plasticity Indices (PI) of the 3 samples used Table 6.1. Results show that as PI increases, hydraulic conductivity at the maximum matric suction point decreases. This is a clear trend with a high correlation coefficient ( $R^2=0.9981$ ) (Figure 6.24).

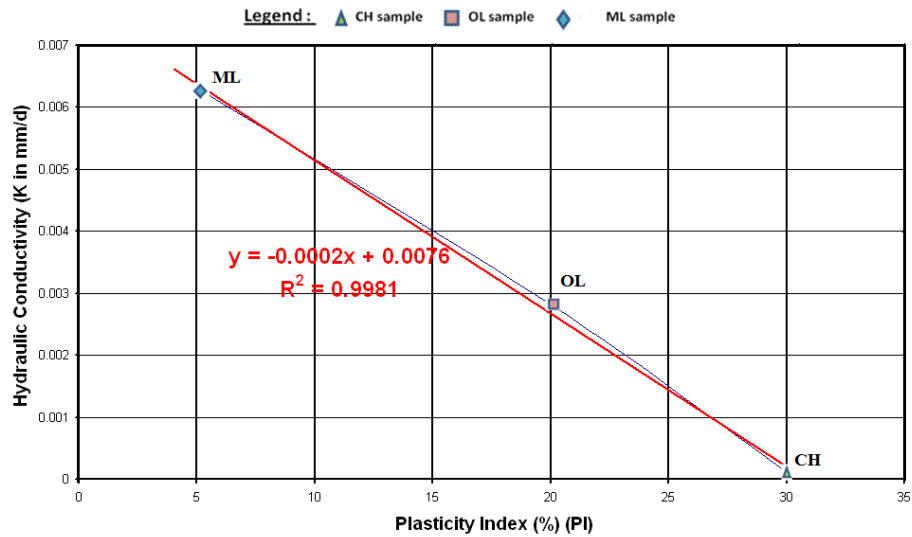


Figure 6.24. Variation of Hydraulic Conductivity at the Maximum Matric Suction against the PI

#### 6.5.4.7. Hydraulic Conductivity at the Maximum Matric Suction against the Colloid Content

Values of the hydraulic conductivity (in mm/day) at the maximum matric suction (in kPa) obtained in the Hyprop test-result graphs presented above were plotted against the colloid content (c) of the 3 samples used Table 6.1. Results show that as colloid content increases, hydraulic conductivity at the maximum matric suction points decreases. This is also a clear trend with a high correlation coefficient ( $R^2=0.9262$ ) (Figure 6.25).

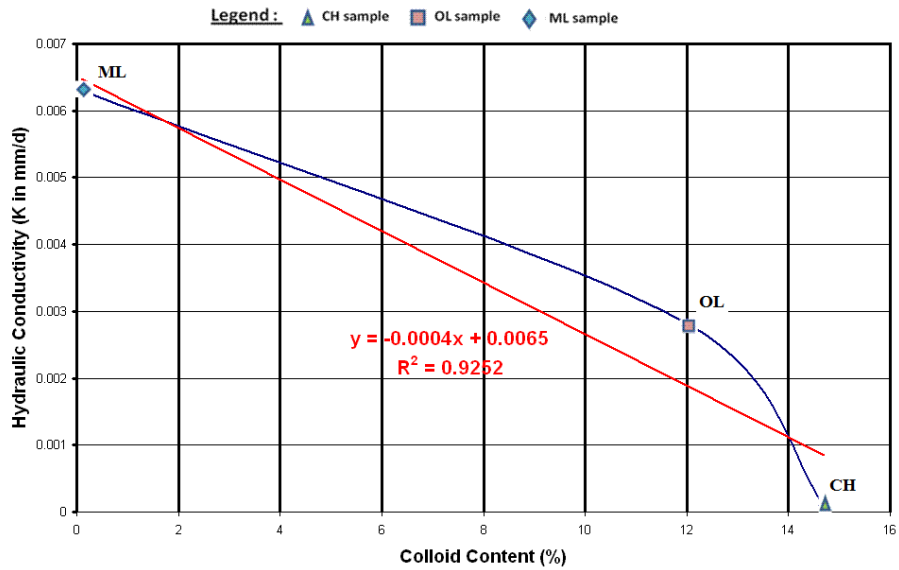


Figure 6.25. Variation of Hydraulic Conductivity at the Maximum Matric Suction point against the Colloid Content

## 6.6. Calibration of the Hyprop Tensiometers

Calibration of Hyprop tensiometers were done by the manufacturer on 28.08.2012, just before testing set was delivered for the normal pressure range of 0-80 kPa. The maximum difference between the applied and the measured pressures were about one half of the applied and measured pressure sensor's maximum tolerance of  $\pm 0.1$  kPa. An accuracy level, which was acceptable ( $R^2=0.99$ ). The calibration plot is given in Figure 6.26.

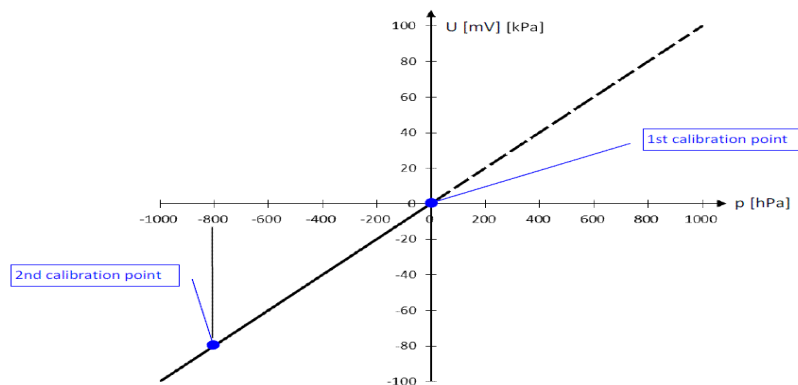


Figure 6.26. Calibration Plot of the Hyprop Tensiometers

## 6.7. Discussion of the Results

The unsaturated fine-grained (UFG) soil testing was performed using the Hyprop testing set for determining the water-retention and hydraulic conductivity characteristics of 3 samples with the USCS types of: CH, OL and ML. Matric suction is an important parameter of unsaturated soils, because it affects the strength of the soil. Following conclusions can be drawn from this experimental study;

- At no overall stresses applied to a soil sample (ie. under atmospheric conditions), matric suction within soil pores do not stay constant, but increases with time up to a maximum point and then decreases.
- Decreasing PI and colloid content (i.e. a UFG sample becoming more granular in nature with a higher void ratio), increase pore and air bubble sizes and time to reach the maximum matric suction. Though the effect of the 2 high PI and high colloid content samples (CH, OL) on the verdict given in the previous sentence was not understandable, the difference between these 2 high PI, high colloid content samples and the low PI, low colloid content (ML) sample on the verdict in the first sentence was clearer with medium to high correlation coefficients ( $0.8429 < R^2 < 0.9498$ ).
- Increasing PI also increases the maximum matric suction (MMS). This is because of if PI increases soil becomes more clayey, which means that pore size will decrease and matric suction will increase (Equation 4.6). Though the correlation coefficient is not very high (0.7699), the general trend is still clear.
- Increasing colloid contents (c), also increases maximum matric suctions (MMS). This is because of increasing colloid content means increasing fines or clay content, which means that pore sizes will decrease and matric suction will increase (Equation 4.6). Tough the correlation coefficient is relatively low (0.5242), the general trend is still apparent.
- Hydraulic conductivity values corresponding to the maximum matric suction points (HC-MMS) were obtained from the Hyprop test-result graphs. HC-MMS plotted against the MMS showed no clear trend for any correlation existence. This needed further study.

- However, HC-MMS plotted against the PI and colloid contents (c) showed quite clear trends with high correlation coefficients ( $0.9262 < R^2 < 0.9981$ ), as HC-MMS decreased with increasing PI or c.

## CHAPTER 7

### CONCLUSIONS

#### 7.1. Conclusion with Tests on Unsaturated Soil's Infiltration Theories

As mentioned previously, twelve main experiments were performed by (Pulat, 2009), but checking his observations against the (Lumb, 1975) wetting band theory was performed in this study, during which time additional three 2-D experiments were performed. In order to determine wetting band thicknesses against these two theories, additional 32 numbers of 1-D experiments were conducted at the Geotechnical Laboratory of Izmir Institute of Technology. In the previous 12 numbers of 2-D main experiments, variables were; two types of soils used, initial water contents and soil densities. Comparison of the wetting band thicknesses, calculated now from the (Lumb, 1975) theory and observations made by (Pulat, H.F., 2010) did not match closely. Lumb's theory gave much lower results between 1.08% - 40.5% of the actually observed wetting band thicknesses (Table 5.3). Original 12 numbers of 2-D results could not be used to check the validity of the (Pradel-Raad, 1993) theory, as soil's (matric) suction measurements were not done then. That's why additional 3 numbers of 2-D experiments were done in this study with the tensiometers. Results of the three additional 2-D main experiments are shown, together with the (Pradel-Raad, 1993) calculation results vs. observed wetting band thicknesses indicated also poor correlations. Pradel-Raad, (1993) theory again gave much lower results (between 2.40% - 4.3%) of the actually observed wetting band thicknesses (Table 5.4). This meant that both theories underestimate actually occurring wetting band thicknesses and need modifications, though predictions from the Lumb, (1975) theory gave slightly better results on average than the predictions from the Pradel-Raad, (1993) theory, according to 2-D experiments.

On the other hand; results of 32 numbers of 1-D tests and calculations using Pradel-Raad's, (1993) and Lumb's, (1975) theories were given in Table 5.5. Results again showed poor correlations to exist between the calculated results (from the theories) and the actual observations made. Theoretical results obtained from both

theories ranged between 3,37% - 8,53% of the actual observations made. This again confirmed that both theories grossly underestimated wetting band thicknesses observed and needed modifications to be made.

## **7.2. Conclusions with Tests on Unsaturated Soil's Hydraulic Properties**

Three unsaturated fine-grained (UFG) undisturbed soils (all which were first saturated and then were allowed to unsaturate by evaporation) tested for their hydraulic properties via a recently developed Hyprop testing set for continuously determining their water-retention and hydraulic conductivity curves. The 3 undisturbed sub-samples were obtained by coring from field obtained "Shelby-Tube" samples having the Unified Soil Classification System (USCS) types of; CH, OL and ML. Though the USCS is the most commonly used soil classification systems globally by engineers, it does not distinguish inorganic clay colloids (particle size < 0.001mm or 1000 nanometers, nm). Such particles can become suspended in water with the presence of infiltrating water. This mechanism allows hazardous contaminants to be attached to colloid particles and transported in groundwater for long distances to spread contamination. In this study colloid contents,  $c$  (%) of the 3 used soils (CH, OL, ML) were obtained using Lazer Diffraction tests conducted at the Gazi University laboratory in Ankara. Following conclusions were drawn from this experimental study.

- At no overall stresses applied to a soil sample (i.e. under atmospheric conditions), matric suction within soil pores do not stay constant, but increases with time up to a maximum point and then decreases.
- By decreasing plasticity index (PI) and colloid content,  $c$  (%) of an unsaturated fine soil sample (i.e. an UFG sample becoming more granular in nature yielding to a higher void ratio and having a decreasing colloid content), increase pore size and air bubble sizes and time to reach the maximum matric suction. Though the effect of the 2 high PI and high colloid content samples (CH, OL) on this verdict was clearly definitive, the difference between these 2 high PI, high colloid content samples and the low PI, low colloid content (ML) sample on this verdict was clearly definitive with medium to high correlation coefficients ( $0,8429 < R^2 < 0,9498$ ).

- By increasing PI, the maximum matric suction (MMS) also increases. Though the correlation coefficient is not very high (0,7699) the general trend was still clear.
- By increasing colloid content,  $c$  (%), the maximum matric suctions (MMS). Also increases. Though the correlation coefficient was relatively low (0,5242), the general trend was still apparent.
- When the hydraulic conductivity values at the maximum matric suction points (HC-MMS) obtained from the Hyprop test-graphs plotted against the maximum matric suction points (MMS) showed no clear trend for any correlation existence. Various soils could be selected giving different MMS so that their hydraulic conductivity at MMS variation could be better observed. This needed further study. However, HC-MMS plotted against the PI and colloid content,  $c$  (%) showed definitive trends with high correlation coefficients ( $0,9262 < R^2 < 0,9981$ ), as HC-MMS decreased with increasing PI or  $c$ .

### **7.3. Significance of this Research for Use in Geotechnical Engineering Practice**

This study introduces a new classification system called USCS-M which distinguishes fine-grained soils part of the USCS into silt, clay and colloid sizes. In most geotechnical engineering projects high contents of last two sizes are undesirable as they cause many geotechnical problems like settlements, pollution transport etc. By distinguishing these three sizes these undesirable results can be better controlled.

This study showed that slope and landslide stability affecting wetting-band theories by Lumb (1975) and Pradel-Raad (1993) needed modifications.

This study also showed that Hyprop set, which uses tensiometer standard (ASTM D3404-91(2013)) could be used to predict soil hydraulic properties on the wet side of the optimum water content in the Proctor curve (i.e. water-retention and hydraulic conductivity variations), which are important parameters of unsaturated soils.

### **7.4. Suggestions for Future Research**

Lumb and Pradel-Raad equations give constant values independent of time. Even after rainfall stops wetting-band keeps moving (increasing) with time. So the equations (Lumb and Pradel-Raad) should take this (time based changing) into account. Another factor is the change of hydraulic conductivity (unsaturated soil permeability) with time. These could be the subject of future detailed study. Future studies to check the effect of various parameters on hydraulic conductivity (HC) and matric suction (MS) can include varying the following parameters:

1. Changing clay contents, Plasticity Index and initial water contents,
2. Taking matric suction and wetting-band thickness values at constant times (e.g. 10mins.) after rainfall starts with intensity kept constant at  $0.05\text{lt/sec/m}^2$ .

## REFERENCES

- Alonso, E., Gens, A., Lloret, A. & Delahaye, C. (1996). Effect of rain infiltration on the stability of slopes. Proc. Ist Int. Conf. on Unsaturated Soils, UNSAT '95, Paris, pp. 241-249.
- Alonso, E.E., Gens, A., Josa, A., (1990). A constitutive model for partially saturated soils. *Geotechnique* 40 (3), 405-430.
- ASTM Test Standards.
- Bao, C.G., Gong, B. and Zhan, L. (1998). Properties of Unsaturated Soils and Slope Stability of Expansive Soil. *Keynote Lecture, 2<sup>nd</sup> Int. Conf. on Unsaturated Soils*. Beijing, China.
- Becher, H. H. (1970) Determination of soils hydraulic properties by evaporation method. *Z. Pflanzenemahr. Bodenk. v. 128 s. 1-12.*
- Benda, L.E., Cundy, T. W., (1990). Predicting deposition of debris flows in mountain channels. *Canadian Geotechnical Journal*. 27, 409-417.
- Bishop, A.W., (1961). The Measurement of Pore Pressure in Triaxial Test, *Pore Pressure and Suction in Soils*, Butterworths, London, p. 38.
- Bouwer, H (1964). Unsaturated flow in groundwater hydraulics. *ASCE journal of the Hydraulic division*, HY5, pp121-144.
- Brankensiek, D. L., (1977). Parameter estimation of the Green and Ampt Infiltration Equation, *Water Resources Research*, pp 1009-1012.
- Burton, A., Bathurst, J.C., (1998). Physically based modeling of shallow landslide sediment yield at a catchment scale. *Environmental Geology* 35, 89-99.
- Brooks, R.H., and A. T. Corey (1964), Hydraulic properties of porous media, *Hydrol. Pap. 3*, 27 pp., Colo. State Univ., Forth Collins.
- Campbell, R.H. (1975). Soil slips, debris flows and rainstorms in the Santa Monica Mountains and vicinity, southern California. *U.S. Geological Survey Professional Paper* 851, 51 p.
- Cho, G. C. and Santamarina, J. C. (2001). Unsaturated particulate materials – Particle-level studies. *Journal of Geotechnical and Geoenvironmental Engineering*, ASCE, 127, No. 1, 84-96.
- Cheng, P.F.K. (1997). Soil infiltration prediction and its significance in slope stability. In Proceedings of the 3<sup>rd</sup> Asian Young Geotechnical Engineers Conference,

- Singapore. Edited by T.S. Tan, S.H. Chew, K.K. Phoon, and T.G. Ng. Photoplates Pt. Ltd., Singapore. pp. 661-669.
- Chen, S. Y. (1996). Relationship between stress-strain model of soils and growing process of landslides. *Rock and soil mechanics* (in Chinese) 17(39), 21-26.
- Chen, S. Y. (1997). A method of stability analysis taken effect of infiltration and evaporation into consideration for soil slopes. *Rock and soil mechanics* (in Chinese) 18(2), 8-12.
- Cruden, D. M. (1991). ‘‘A Simple Definition Of A Landslides.’’ *Bulletin IAEG*, 43:27-29.
- Dane, J. H., Hopmans, J. W. (2002). Pressure plate extractor, in Dane, J. H., Topp, E. C. (eds.). *Methods of Soil Analysis, Part 4, Physical methods*, SSSA Book Ser. 5, SSSA, Madison, WI, USA, pp. 688-690.
- Du, R. H. (1991). Study of landslide and debris flow at Three Gorges Reservoir Area, Yangtze River. Chengdu. *Sichuan Press of Science and Technology* (in Chinese) 1991, 33-36.
- Durner, W., Flühler, H. (2005). Soil Hydraulic Properties, in Anderson, M. G., McDonnell, J. J. (eds.). *Encyclopedia of Hydrological Sciences*, Chapter 74. John Wiley & Sons, Ltd., pp. 1103-1120.
- Durner, W., Or, D. (2005). Soil Water Potential Measurement, in Anderson, M. G., McDonnell, J. J. (eds.). *Encyclopedia of Hydrological Sciences*, Chapter 73. John Wiley & Sons, Ltd., pp. 1089-1102.
- Egeli, İ. (1981). Pore Pressures and Volume Changes in Undrained Unsaturated Clays. Ph.D. Thesis submitted to Imperial College of Science and Technology – ICST (Univ. of London) Civil Engineering Dept. –Soil Mechanics, London, U.K.
- Egeli, İ. (1992). Some Tests for Studying Volume Change and Pore Water Pressure Behaviour of Unsaturated Clays on the Wet Side of Optimum Water Content. In *Proceedings of the 45<sup>th</sup> Canadian Geotechnical Conference*. 26-28 October 1992, Royal York Hotel, Toronto-Ontario, Canada. Vol. II-1/1-10. (Proceedings of International Conferences).
- Fredlund, D. G., Morgenstern, N.R. & Widger, R.A. (1978). The shear strength of unsaturated soils. *Canadian Geotechnical Journal*, vol 15, No3 pp 313-321.
- Fredlund, D. G., and Rahardjo, H. (1993). *Soil mechanics for unsaturated soil mechanics*. Wiley Inter Science, New York.
- Fredlund, D. G., and Xing, A. (1994). Equation for the Soil-Water Characteristic Curve. *Canadian Geotechnical Journal*. 31: 521-532.

- Fleureau, J. M., Kheirbek-Soud, S and Taibi, S. (1995). Experimental aspects and modeling of the behavior of soils with a negative pressure. *Proc. of 1st International conference on unsaturated soils*, Paris, Vol.1, 57-62.
- Fourier, A. B., Rowe, D. and Blight, G. E. (1999). The effect of infiltration on the stability of the slopes of a dry ash dump. *Geotechnique*, 49(1), 1-13.
- Fredlund, D. G. (1995). The scope of unsaturated soil mechanics: An overview. *Proc. of 1<sup>st</sup> International conference on unsaturated soils*, Paris, Vol. 1, 1155-1177.
- Fredlund, D. G. (1995a). Prediction of Unsaturated Soil Functions using the Soil-Water Characteristic Curve. B.B.Symposium, 13-16 December, Singapore.
- Fredlund, D. G, Xing, A., Fredlund, M. D., and Barbour, S. L. (1996). The relationship of unsaturated soil shear strength to the soil-water characteristic curve. *Canadian Geotechnical Journal.*, 33, 440-448.
- Gasmo, J. M., Rahardjo, H., Leong, E. C. (2000). Infiltration effects on stability of a residual soil slope. *Computers and Geotechnics*, 26, 145-165.
- Geiger, S. L., and Durnford, D. S. (2000). Infiltration in Homogeneous Sands and a Mechanistic Model of Unstable Flow. *Soil Science Society of America Journal*. 64: 460-469.
- Glass, R. J., Steenhuis, T. S., and Parlange, J. Y. (1989). Wetting Front Instability, Experimental Determination of Relationships between System Parameters and Two Dimensional Unstable Flow Field Behavior in Initially Dry Porous Media. *Water Resource Research*. 25: 1195-1207.
- G. J. Bouyoucos. (1936). Directions for Making Mechanical Analysis of Soils by the Hydrometer Method. *Soil Sci*. 42(3).
- Green, W. H. and Ampt, G. A. (1911). Studies on Soil Physics I. The Flow of Air and Water through Soils. *Journal of Agricultural Research*. 4: 1-24.
- Green, R. E., and J. C. Corey. (1971). Calculation of hydraulic conductivity: a further evaluation of some predictive methods. *Soil Sci. Soc. Am. Proc*. 35:3-8.
- Haan, C. T., B. J. Barfield, and J. C. Hayes. (1994). Infiltration, Design Hydrology and Sedimentology for Small Catchments, *Academic Press*, New York, USA, p. 54-67.
- Haefeli, R., (1948). The stability of slopes acted upon by parallel seepage, *Proc. Int. Conf. Soil Mech. Found. Eng.*, 1, 57-62.
- Hoek, E. and Brown, E.T. 1980. Empirical Strength Criterion for Rock Masses. *J. Geotech. Engng*
- Hollingsworth, R. and Kovacs, G. S. (1981). Soil slumps and debris flows, prediction and protection. *Bulletin of Association of Engineering Geologists* 18, 17-28.

- Huang, L. J. and Lin, X. S. (2002). Study on landslide related to rainfall. *Journal of Xiangtan Normal University* (in Chinese, Natural Science Edition) 24, 55-62.
- Iverson, R. M., and J. J. Major. (1987). Rainfall, groundwater flow and seasonal motion at Minor Creek landslide, northwestern California: Physical interpretation of empirical relations, *Geol. Soc. Am. Bull.*, 99, 579-594.
- Iverson, R. M., (2000). Landslide triggering by rain infiltration, *Water Resources Research*, Vol. 36, No. 7, pp 1897-1910. *U.S. Geological Survey*, Vancouver, Washington.
- Jensen, M. E., Burman, R. D., and Allen, R. G. (1990). Evapotranspiration and irrigation water requirements. *ASCE Manuals and Reports on Engineering Practice No. 70*, ASCE, New York, N. Y.
- Jury, W. A., Z. Wang and A. Tuli. (2003). A conceptual model of unstable flow in unsaturated soil during redistribution. Available at [www.vadosezonejournal.org](http://www.vadosezonejournal.org). *Vadose Zone J.* 2:61-67.
- Khalili, N., Geiser, F., and Blight, G. E. (2004). Effective stress in unsaturated soils: review with new evidence. *Int. J. Geomech. ASCE*, 4(2), 115-126.
- Klute, A., and C. Dirksen. (1986). Hydraulic conductivity and diffusivity: Laboratory methods. p. 687-734. In A. Klute (ed.) *Methods of soil analysis. Part 1.* 2<sup>nd</sup> ed. Agron. Monogr. 9. ASA and SSSA, Madison, WI.
- Klute, A. and Dirksen, H. E. (1989). Hydraulic conductivity and diffusivity: laboratory methods. In *Method of Soil Analysis*. Edited by A. Klute. Part 1. American society Agronomy, Madison, Wis. Pp. 687-734.
- Kim, J., Park, S. and Jeong, S. (2006). Effect of Wetting Front Suction Loss on Stability of Unsaturated Soil Slopes. *Unsaturated Soils, Seepage and Environmental Geotechnics*, ASCE. 148: 70-77.
- Kirkby, M. J., (1987). General models of long-term slope evolution through mass movement. In: Anderson, M. G., Richards, K. S. (Eds.), *Slope Stability*. Wiley, Chicester, pp. 359-379.
- Lan, H. X., Wu, F. Q., Zhou, C. H. et al. (2003). Rainfall-induced landslide hazard spatial analysis and prediction using GIS. *Chinese Science Bulletin* 48(7), 703-708.
- Leong, E. C., Low, B. K. and Rahardjo, H. (1999). Suction profiles and stability of residual slopes. *Proceedings of Slope Stability Engineering*, edited by Yagi, Yamagami and Jiang, Balkema, 387-392.
- Liu, Y., Bierck, B. R., Selker, J. S., Steenhuis, T. S. and Parlange, J. Y. (1993). High Density.

- Li, X. H. and Lin, H. and Chen, X. Q. et al. (2001). GIS aided study and numerical simulation of initiation mechanism of landslide due to precipitation. *Journal of Engineering Geology* (in Chinese) 33(8), 133-140.
- Lumb, P. B. (1962). The Properties of Decomposed Granite. *Geo-technique*. 12: 226-243.
- Lumb, P. B. (1975). Slope Failures in Hong Kong. *Quarterly Journal of Eng. Geol.*, Geological Society of London, 8: 31-65, UK.
- Mein, R. G. and Farrell, D. A. (1974). Determination of Wetting front Suction in the Green-Ampt Equation. *Soil Science Society of America, Proceedings*. 38: 872-876.
- Moret-Fernandez, D., J.L. Arrue, V. Perez and M.V. Lopez (2008): A TDR-pressure cell design for measuring the soil-water retention curve. *Soil and Tillage Research*, 100(1-2): 114-119. DOI:10.1016/j.still.2008.05.009
- Morris, P. H., Graham, J. and Williams, D. J. (1992). Cracking in drying soils. *Canadian Geotechnical Journal*, 29, 263-277.
- Mualem, Y. (1976). A new model for predicting the hydraulic conductivity of unsaturated porous media. *Water Resources Research*, 12: 513-522.
- Mualem, Y. (1986). Hydraulic conductivity of unsaturated soils: Prediction and formulas. In *Methods of Soil Analysis, Part 1*. A. Klute, ed. American Society of Agronomy. Madison, WI. pp. 799-823.
- Ng, C. W. W., Chen, S. Y. and Pang, Y. W. (1999). Parametric study of effect of rain infiltration of unsaturated slopes. *Rock and Soil Mechanics*, Vol. 20, No. 1, 1-14 (In Chinese).
- Ng, C. W. W. and Shi, Q. (1998). A numerical investigation of the stability of unsaturated soil slopes subjected to transient seepage. *Computers and Geotechnics*, Vol. 22, No. 1, 1-28.
- Ozer, M., Orhan, M., Isık, N. S. (2009). Determination of Particle Size Distribution of Soils by using Lazer Diffraction Method (in Turkish), Proc. of 3.<sup>rd</sup> Geotech. Symp., Çukurova Univ., Adana, Turkey.
- Peck, A. J. (1971). Redistribution of soil water after infiltration. *Aust. J. Soil Res.* 9:59-71.
- Peters, A., and W. Durner (2006a). Improved estimation of soil water retention characteristics from hydrostatic column experiments, *Water Resources. Res.*, 42, W11401, doi: 10.1029/2006WR004952.
- Pierson, T. C. (1980). Piezometric response to rainstorms in forested hillslope drainage depressions. *Journal of Hydrology* (New Zealand) 19,1-10.

- Plagge, R. (1991). Bestimmung der ungesättigten hydraulischen Leitfähigkeit im Boden. PhD thesis, Berlin University of Technology, Institute of Ecology, Department Soil Science.
- Pradel, D., and Raad, G. (1993). Effect of Permeability on Surficial Stability of Homogeneous Slopes. *Geotechnical Engineering*. 119, No. 2, 3 15-332.
- Premchitt, J., Brand, E. E., Chen, P. Y. M. (1994). Rain induced landslides in Hong Kong, 1972-1992. *Asia Engineer*, 43-51.
- Priesack, E., Durner, W., (2006). Closed form expression for the multi-model unsaturated conductivity function. *Vadose Zone J.* 5, 121-124.
- Pulat, H., F. (2009). An experimental and analytical study of various soil slopes in laboratory conditions. *İzmir Institute of Technology*, MSc. Thesis.
- Rahardjo, H., E. C. Leong, and R. B. Rezaur (2003). Response of a residual soil slope to rainfall. NRC Research Centre.
- Richards, L. A. (1931). Capillary Conduction of Liquids Through Porous Mediums. *Physics* 1, 318-333.
- Selby, M. J., (1993). Hillslope Materials and Processes, Second Edition. *Oxford University Press*, Oxford.
- Schindler, U. (1980). Ein Schnellverfahren zur Messung der Wasserleitfähigkeit im teilgesättigten Boden an Stechzylinderproben. *Arch. Acker-Pflanzenbau Bodenkd.* 24:1-7.
- Schindler, U., Müller, L., (2006). Simplifying the evaporation method for quantifying soil hydraulic properties. *J. Plant Nutr. Soil Sci.* 169, 623-629. doi: 10.1002/jpln.200521895.
- Schindler, U., Durner, W., von Unold, G., Mueller, L. (2010). Evaporation method for measuring unsaturated hydraulic properties of soils. Extending the range. *Soil Sci. Soc. Am. J.*, in press.
- Schwab, G. D., D. D. Fangmeier, W. J. Elliot, and R. K. Frevert. (1993). *Other factors. Soil and Water Conservation Engineering*. pp.51.
- Sheng, M., Tang, M., Chen, H., Yang, B. W., Zhang, FF., Huang, Y. H. (2008). Influence of arbuscular mycorrhizae on photosynthesis and water status of maize plants under salt stress. *Mycorrhiza*, 18: 287-296.
- Skaggs, R. W. (1980). Methods for design and evaluation of drainage-water management systems for soils with higher water tables. *Drainmod Reference Report*.
- Skempton, A. W., and DeLory, F. A. (1957). Stability of natural slopes in London clay. *Proc. 4<sup>th</sup> Int. Conf. on Soil Mech. and Found. Engrg.*, Vol. 2, 378-381.

- Slosson, J. E., and Khron, J. P. (1979). AEG building code review, mudflow/debris flow damage, February 1978 storm-Los Angeles area. *California Geology*, 1, 8-11.
- Stanic, B. (1984). Influence of Drainage Trenches on Slope Stability. *Journal of Geotechnical Engineering*, Vol. 110, No.11, November, 1984.
- Sun, D. A., Matsuoka, H., Yao, Y. P., and Ichihara, W. (2000). An elastoplastic model for unsaturated soil in three dimensional stresses. *Soil Found.*, 40(3), 17-28.
- Tarantino, A. and Bosco, G. (2000). Role of soil suction in understanding the triggering mechanisms of flow slides associated to rainfall. *Second International Conference on debris flow hazards mitigation*, 16-18 August, 2000, Taipei, Taiwan 81-88. A. A. Balkema, Rotterdam.
- Tindall, J. A. and Kunkel, J. R. (1999). *Unsaturated Zone Hydrology*, New Jersey, Prentice Hall.
- Toll, D. G. and Ong, B. H. (2003). Critical state parameters for an unsaturated residual sandy clay. *Geotechnique* 53(1): 93-103.
- Vanapalli, S. K., Fredlund, D. G., Pufahl, D. E., Clifton, A. W., (1996). Model for the prediction of shear strength with respect to soil suction. *Canadian Geotechnical Journal* 33, 379-392.
- Van Genuchten, M. T., (1980). A closed-form equation for predicting the hydraulic conductivity of unsaturated soils. *Soil Sci. Soc. Am. J.* 44, 892-898.
- Wallace, K. (1975). The analysis of surface infiltration into earth structures. 4<sup>th</sup> *Southeast Asian Conf. on Soil Engrg.*, Kuala Lumpur.
- Wang, Z., Tuli, A. and Jury, W. A. (2003). Unstable Flow during Redistribution in Homogeneous Soil. *Vadose Zone Journal*. 2: 52-60.
- Weber, R. F., Treiman, J. A., Tan, S. S., and Miller, R. V. (1979). Landslides in the Los Angeles region, California, effects of February-March, 1978 rains. *Open File Report 79-4LA*, California Division of Mines and Geology, Sacramento, Calif.
- Wendroth, O., W. Ehlers, J. W. Hopmans, H. Kage, J. Halbertsma, and J. H. M. Wösten. (1993). Reevaluation of the evaporation method for determining hydraulic functions in unsaturated soils. *Soil Sci. Soc. Am. J.* 57:1436-1443.
- Wilson, R. C. and Dietrich, W. E. (1987). The contribution of bedrock groundwater flow to storm runoff and high pore pressure development in Erosion and Sedimentation in the Pacific Rim. *Int. Assoc. Hyd. Sci. Pub.* 165, 49-60.
- Wind, G. P. (1966). Capillary conductivity data estimated by a simple method, in Proc. UNESCO/IASH Symp. Water in the Unsaturated Zone. Wageningen, The Netherlands, pp. 181-191.

- Wroth, C. P. and Houlsby, G.T. (1985). Soil mechanics: property characterization and analysis procedure. *Proc. 11<sup>th</sup> ICSMFE*, San Francisco, Vol.1, 1-55.
- Xie, S. Y. and Xu, W. Y. (1999). Mechanism of landslide induced precipitation. *J. Wuhan Univ. of Hydr. and Elec. Eng.* (in Chinese) 32(1), 21-23.
- Youngs, E. G. (1957). Moisture profiles during vertical infiltration. *Soil Science*, volume 84, (July-Dec.), pp 283-290.
- Young, M. H., Sisson, J. B. (2002). Tensiometry, in Dane, J. H., Topp, E. C. (eds.): *Methods of Soil Analysis, Part 4, Physical methods*. SSSA Book Ser. 5, SSSA, Madison, WI, USA, pp. 575-608.